INVESTIGATION OF IONICALLY-DRIVEN STRUCTURE-PROPERTY RELATIONSHIPS IN POLYELECTROLYTE NETWORKS

by

Jessica Lauren Sargent

A Dissertation

Submitted to the Faculty of Purdue University

In Partial Fulfillment of the Requirements for the degree of

Doctor of Philosophy

School of Materials Engineering

West Lafayette, Indiana

August 2020

THE PURDUE UNIVERSITY GRADUATE SCHOOL
STATEMENT OF COMMITTEE APPROVAL

Dr. Kendra A. Erk, Co-Chair
School of Materials Engineering

Dr. John A. Howarter, Co-Chair
School of Materials Engineering

Dr. Carlos J. Martinez
School of Materials Engineering

D**r. Jeffrey P. Youngblood**
School of Materials Engineering

Approved by:
Dr. David F. Bahr

To my family, who has supported me in every way throughout this journey and beyond

ACKNOWLEDGMENTS

I would like to thank my advisors, Professor Kendra Erk and Professor John Howarter, for their great support and guidance throughout my graduate career. Thank you for your assistance and encouragement through the many challenges encountered throughout my M.S. and Ph.D. work, both personally and professionally. Thank you for your patience and support as I have pursued more obscure projects outside of the regular scope of your research groups and taken on extra responsibilities with the Women in Engineering Program and MSE Graduate Student Association. I would also like to acknowledge my committee, Professor Jeffrey Youngblood and Professor Carlos Martinez, for their valuable discussions and insight across a wide range of polymer science topics. This work was supported by a National Science Foundation Career grant (CMMI 1454360) and a Graduate Assistance in Areas of National Need (GAANN) fellowship.

Thank you to my fellow group members: Dr. Eduard Caicedo-Casso, Baishakhi Bose, Cole Davis, Ryan Szeto, Caitlin Adams, Dr. Nelyan Lopez-Perez, Hyungyung Jo, Michael Toomey, Dr. Matthew Korey, and Dr. MD Nuruddin. I have thoroughly enjoyed working in such a supportive and collaborative environment in the Purdue MSE department, and you have each offered invaluable support and advice throughout my time here. Additional thanks to Dr. Gamini Mendes, Dr. Logan Kearney, Dr. Anna Walter, and Dr. Travis Thornell, who have all offered their personal time to teach and advise me in different capacities, even when I was not their group-mate and after they had successfully completed their degrees. I have had an excellent experience working with each of you.

Thank you to the wonderful undergraduate researchers I have had the opportunity to mentor: Xunkai Chen, Mitchell Brezina, and Sebastian Aldwin. I hope that I have been able to offer

valuable advice and support, as I have certainly learned from each of you along the way. I look forward to seeing what the future holds for the three of you.

Finally, thank you to my family and friends who have blessed me with their love and support throughout this journey. Thank you to Mom, Dad, Jacob, and Joseph for always being there for me no matter how far apart we might be. You have all been my rocks and have sacrificed so much to support me – especially your sleep, Mom. You all have so often given up your own summers and holiday breaks to make the 10 hour drive to Lafayette any time I moved, faced a new health challenge, or even simply wasn't able to take the time off to travel down to you. Thank you to my loving husband, Kris, who has supported and cared for me through the highs and the lows of the past several years, even when you barely knew me. You brought me dinner on the many late nights in the lab where I would not have eaten otherwise, you've been immensely patient and supportive through trying to balance graduate school and a new marriage, and you've looked after me with the utmost care through some unexpected and lengthy medical challenges along the way. Thank you to caring friends Kate and Eric Wright, Peggy and Alan Brubaker, Germaine Woten, and Amanda Barton for your Christ-like love and support over the past three years. To all of these family and friends, thank you for helping me continue to grow in strength and faith, constantly reminding me that God has a plan for each of us and to trust in Him. I would not have made it to this day without you. I love you.

TABLE OF CONTENTS

LIST OF TABLES

LIST OF FIGURES

LIST OF ABBREVIATIONS AND SYMBOLS

AA	acrylic acid
AM	acrylamide
ANa	sodium acrylate
DLS	dynamic light scattering
EC	electrical conductivity
FTIR	Fourier-transform infrared spectroscopy
ITC	isothermal titration calorimetry
MBAM	*N,N'*-methylenebisacrylamide
PANa-PAM	poly(sodium acrylate-*co*-acrylamide)
PANa-PAM-SiO_2	poly(sodium acrylate-*co*-acrylamide) containing silica nanoparticles
SAXS	small-angle x-ray scattering
SANS	small-angle neutron scattering
TEOS	tetraethyl orthosilicate
UV-Vis	ultraviolet-visible light spectrometry
XRD	x-ray diffraction
A	absorbance
C *or* $[C]$	concentration
d	diameter
l	path length
l_p	polymer persistence length
M_c	molecular weight between crosslinks
Q	hydrogel swelling ratio
Q_{equil}	hydrogel equilibrium swelling ratio in DI water
q	scattering vector
ε	molar absorptivity coefficient
λ	wavelength
μ	chemical potential
θ	scattering angle
ξ	polymer network mesh size

ABSTRACT

Despite the abundant current applications for ionic hydrogels, much about the stimuli-responsive behavior of these materials remains poorly understood. Due to the soft nature of these materials, the number of traditional characterization methods which can be applied to these systems is limited. Many studies have been conducted to characterize bulk property responses of these materials, and experimental studies have been produced examining the distribution of free ions around single polyelectrolyte chains. However, little experimental work has been published in which molecular-scale interactions are elucidated in confined polyelectrolyte networks. Furthermore, the way in which responsive properties, other than bulk swelling capacity, scale with ionic fraction in mixed polyelectrolyte-non-polyelectrolyte hydrogel systems has not been thoroughly investigated.

The distribution and strength of polymer-counter-ion bonds has a remarkable effect on hydrogel properties such as absorption capacity, mechanical strength, and size and chemical selectivity. In order to tailor these properties for targeted applications in ionic environments, it is imperative that we thoroughly understand the character of these polymer-ion interactions and their arrangement within the bulk hydrogel. In order to do so, however, non-traditional methods of analysis must be employed.

This dissertation focuses on a model part-ionic hydrogel system, poly(sodium acrylate-*co*-acrylamide), in order to assess not only the polymer-counter-ion interactions but also the impact of gel ionic fraction on these interactions and the responses which they induce in gel performance properties. A model alkali (NaCl), alkaline earth ($CaCl_2$), and transition ($CuSO_4$) metal salt are employed to investigate changes in polymer properties from the macroscale to the nanoscale. The aim of this dissertation is to lay the foundation for the development of fundamental structure-

property relationships by which we may fully understand the ionically-induced performance properties of polyelectrolyte networks.

1. INTRODUCTION

This dissertation presents a series of investigations regarding superabsorbent polymer gels known as hydrogels. Polymeric hydrogels are lightly-crosslinked polymer networks containing hydrophilic pendant groups that interact favorably with water molecules in order to absorb many times their weight in aqueous solutions. The broad range of chemistries that can be incorporated into such polymer networks has led to the application of hydrogels in many fields, including highly specialized materials that require on-demand changes in polymer properties in response to external stimuli. The ability to tailor such hydrogel materials for a specific application is currently restricted by the limited understanding of molecular-scale interactions between the polymer and its environment. In particular, specific noncovalent chemical interactions between solute molecules and polymer functional groups have yet to be fully elucidated. Without a thorough understanding of the structure-property relationships defined by these interactions, much of our development of superabsorbent polymers and polymeric composites may never reach optimal performance.

1.1 Stimuli-responsive Hydrogels and Their Applications

Stimuli-responsive hydrogels are a specialized group of superabsorbent polymers that contain chemically or thermally-reactive functional groups. Such materials have found application in fields ranging from medicine[1-6] to infrastructure,[7-12] where controlling changes in hydrogel properties *in situ* is of particular interest. Many of the tunable properties of these gels are dependent upon multiple aspects of the character of the environment in which the hydrogel is functioning,[4,6,10] further complicating the development of materials for changing environments. As an example of a stimuli-responsive hydrogel, polymer carriers designed for drug-delivery must behave in a way under pre-treatment conditions such that all of the drug molecules are confined within the polymer

network, then, upon encountering a change in pH, temperature, or other stimulus at the diseased site, the hydrogel character must change in order to release its payload to the targeted area.[4]

1.1.1 pH-responsive hydrogels

Many recent advances in stimuli-responsive hydrogels have focused on polyelectrolyte gels that exhibit pH- and ion-responsive behavior in order to control the diffusional, mechanical, colorimetric, thermal, and chemical reactivity properties of the materials in a wide range of environments. The inclusion of functional groups capable of undergoing ionization has led to a class of materials for which their swelling, binding, and transport properties can be tightly controlled.[4] As with ionic small molecules, the functional groups of pH-sensitive hydrogels undergo deprotonation at pH > pK_a, producing charged functional groups that are constrained by the connectivity of the polymer backbone. Coulombic repulsion between these groups favors solvation of the groups by water[4] and causes the polymer chains to stretch, resulting in pH-dependent swelling of the hydrogel. When ionic species are present in the aqueous medium, oppositely-charged counter-ions are driven into the polymer matrix by osmotic pressure[13] and cause collapse of the polymer chains. In the case of monovalent ions, this collapse is primarily attributed to electrostatic screening, wherein counter-ions condense onto the polymer chain and form a double-screening layer that shields electrostatic effects between the like-charged moieties on the chain.[14-17] However, higher valency ions have the capacity to interact with multiple functional groups in the polymer and produce an additional bridging effect.[4,6,18] The effects of multivalent counter-ions on the equilibrium swelling of pH-sensitive hydrogels have been documented frequently, yet much about the distribution and binding of multivalent counter-ions within the polymer matrix remains unknown.

Unfortunately, this and other significant gaps remain in our understanding of these properties. In particular, a thorough understanding of the ways in which all of these properties are interrelated remains highly elusive. Experimental characterization of pH-responsive hydrogels has thus far depended heavily on either macroscale characterization (*e.g.*, swelling ratio, compression modulus) or nanoscale characterization that cannot be executed on the material while in its end-use state (*e.g.*, electron microscopy of dried gels). While these methods are informative, they make it challenging to fully develop fundamental structure-property relationships due to their limitations on capturing the molecular and nanoscale interactions occurring in the material while swollen.

1.1.2 Osmotic pressure-driven swelling

A significant factor in these structure-property relationships for pH-responsive gels is osmotic pressure, as described previously. Computational theory has made exceptional strides in modeling osmotic pressure-driven swelling in simple polyelectrolyte systems,[6,19-24] and qualitatively matching experimental data for such systems has been generated.[14,19] However, a majority of the computational models concerned with molecular-level interactions have been applied only to unconfined, linear polyelectrolyte chains.[14,25,26] These models do not necessarily take into account all parameters influencing confined polyelectrolyte systems,[4,15] and the conformational changes observed in linear molecules,[25] particularly as induced by multivalent ions, often do not directly translate to crosslinked networks.

Some computational models have been derived specifically for polyelectrolyte gels, but they have largely focused on the osmotic pressure-driven diffusion of mobile ions into the hydrogel network,[20,22,24] and few[19] provide insight into specific polymer-ion interactions. Furthermore, the limitations of computational modeling mean that such methods cannot yet be applied to several of the more complex mixed-polymer systems used in many applications today. As such, decisions

regarding chemical composition of hydrogel materials are largely made based on the behavior of linear polymers of the same composition or chosen through Edisonian experiments by varying different compositional parameters and observing macroscale property changes.

1.2 Anionic Hydrogels and the Poly(sodium acrylate-*co*-acrylamide) System

1.2.1 Motivation for using PANa-PAM

The work presented here focuses specifically on a mixed-polymer system, poly(sodium acrylate-*co*-acrylamide) (PANa-PAM), which contains anionic functionalities (*i.e.*, sodium acrylate, or neutralized acrylic acid) and neutral hydrophilic functionalities (*i.e.*, acrylamide). Not only is this system of particular interest to recent research efforts in improved internal curing of high-performance concrete,[9-11,16] but this combination is also a model system for more fundamental studies of ionic interaction between a pH-sensitive hydrogel and saline environments.

Anionic hydrogels are commonly employed in systems that involve inorganic salts, such as heavy metal-contaminated waters, as metal cations can be absorbed and confined within the gel by their attraction to anionic polymer groups. Acrylic acid ($pK_a \approx 4.5$) (Figure 1.1a) forms an anionic functionality, COO^-, at $pH > pK_a$,[9] making the hydrogel highly pH-dependent within the pH range encountered in many aqueous systems. Meanwhile, acrylamide (Figure 1.1b), although partially hydrolyzed at pH > 12,[27] offers good swelling properties and structural support while remaining relatively insensitive to pH or ionic strength in the pH range of interest for such investigations.

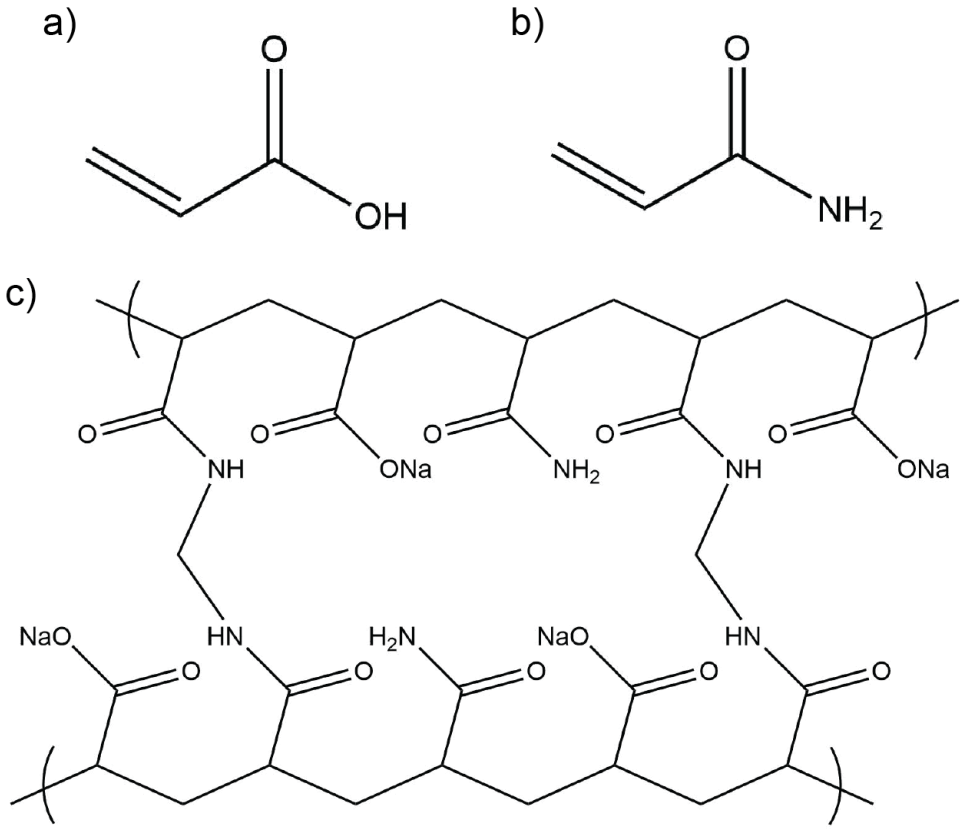

Figure 1.1. Acrylic acid monomer (a), acrylamide monomer (b), and crosslinked PANa-PAM network (c).

Furthermore, pure polyacrylamide gels are widely used in commercial applications, particularly in biochemistry,[28-34] and pure poly(sodium acrylate) gels have been employed in myriad investigations regarding the swelling effects of counter-ions.[6,8,21,35-39] Inspiration throughout this project has been drawn from such studies, particularly by Ferenc Horkay and associates.[6,21,35,36,40] Horkay, *et al.* have produced studies focused on counter-ion competition in poly(sodium acrylate) and investigation of polymer conformation through the use of mechanical analysis and x-ray or neutron scattering. Such studies are highly valuable to expanding our investigation into a mixed PANa-PAM system and advancing the development of structure-property relationships for polyelectrolyte gels in ionic environments.

In order to synthesize a crosslinked network, the two monomers are polymerized via free radical polymerization in the presence of the crosslinking agent *N,N'*-methylenebisacrylamide (MBAM) to produce a structure as illustrated in Figure 1.1c. The resultant crosslinked copolymer offers a hydrogel platform with good swelling, variable crosslink density, and tunable pH-sensitivity, which provides a model platform for systematic investigation of changes in the gel induced by ionic interactions. This copolymer has been proven to have facile, consistent synthesis, allowing for numerous experimental studies without concern for significant variation between reaction batches.

1.2.2 Fundamental background on polyacrylate gels in ionic media

It is well established that the valency of counter-ions in solution impacts the swelling behavior of pH-sensitive hydrogels, and poly(acrylic acid)-based gels offer a simple polymer chemistry for investigating anionic hydrogel performance. To give an example of the valence-sensitivity of poly(sodium acrylate) gels, the swelling ratio (*i.e.*, the mass of water absorbed divided by the mass of the dry polymer), Q, of this gel in a 1 mM salt solution decreases from $Q \approx 400$ in 100% monovalent salt to $Q \approx 4$ in a 1:2 ratio of monovalent to divalent salts.[6]

A follow-up investigation by the same researchers expanded their interrogation on a more fundamental level to develop quantitative relationships between the shear modulus of the same hydrogel system and its equilibrium swelling as a function of concentration of a single monovalent, divalent, or trivalent-cation salt in solution.[21] This and similar studies provided not only foundational insight into polyelectrolyte responses to multivalent counter-ions. It also generated motivation to better understand the importance of counter-ion character beyond its valency. As will be discussed in detail later, metal cations of the same valency but belonging to different groups in the periodic table (*e.g.*, alkaline earth metals versus divalent transition metals) alter multiple

properties of the gel in significantly different ways. In particular, these studies prompted us to probe the idea of counter-ion chelation, or the formation of dative (*i.e.*, strong coordinate-covalent) bonds by certain classes of metal cations.

1.3 Non-destructive Characterization of Polymeric Materials

This dissertation reports investigations into the PANa-PAM system by several characterization techniques that provide information from the macroscale to the atomic scale in order to fully elucidate structure-property relationships across length-scales, as illustrated in Figure 1.2. A commonality between these techniques, however, is that all of the methods employed are nondestructive in nature. Unlike common polymer characterization methods such as thermogravimetric analysis (TGA) or various types of electron microscopy, the nondestructive characterization techniques used here provide valuable tools for understanding material phenomena *in situ* and in a manner by which the material can still function as intended following the analysis.

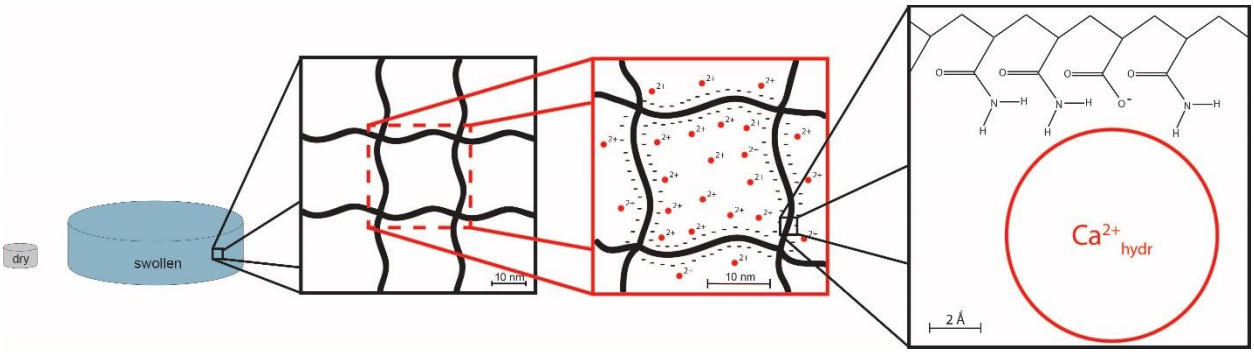

Figure 1.2. Illustration indicating relative dimensions within a PANa-PAM hydrogel from the macroscale to the atomic scale.

1.3.1 Macroscale properties

In all hydrogel experiments, it remains valuable to collect information regarding macroscale changes in polymer properties, especially when attempting to develop structure-

property relationships by which macroscale and molecular-scale interactions can be connected. The primary macroscale characterization methods used in the studies herein are gravimetric swelling measurements and mechanical compression tests.

Gravimetric swelling tests are conducted to provide information on the swelling capacity of a gel in a given environment, as well as to measure the rate at which solution is absorbed or released by the gel. Highly accurate measurements for water and solute diffusion rates can be performed using swell tests, although these require the synthesis of uniform microgel spheres. In the current studies, gravimetric swelling is used primarily to understand the equilibrium properties of hydrogels exposed to different types and concentrations of solutes and how long it takes to reach that equilibrium state. This method will be described in further detail in Chapter 2.

Mechanical compression tests are conducted in Chapter 4 of this work using a Texture Analyzer. This device is essentially a scaled-down version of the Instron-type mechanical testers commonly used on harder materials and larger samples. It is optimized for use in soft materials and adhesives, allowing measurements down to millinewton and micrometer levels of precision. The texture analyzer can be used for tensile, compression, three-point-bending, and shear measurements. While only compression measurements were performed in the studies presented here, three-point-bending or tensile measurements of these gels are proposed in Chapters 5 and 6 as valuable methods for rounding out the investigations described in Chapter 5.

1.3.2 Scattering

X-ray and neutron scattering provide spatially-averaged measurements at the nanoscale in order to understand the distribution of species and conformation of polymer chains within a swollen hydrogel network. Both methods can be optimized to do no damage to samples, although it is possible to “burn” polymeric materials in these methods if exposed to the high-energy beam

for extended lengths of time. Although analysis must be conducted under vacuum, samples can be encapsulated in low-scattering glass capillaries or sandwiched between polyethylene or polyimide films in order to protect them from the vacuum chamber environment. Small-angle x-ray scattering has been particularly valuable to the study described in Chapter 2 and is further elaborated upon there.

1.3.3 Spectroscopy

Multiple types of spectroscopy have been used extensively in the studies presented in this dissertation. UV-Vis spectrometry, Fourier-transform infrared (FTIR) spectroscopy, and Raman spectroscopy can all provide valuable information regarding the contents of a hydrogel in a given environment. UV-Vis spectrometry and FTIR spectroscopy are both absorbance-based, meaning that the absorption of light at a given wavelength can be correlated to the concentration of various species and the character of atomic bonds.

UV-Vis allows for precise measurements of solution concentration of any photochromic material. In this case, it is employed in Chapter 5 to indirectly measure the amount of copper (II) ions absorbed by hydrogel samples. In FTIR, each type of chemical bond absorbs a unique wavelength of infrared light, which makes it useful for characterization of bond arrangements within a polymer. Unfortunately, FTIR often cannot achieve high resolution at the low wavenumbers at which metal-polymer coordination bonds absorb, and the absorption band for O-H bonds in water molecules is significantly stronger than most other bonds that absorb at the same range of wavelengths. FTIR was therefore explored but not heavily utilized in the experiments described in Chapter 5.

Instead, Raman spectroscopy quickly became the preferred method due to its superior resolution at low wavenumbers and the minimal spectral contributions from water bonds. These

differences are attributable to the measurement of Raman scattering instead of light absorption. Raman employs a monochromatic light source (*i.e.*, laser), but instead of measuring absorption of the light at that wavelength, Raman measures scattering off of the various vibration modes present in interatomic bonds. The shift in wavelength of the scattered light wave can be plotted as a Raman shift in which the resulting wavenumbers match those reported by FTIR. In addition to scattering off of the same bond vibrations that absorb infrared light, Raman scattering can occur off of secondary vibration modes, offering additional information about bond strength and symmetry. Raman scattering is described in more detail in Chapter 5.

1.4 Dissertation Outline

This dissertation is broken down into 4 main areas of interest related to connecting molecular-scale interactions with ionically-driven property changes in polyelectrolyte gels. Together, these investigations offer new insight into these relationships in order to assist researchers in making informed decisions on hydrogel composition when designing for targeted ionic environments. Chapter 2 examines PANa-PAM hydrogels and their nanocomposites containing spherical silica particles. Using swelling and scattering experiments to understand the spatial distribution of ionic interactions throughout the gel and alterations to polymer conformation caused by these interactions, we seek to explain the macroscale changes observed with the introduction of monovalent and divalent counter-ions. Chapter 3 explores the crystallization of simple salts in PANa-PAM hydrogels in which we gain a clearer understanding of ionic crosslinks induced by divalent counter-ions, the hysteretic effects of monovalent counter-ions, and the impact of polymer composition on salt crystallization within the hydrogel mesh. Chapter 4 investigates the swelling and mechanical performance of high and low ionic-content PANa-PAM gels in the presence of alkali, alkaline earth, and transition metal counter-ions. Explanations are formulated

regarding the molecular-scale interactions that produce different hydrogel properties depending upon the character of the multivalent counter-ions present in the gel. Chapter 5 presents an in-depth study of copper (II) ion uptake in PANa-PAM hydrogels and the specific changes induced in each interatomic bond present in the polymer network by strong counter-ion chelation. This study also takes these changes in bond vibrations a step further in order to use a transition metal cation as a signaling molecule for determining the content and character of other counter-ions previously present in the network. Chapter 6 summarizes the conclusions and structure-property relationships determined from the research presented in Chapters 2 through 5, the implications of these conclusions for the design of novel superabsorbent materials and the up-cycling of used superabsorbents, and suggestions regarding future studies on these topics.

1.5 References

1. Calo, E.; Khutoryanskiy, V. V., Biomedical applications of hydrogels: A review of patents and commercial products. *Eur. Polym. J.* **2014,** *11*, 24.
2. Garcia-Astrain, C.; Guaresti, O.; Gonzalez, K.; Santamaria-Echart, A.; Eceiza, A.; Corcuera, M. A.; Gabilondo, N., Click gelatin hydrogels: Characterization and drug release behaviour. *Mater. Lett.* **2016,** *182*, 134-137.
3. Karimi, A.; Wan Daud, W. M. A., Harmless hydrogels based on PVA/Na^+-MMT nanocomposites for biomedical applications: Fabrication and characterization. *Polym. Compos.* **2015,** *38* (6).
4. Nayak, S.; Lyan, L. A., Soft Nanotechnology with Soft Nanoparticles. *Angew. Chem. Int. Ed.* **2005,** *44*, 7686-7708.
5. Xu, Y.; Han, J.; Lin, H., Fabrication and characterization of a self-crosslinking chitosan hydrogel under mild conditions without the use of strong bases. *Carbohydr. Polym.* **2017,** *156*, 372-379.
6. Horkay, F.; Tasaki, I.; Basser, P. J., Osmotic Swelling of Polyacrylate Hydrogels in Physiological Salt Solutions. *Biomacromolecules* **2000,** *1*, 84-90.

7. Ozay, H.; Ozay, O., Rhodamine based reusable and colorimetric naked-eye hydrogel sensors and their applications in wastewater treatment. *Chem. Eng. J.* **2013,** *232,* 364-371
8. Pakdel, P. M.; Peighambardoust, S. J., A review on acrylic based hydrogels and their applications in wastewater treatment. *J. Environ. Manage.* **2018,** *217,* 123-143.
9. Krafcik, M. J.; Erk, K. A., Characterization of superabsorbent poly(sodium-acrylate acrylamide) hydrogels and influence of chemical structure on internally cured mortar. *Mater. Struct.* **2016**, *49*, 4765-4778.
10. Krafcik, M. J.; Macke, N. D.; Erk, K. A., Improved Concrete Materials with Hydrogel-Based Internal Curing Agents. *Gels* **2017,** *3* (46).
11. Krafcik, M.; Bose, B.; Erk, K., Synthesis and Characterization of Polymer-Silica Composite Hydrogel Particles and Influence of Hydrogel Composition on Cement Paste Microstructure. *Adv. Civ. Eng. Mater*. **2018,** *7* (4), 590-613.
12. Hu, X.; Zou, C., Pentaerythrityl tetra-B-cyclodextrin: Synthesis, characterization and application in multiple responses hydrogels. *Colloids Surf., A* **2017,** *529,* 571-579.
13. Kiatkamjornwong, S.; Chomsaksakul, W.; Sonsuk, M., Radiation modification of water absorption of cassava starch by acrylic acid/acrylamide. *Radiat. Phys. Chem.* **2000,** *59,* 413-427.
14. Muthukumar, M., 50th Anniversary Perspective: A Perspective on Polyelectrolyte Solutions. *Macromolecules* **2017,** *50* (24), 9528-9560.
15. Flory, P. J.; Rehner, J., John, Statistical Mechanics of Cross-Linked Polymer Networks. *J. Chem. Phys.* **1943,** *11* (11), 521-526.
16. Zhu, Q.; Barney, C. W.; Erk, K. A., Effect of ionic crosslinking on the swelling and mechanical response of model superabsorbent polymer hydrogels for internally cured concrete. *Mater. Struct.* **2015,** *48*, 2261-2276.
17. Muthukumar, M., Double screening in polyelectrolyte solutions: Limiting laws and crossover formulas. *J. Chem. Phys.* **1996,** *105,* 5183-5199.
18. Farina, R.; Laugel, N.; Yu, J.; Tirrell, M., Reversible Adhesion with Polyelectrolyte Brushes Tailored via the Uptake and Release of Trivalent Lanthanum Ions. *J. Phys. Chem. C* **2015,** *119*, 14805-14814.

19. Sing, C. E.; Zwanikken, J. W.; de la Cruz, M. O., Effect of Ion-Ion Correlations on Polyelectrolyte Gel Collapse and Reentrant Swelling. *Macromolecules* **2013,** *46*, 5053-5065.
20. Caykara, T.; Dogmus, M., Swelling-Shrinking Behavior of Poly(Acrylamide-co-Itaconic Acid) Hydrogels in Water and Aqueous NaCl Solutions. *J. Macromol. Sci., Part A: Pure Appl. Chem.* **2005,** *42* (1), 105-111.
21. Horkay, F.; Tasaki, I.; Basser, P. J., Effect of Monovalent-Divalent Cation Exchange on the Swelling of Polyacrylate Hydrogels in Physiological Salt Solutions. *Biomacromolecules* **2001,** *2*, 195-199.
22. Okay, O.; Sariisik, S. B.; Zor, S. D., Swelling Behavior of Anionic Acrylamide-Based Hydrogels in Aqueous Salt Solutions: Comparison of Experiment with Theory. *J. Appl. Polym. Sci.* **1998,** *70*, 567-575.
23. Li, H.; Lai, F., Multiphysics modeling of responsive characteristics of ionic-strength-sensitive hydrogel. *Biomed Microdevices* **2010,** *12*, 419-434.
24. Feng, L.; Jia, Y.; Chen, X.; Li, X.; An, L., A multiphasic model for the volume change of polyelectrolyte hydrogels. *J. Chem. Phys.* **2010,** *133*, 114904.
25. Morfin, I.; Horkay, F.; Basser, P. J.; Bley, F.; Hecht, A.-M.; Rochas, C.; Geissler, E., Adsorption of Divalent Cations on DNA. *Biophys. J.* **2004,** *87*, 2897-2904.
26. Nishida, K.; Kaji, K.; Kanaya, T., High concentration crossovers of polyelectrolyte solutions. *J. Chem. Phys.* **2001,** *114* (19), 8671-8677.
27. Ben Jar, P.-Y.; Wu, Y. S., Effect of counter-ions on swelling and shrinkage of polyacrylamide-based ionic gels. *Polymer* **1997,** *38* (10), 2557-2560.
28. Lee, C.; Levin, A.; Branton, D., Copper Staining: A Five-Minute Protein Stain for Sodium Dodecyl Sulfate-Polyacrylamide Gels. *Anal. Biochem.* **1987,** *166*, 308-312.
29. Vanfleteren, J. R.; Peeters, K., Chromatographic recovery of polypeptides from copper-stained sodium dodecyl sulfate polyacrylamide gels. *J. Biochem. Biophys. Methods* **1990,** *20*, 227-235.
30. Jewett, S. L.; Rocklin, A. M., Two Applications UsingN,N*-Diethyldithiocarbamates a Stain for Copper in Native Polyacrylamide Gels of Superoxide Dismutase. *Anal. Biochem.* **1996,** *237*, 65-69.

31. Wang, Z.; Liu, X.; Baeyens, W. R. G.; Delanghe, J. R.; Ouyang, J., Copper(II)-Alizarin Red S Complex as an Efficient Chemiluminescent Probe for the Detection of Human Serum Proteins after Polyacrylamide Gel Electrophoresis. *J. Proteome Res.* **2008,** *7*, 5075-5081.
32. Saito, S.; Kawashima, K.; Ohshima, H.; Enomoto, K.; Sato, M.; Yoshimura, H.; Yoshimoto, K.; Maeda, M.; Shibukawa, M., Separation of metalloproteins using a novel metal ion contaminant sweeping technique and detection of protein-bound copper by a metal ion probe in polyacrylamide gel electrophoresis: distribution of copper in human serum. *Analyst* **2013,** *138*, 6097-6105.
33. Zhu, X.; Shi, H.; Shen, Y.; Zhang, B.; Zhao, J.; Li, G., A green method of staining DNA in polyacrylamide gel electrophoresis based on fluorescent copper nanoclusters synthesized *in situ*. *Nano Res.* **2015,** *8* (8), 2714-2720.
34. Ozcesmec, M.; Bas, S. S.; Akkurt, B.; Bolkent, S.; Hamuryudan, E., Synthesis, characterization and staining performance of peripherally and non-peripherally substituted metallo-phthalocyanines bearing 1,3-bis-(trimethylamino)-2-propoxy groups. *New. J. Chem.* **2020,** *44*, 7786-7794.
35. Horkay, F.; Hecht, A. M.; Rochas, C.; Basser, P. J.; Geissler, E., Anomalous small angle x-ray scattering determination of ion distribution around a polyelectrolyte biopolymer in salt solution. *J. Chem. Phys.* **2006,** *125* (23).
36. Horkay, F.; Basser, P. J.; Hecht, A.-M.; Geissler, E., Calcium Induced Volume Transition in Polyelectrolyte Gels. *Macromol. Symp.* **2003,** *200* (1), 21-30.
37. Tomida, T.; Hamaguchi, K.; Tunashima, S.; Katoh, M.; Masuda, S., Binding Properties of a Water-Soluble Chelating Polymer with Divalent Metal Ions Measured by Ultrafiltration. Poly(acrylic acid). *Ind. Eng. Chem. Res.* **2001,** *40*, 3557-3562.
38. Roma-Luciow, R.; Sarraf, L.; Morcellet, M., Complexes of poly(acrylic acid) with some divalent, trivalent and tetravalent metal ions. *Euro. Polym. J.* **2001,** *37*, 1741-1745.
39. Thornell, T. L. Synthesis and Characterization of Model Acrylic-based Polymer Gels. Purdue University, West Lafayette, IN, 2018.
40. Horkay, F.; Douglas, J. F., Polymer Gels: Basics, Challenges, and Perspectives. In *Gels and Other Soft Amorphous Solids*, Horkay, F.; Douglas, J. F.; Del Gado, E., Eds. American Chemical Society: 2018; Vol. 1296, pp 1-13.

2. INVESTIGATION OF NANO-SCALE BEHAVIOR OF HYDROGEL NANOCOMPOSITES IN IONIC MEDIA

2.1 Introduction to Hydrogel Nanocomposites

In the interest of improving hydrogel performance, many researchers have turned to nanocomposite hydrogel systems.[1-5] The incorporation of a particulate system may offer improvements to a wide range of performance properties,[2,3] but doing so may also induce secondary reactions within the gel, particularly with environmental changes (*e.g.*, changes in pH that alter the ionization of charged functionalities in the gel).[4,5] This can offer beneficial handles for tuning properties and chemical reactions, but in doing so, it further complicates the phenomena that must be understood for efficient application of these materials.

The incorporation of any additional species into a polymer network introduces changes to the arrangement of polymer chains within the gel and alters overall interactions between the network and its environment. A significant knowledge gap in the current literature regarding hydrogels and hydrogel nanocomposites is an understanding of the distribution of various species and weaker, noncovalent bonds within these systems. This study therefore seeks to push beyond conventional characterization methods (*i.e.*, gravimetric swelling, electron microscopy of dry materials) to elucidate interactions within hydrogels and hydrogel nanocomposites across multiple length-scales and connect newly determined nanoscale interactions to the more widely-investigated macroscale performance of such materials.

In this study, a hydrogel composed of a poly(sodium acrylate-*co*-acrylamide) (PANa-PAM) network, with and without spherical silica (SiO_2) nanoparticles incorporated into the network, is investigated at various degrees of swelling in deionized water, monovalent salt solutions, and divalent salt solutions.

2.2 Background and Previous Analysis Approaches

2.2.1 Hydrogel-silica nanocomposites

Nanosilica has recently garnered extensive interest as an inorganic filler for hydrogel composites.[4-10] Silica is appealing to developers in many fields due to its chemical stability,[11] biocompatibility,[7,10] ease of functionalization,[7-9,12] and size-selective synthesis routes.[7,13] Silica has been broadly recognized to produce additional crosslink-like effects within the polymer network, which improves mechanical[9] and thermal stability[8,9] but decreases overall hydrogel swelling capacity.[5-7] Authors attribute these effects to physical crosslinks,[7,8] but little work has been performed to investigate the molecular-scale interactions that produce these crosslinks.

The incorporation of silica nanoparticles in an ionic hydrogel matrix contributes an additional layer of complexity to our understanding of hydrogel behavior in ionic media due to the surface charge of bare silica. Although the magnitude of charge may vary, the effective charge of silica nanoparticles is generally negative due to hydroxyl groups that appear on the particle surface. This charge is expected to induce electrostatic repulsion between nanoparticles and anionic polymer functionalities such as sodium acrylate. Literature has reported good dispersion of bare nanosilica within such matrices,[5,7] but the causes of this behavior have not been thoroughly established.

PANa-PAM-SiO_2 composites have been heavily investigated as an additive in internally-cured high performance concrete.[4,5,14] Several compositions have been studied in attempts to optimize the controlled release of pore solution during curing and the formation of calcium-silicate-hydrate (CSH) in the voids left behind by gel particles. Krafcik, *et al.* determined that a balance must be struck between the increased swelling capacity provided by the PANa functionalities, the faster de-swelling that occurs in high-PANa hydrogels in cement pore solution,

and the reduction in maximum swelling capacity produced by the addition of nanoparticles. In terms of nanoparticle-hydrogel interactions, the results of this study were taken as support for a proposed preferential association between SiO_2 and PAM and the possibility of rapid complexation of the negatively charged silica particles with cations in the pore solution.[5] This and preceding studies[4,15,16] made significant strides in understanding the macroscale effects of ionic fraction, silica content, and ionic solution and provided an excellent foundation on which to build a better understanding of the nanoscale interactions that remain convoluted.

2.2.2 Conventional hydrogel characterization methods

In order to fully understand these nanoscale interactions, the bonding between each participating component (*i.e.*, nanoparticle, PANa functional group, PAM functional group, water, and free ion in solution) must be differentiated, as well as the spatial arrangement of these components within the larger gel network resolved. Some of the traditional macroscopic, microstructural, chemical, and thermal characterization methods employed in the study of hydrogel nanocomposites are outlined here with an emphasis on the benefits and shortcomings of each technique. Following this outline, we introduce less common analysis techniques that may be employed to advance our understanding of nanoscale phenomena in hydrogel composites.

Swelling ratio

The most straightforward and widely-employed method for characterizing hydrogels is through the swelling ratio (Q) defined by

$$Q = \frac{m_{swollen} - m_{dry}}{m_{dry}} \tag{2.1}$$

where $m_{swollen}$ refers to the mass of the swollen hydrogel and m_{dry} refers to the mass of the dry hydrogel prior to swelling. This is most often obtained by the gravimetric ("tea bag") method.[17]

This method provides a facile means for comparing swelling behavior between hydrogel compositions or environments. However, these measurements are highly susceptible to inaccuracies arising during the measurement procedure (*e.g.*, the amount of excess water removed before weighing the wet bag and sample) and are most likely to overestimate the material's true swelling capacity.[17] This method is efficient for evaluation of bulk swelling and relative changes in swelling performance, but it does not clarify any specific interactions within the material. For example, the amount of bound versus unbound water within the hydrogel provides significantly more insight into interactions between water molecules and polymer chains, but these values can only be determined accurately through more complex nanoscale probing such as positron annihilation lifetime spectroscopy (PALS).[18,19]

Electron microscopy

Electron microscopy provides valuable tools for investigating the microstructure and phase distribution within hydrogels.[7] While these imaging techniques are useful in visualizing hydrogel structure, none of these techniques can be performed on the hydrogel in its swollen state. The polymer can be freeze-dried in order to preserve the expanded structure of the swollen gel, but even rapid removal of water from the hydrogel allows for possible alteration of the network structure and composition from its swollen state. Specifically, both freeze-drying and imaging under vacuum pose the threat of removing or displacing unbound or weakly-bound counter-ions within the hydrogel matrix, thereby undermining any attempt to characterize the interaction of aqueous ionic species with the components of the hydrogel.

Bond characterization

Traditional spectroscopy methods, such as ultraviolet-visible light (UV-Vis) spectrometry and infrared (FTIR) spectroscopy, are often employed to characterize the chemical composition of hydrogel materials. These techniques allow one to confirm the presence of a desired molecular species, determine relative amounts of a species present in different samples, and possibly even gain insight into noncovalent bonds formed between the functionalities within the nanocomposite. Combining such analysis with a thermal characterization technique such as thermogravimetric analysis (TGA) can more completely assess bonds present in the material. In TGA, strong chemical bonds or their absence can be discerned as bonds are broken and organic species are degraded with increasing temperature.[7] Despite the additional valuable insight these analysis techniques offer, these methods are still poorly suited for investigating hydrogels in their swollen state and therefore cannot be used to fully understand the molecular interactions between hydrogel and environment that are of interest to the current investigation.

2.2.3 Specialized characterization techniques

As noted above, this study aims to employ some less common, more specialized characterization techniques to address the challenges encountered with more traditional characterization methods. The experiments described in the Methods section below focus on only a few of the techniques needed in order to fully elucidate the distribution of species and noncovalent bonds within this hydrogel material, but we will introduce additional techniques here that would offer valuable contributions in future studies to complete our understanding of the system.

Small-angle scattering

Small-angle scattering of neutrons and x-rays offers an immense amount of information regarding the arrangement of ions, polymer chains, and particles within the hydrogel network. All information gathered through these experiments is spatially averaged across a sample, and thus these techniques alone are not enough to fully describe the system. Nonetheless, the combination of neutron and x-ray scattering has been successfully applied to hydrogel systems[20-23] and may offer significant insight into the distribution of species.

The two energetic particle sources provide different but complimentary information due to their scattering mechanisms. Small-angle neutron scattering (SANS) measures the scattering of accelerated neutrons from collisions with atomic nuclei and magnetic dipole interactions with unpaired electrons. As such, this technique exhibits higher sensitivity to lighter elements when compared to small-angle x-ray scattering (SAXS), which measures the scattering of an x-ray beam off of electron clouds.

SANS is particularly valuable for probing organic materials in solution, since the signal interference by solvent molecules, which is significant in SAXS, can be mitigated through the use of deuterated solvents. Because of the different interaction mechanism (*i.e.*, scattering off of nuclei versus electron clouds), a deuterium atom is "seen" as identical to a hydrogen atom in SAXS but as twice the size of a hydrogen atom in SANS. As previously mentioned, neutrons are most sensitive to light atoms, and so without delving into the physics of neutron scattering, it can be understood that neutron scattering off of a deuterium atom will be significantly less than off of a hydrogen atom.[24] Therefore, using a deuterated solvent allows one to achieve high contrast between organic materials possessing many hydrogens (*e.g.*, the saturated carbon-carbon backbone of many organic polymers) and the solvent (water) molecules with which it is hydrated.

As a complement to SANS, SAXS is incapable of the same resolution at the level of individual atoms but provides better resolution of supramolecular assembles.[24] X-ray scattering can probe multiple length scales in a single experiment while allowing for fast data collection using small amounts of sample. SAXS can provide information regarding persistence and correlation lengths, distances between features, dimensions of electron-dense features, and distributions of stronger-scattering molecules such as silica and metal cations within the organic network.

While the combination of SANS and SAXS is ideal for robust characterization of these materials, neutron sources are expensive to maintain and difficult to access, while x-ray scattering can be performed at the benchtop scale. Therefore, only SAXS experiments were achievable in the current study.

Atomic force microscopy

In literature, atomic force microscopy (AFM) has often been employed to study the surface roughness and nanoparticle distribution within hydrogels in the dry state.[3,25,26] This said, AFM itself is not an uncommon characterization technique. However, traditional AFM does not allow for the phase analysis of water-containing hydrogels, due to the strong attractive forces that water's high surface tension exert on the AFM probe tip. Even in thoroughly dried samples, capillary forces from trace amounts of water have been reported to obscure data.[27] Mechanical analysis on swollen gels is achievable[27,28] but is not highly valuable to the current study.

This work therefore proposes the application of AFM within an aqueous environment for the investigation of hydrogel nanocomposites. Significant advances have been made in recent years regarding AFM measurements obtained by fully submerging the probe tip in the fluid environment surrounding the sample. Specifically, the Raman group at Purdue University has

published extensively on cutting-edge developments in multiple modes of AFM imaging for probing biological structures under natural aqueous conditions.[29-32] Additionally, other research groups at Purdue University have conducted force measurements in aqueous environments[33,34] and high relative humidity environments.[35]

From this literature, imaging of swollen hydrogels using AFM has been assessed as experimentally feasible and highly valuable for spatially discrete measurements of nanoparticle and noncovalent bond distribution. Unfortunately a collaboration with a research group which specializes in such experiments was not achievable during the available time frame of this study.

Isothermal titration calorimetry

In conjunction with determining the spatial arrangement of counter-ions and nanoparticles within the PANa-PAM-SiO_2 matrix, it is important to understand the extent of attraction between free ions and various components of the hydrogel nanocomposite. In literature, it has been found that certain multivalent cations form "stronger" but reversible bonds with anionic groups in a hydrogel network,[36] which has raised the question of whether counter-ions form true ionic bonds in the network or simply form a cloud of opposite charge around the fixed charges. The answer to this could be resolved through the use of thermodynamic measurements such as isothermal titration calorimetry (ITC).

In a previous study, Eichenbaum determined that the Gibbs free energy associated with ion binding in the hydrogel system that he was investigating indicated that the counter-ions associated with the hydrogels remained partially hydrated, suggesting what he termed "weak field" binding sites.[37] In the current PANa-PAM-SiO_2 system, ITC could be similarly employed in order to decouple the binding energies of counter-ions to each component of the network. The difference in binding energy for the same counter-ion to acrylate, acrylamide, and silica pendant groups could

provide a quantitative measure of the distribution of counter-ions between the network components, which would provide additional insight into the spatial arrangement of counter-ions and polymer within the PANa-PAM-SiO_2 network. However, in order to perform such measurements, the hydrogel material must be suspended in solution and exhibit rapid transport of water and ions. This is typically achieved through the use of microgels produced through suspension polymerization,[17] and the bulk hydrogels used in the current study could not be ground to a particle size small and uniform enough to be used in ITC experiments.

As mentioned previously, several of the techniques discussed in the section above have been proposed and investigated as potential methods by which to fully characterize the PANa-PAM-SiO_2 hydrogel system, but not all of these techniques were pursued in the final study presented below.

2.3 Experimental Methods

2.3.1 Materials

Ammonia solution, ethanol (anhydrous), tetraethyl orthosilicate (TEOS), *N,N'*-methylenebisacrylamide (MBAM), sodium metabisulfite ($Na_2S_2O_5$), sodium persulfate ($Na_2S_2O_8$), acrylamide (AM), sodium hydroxide (NaOH), sodium chloride (NaCl), and calcium chloride ($CaCl_2$) were all obtained from Sigma-Aldrich (St. Louis, MO) and used as received. Acrylic acid (anhydrous, 200 ppm MEHQ inhibitor) (AA) from Sigma-Aldrich was filtered through a pre-packed column (Sigma-Aldrich) to remove MEHQ inhibitor prior to polymerization. Deionized (DI) water (18.1-18.3 MΩ cm^{-1}) was purified in-house using a Barnstead Nanopure system (Dubuque, IA).

Gravimetric swelling tests were conducted using T-Sac Size 3 tea filter bags. All swelling solutions were prepared using DI water. Dynamic light scattering measurements were obtained using a Malvern Zetasizer Nano ZS (Westborough, MA). Small-angle x-ray scattering measurements were obtained using an Anton Paar SAXSpoint 2.0 (Graz, Austria).

2.3.2 Synthesis

Nanoparticle synthesis

Monodisperse silica nanoparticles were synthesized using the method established by Stöber, *et al.*[13] Ammonia (12.5 mL) and ethanol (250 mL) were combined in a 500 mL roundbottom flask with a stir bar, sealed with a rubber septum, and stirred at room temperature for 10 minutes. TEOS (20 mL) was added to the reaction vessel, and the reaction was allowed to stir at room temperature for 4.5 hours.

After synthesis, the particles were purified by the following method. The solution was divided into 50 mL centrifuge tubes (Fisher Scientific, Waltham, MA) and centrifuged at 6000 rpm for 30 minutes or until the supernatant appeared clear. The supernatant was decanted off into a waste container. Each tube was refilled with ethanol and sonicated to re-disperse nanoparticles. The solutions were then centrifuged again at 6000 rpm to separate the nanoparticles to the bottom of the tubes. This rinsing process was repeated three times. After decanting the supernatant the final time, the particles were collected and transferred to a scintillation vial and dried under vacuum at 60°C overnight. Dried particles were stored in a dessicator.

Hydrogel synthesis

Poly(sodium acrylate-*co*-acrylamide) (PANa-PAM) and poly(sodium acrylate-*co*-acrylamide) with silica nanoparticles (PANa-PAM-SiO_2) hydrogels were synthesized using a modified procedure adapted from Krafcik, *et al.*[5] Sodium hydroxide (NaOH) solution of 9.8 M was prepared ahead of time and stored. Stock solutions were prepared of MBAM (15 mg/mL), $Na_2S_2O_5$ (30 mg/mL), and $Na_2S_2O_8$ (30 mg/mL). The amounts of each reagent used in these syntheses are provided in Table 2.1. Syntheses were carried out in 50 mL centrifuge tubes (Fisher Scientific). After mixing, all samples were placed in an oven at 60 °C overnight to drive reaction to completion. Centrifuge tubes were cut open to remove products. Each product was broken into pieces and rinsed in DI water for 5 days, changing the rinse water daily. Excess water was decanted off of the samples, and the samples were allowed to air-dry in a fume hood for one week. Remaining trace water was then removed by placing samples in a vacuum oven at room temperature overnight.

Hydrogel nanocomposites were synthesized and rinsed in a similar manner. An ultrasonic horn (Sigma-Aldrich) was employed to disperse nanoparticles in the DI water used for the reaction prior to the addition of other reagents. Visible cloudiness of the solution and uniform swelling of the subsequent gel confirms that good distribution of the nanoparticles was maintained throughout the synthesis process.

Table 2.1. Reagent amounts for hydrogel and hydrogel nanocomposite syntheses.

Hydrogel Composition	DI Water (mL)	AA (mL)	AM (g)	9.8 M NaOH (mL)	MBAM solution (mL)	$Na_2S_2O_5$ solution (mL)	$Na_2S_2O_8$ solution (mL)	SiO_2 nanoparticles (g)
17% ANa/83% AM	18.6	1.5	7.5	2.4	12	1.5	1.5	0
17% ANa/83% AM 8.5% SiO_2	18.6	1.5	7.5	2.4	12	1.5	1.5	0.765

2.3.3 Characterization

Nanoparticle size distribution

Dried SiO_2 nanoparticles were dispersed in DI water for size measurements. Concentrations of 1, 2, and 5% SiO_2 by weight were prepared by sonication using an ultrasonic horn and filtered into a 1 cm polystyrene cuvette (Sigma-Aldrich) through a 0.45 μm PTFE syringe filter (Sigma-Aldrich). All light scattering measurements were conducted at 23 °C using an input laser wavelength of λ = 633 nm and non-invasive backscatter (NIBS) collection at a scattering angle of θ = 173°. Data was obtained as an average of 14 collection frames. DLS measurements indicated the nanoparticles were 80.7 ± 9.4 nm in diameter.

Hydrogel swelling capacity

Dry hydrogel pieces were ground to a fine powder as in previous studies,[15] and gravimetric swell tests were conducted using the "tea bag" method.[17] Equilibrium swelling capacities were obtained by allowing hydrogel-filled tea bags to soak in each solution for at least 12 hours. Each experiment was performed in triplicate. Swell tests were conducted in DI water, 0.01-1 M NaCl, and 0.01-1 M $CaCl_2$. The pH of the $CaCl_2$ solutions was adjusted using 0.1 M HCl until a pH of 7 was obtained as determined using pH test strips (Fisher Scientific).

Nanocomposite analysis

Small-angle x-ray scattering measurements

SAXS samples were prepared using a 10 x 10 mm solids sample holder (Anton Paar). One-mil (0.0254 mm) thick polyimide tape (Kapton) was placed on one side of each holder cell, a small amount of swollen polymer was scooped into the cell, and a second layer of polyimide tape was

placed on the opposite side of the cell in order to sandwich the gel and seal the cell against vacuum. It was determined that the Kapton tape seal could only withstand vacuum for 30-60 minutes before samples began losing water, and so experiments were monitored between frame collections using the viewing window on the SAXS chamber. The sample holder was mounted on a VarioStage (Anton Paar) assembly for all scattering experiments. All samples were analyzed under vacuum using a copper Kα (λ = 1.54 Å) x-ray source and hybrid photon-counting (HPC) detector. Scattering measurements were collected at a scattering distance of 576 mm. For each data set, three frames of 600 seconds each were collected and averaged. Scattering data was reduced to 1-D plots using SAXSAnalysis 17.0 (Anton Paar) software. A standard operating procedure for SAXSAnalysis data reduction is provided in Appendix B.

Scattering data model-fitting

Mathematical models were fitted to the 1-D scattering curves in order to deconvolute scattering contributions from different features of the hydrogel network. This model-fitting was performed in the SAS data analysis software Igor Pro using Nika and Irena plug-in packages designed for SAXS data reduction and modeling.[38,39] In order to obtain numerical data, bounds were set for the scattering curve to omit scattering from the beamstop at low q and in the noise region at high q, where q is the scattering vector. Relationships between the scattering vector, scattering angle, and feature size are detailed in Appendix A. The scattering function was fitted to models of spherical particles, and each curve required 3 to 4 populations in order to obtain a good fit. A form factor of "spheroid" and structure factor of "hard spheres" was used for each population. Populations were fit individually before turning on all 3 or 4 models to fit the full curve. Bounds were set manually for each variable based on *a priori* knowledge of the polymer system (*e.g.*, theoretical length-scales based on macroscale experimental observations), and at least one variable

(*i.e.*, scale, minimum size, mean size, or standard deviation) was fixed. The Igor algorithm could then be run until the model converged, and each variable could be adjusted and fixed or released before running the algorithm again in order to optimize the fit.

2.4 Results and Discussion

2.4.1 Effects of silica and counter-ions on swelling capacity

Gravimetric swelling tests remain a valuable part of any hydrogel characterization study. These data offer insight at the macroscale into how the hydrogel network is impacted by the addition of nanoparticles and counter-ions in the absorbed solution, and these insights can be combined with nanoscale characterization experiments such as SAXS to draw conclusions regarding changes in network conformation and noncovalent interactions. Equilibrium swelling ratios (Q_{equil}) for the two compositions investigated in this study are presented in Table 2.2.

Table 2.2. Equilibrium swelling ratio (Q_{equil}) of hydrogels and hydrogel nanocomposites in DI water and saline solutions.

Swelling Solution	DI water	0.01 M NaCl	0.1 M NaCl	1 M NaCl	0.01 M $CaCl_2$	0.1 M $CaCl_2$	1 M $CaCl_2$
Neat Hydrogel, Q_{equil}	73.7	29.2	28.0	21.4	--	14.8	15.1
Reduction from Swelling in DI Water		60.4%	62.0%	71.0%	--	79.9%	79.5%
Nanocomposite, Q_{equil}	63.3	46.7	25.1	18.7	18.7	16.7	19.5
Reduction from Swelling in DI Water		26.2%	60.3%	70.5%	70.5%	73.6%	69.2%

Several conclusions can be drawn from the table above. First, the incorporation of silica restricts the swelling capacity of the PANa-PAM hydrogel network. This is expected, as the incorporation of nanoparticles introduces additional crosslinks to the network.[2,5] More interesting is the reduction in Q_{equil} induced with exposure to saline solutions. In both neat hydrogel and nanocomposite, the reduction caused by divalent salt is comparable at all concentrations,

suggesting that the ionic functionalities within the gel are fully occupied by calcium ions. The theoretical fixed charge concentration of the hydrogel can be calculated using an approach developed by Peppas, *et al.*[40] (see Appendix A) and is determined to be $C = 0.0096$ M. This is less than 50% of the positive charge concentration of the lowest concentration of $CaCl_2$ solution (*i.e.*, $C = 0.02$ M) and supports the theory above. However, the same behavior is not observed in NaCl solutions. A possible explanation of this disparity is given below.

In DI water, hydrogel swelling is limited by the finite extensibility of the polymer chains themselves. In saline solutions, the chemical potential (μ), which is dependent on the distribution of ions, inside and outside the polymer matrix must be equivalent at equilibrium swelling. Therefore at solution concentrations higher than the concentration of fixed charges in the gel, additional ions must be present inside the gel as free ions in order to balance osmotic pressure. It is anticipated that the as-synthesized hydrogel retains Na^+ ions as the counter-ion to each acrylic acid functionality in the polymer network upon drying. In this case, when a Ca^{2+} ion displaces two Na^+ ions, the displaced ions may remain within the free solution contained in the hydrogel in order to maintain the osmotic pressure and chemical potential balance. Meanwhile, the Ca^{2+} ions form new ion-bridge crosslinks in the gel, collapsing the gel to a pseudo-equilibrium collapsed state at the point that all fixed charges are linked by Ca^{2+} ions. In the case of monovalent salt solution, however, no additional crosslinks are formed to establish a collapsed state at lower concentrations. As more Na^+ ions are forced into the gel by the osmotic pressure gradient, these ions successively screen more of the electrostatic repulsion between polymer chains, allowing further decreases in swelling as the concentration continues to increase above the concentration of fixed charges in the network.

At all salt concentrations, the reduction in Q_{equil} in the nanocomposite is less pronounced than in the neat hydrogel. As previously proposed,[5] this behavior suggests that counter-ions complex first with the silica nanoparticles. From the continued decrease in Q_{equil} with increasing NaCl concentration, it is likely that beyond a threshold concentration (*e.g.*, the point at which the silica nanoparticles are saturated by counter-ions), counter-ions do then organize around polymer chains to further reduce electrostatic repulsion.

2.4.2 Size and distribution of network components

SAXS measurements show features of these hydrogels not observable by macroscale characterization methods. Because the hydrogels are amorphous, scattering data does not offer neat crystalline reflection patterns but instead presents a curve, as shown in Figure 2.1, containing overlapping contributions from features of different dimensions. Model-fitting is thus required to obtain all the information these data have to offer. Figure 2.1a presents scattering curves for neat PANa-PAM hydrogel in DI water at different swelling ratios (Q). One would expect that as Q increases, the polymer chains in the network are stretched, decreasing the curvature of the chain and increasing the persistence length (l_p), which can be defined as the distance over which the bond vectors are locally correlated[41] and is often considered a measure of chain stiffness. However, only a minimal change in l_p is observed in the SAXS experiments conducted in this study, regardless of swelling ratio or salt concentration. (Figure 2.1) Upon further investigation, these values agree well with the l_p values reported in literature for similar polymer structures.[42,43] The lack of change in l_p has been attributed to steric hindrance between chain side groups and excluded volume effects which essentially fix the local conformation of the polymer chain when hydrated.[42] It is believed, however, that this only holds for low swelling values at which the chains remain highly coiled and do not approach the finite extensibility limit of the polymer segments. This

phenomenon may also be a product of long and uneven chains in the hydrogel that likely resulted from an erroneously low initiator concentration in the synthesis of the gels used in this study. As such, this trend may be observed to change in correctly-synthesized gels.

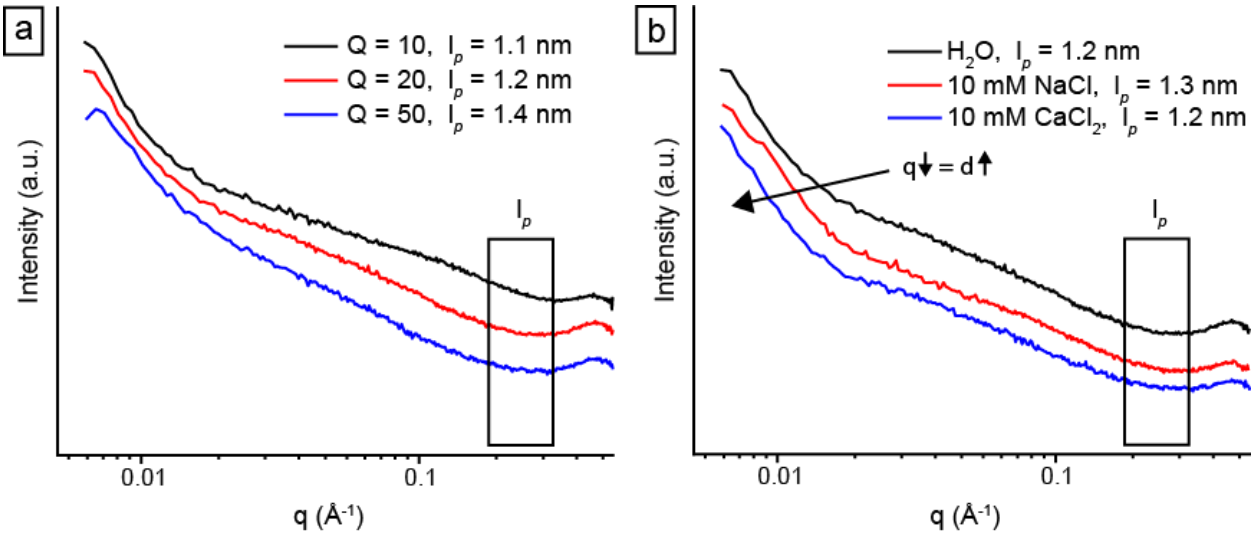

Figure 2.1. Scattering curves of neat PANa-PAM hydrogels in DI water at multiple swelling ratios (a) and compared saline solutions at an intermediate swelling ratio of Q = 20 (b).

In order to gain any more information at the length-scale of the polymer persistence length, additional nanoscale characterization such as PALS is likely necessary. However, further information can be gleaned from the lower q-range in Figure 2.1b. Here, a shift to lower q-values can be observed when moving from DI water to NaCl solution to $CaCl_2$ solution at the same swelling ratio (Q ~ 20). The feature sizes for all three swelling ratios (Q = 10, 20, 50) in DI water and two concentrations of each salt solution are plotted in Figure 2.2. It can be seen that the feature size at this length-scale, from here on referred to as the "aggregate size," remains practically constant for swelling in DI water and both concentrations of NaCl at all values of Q. In $CaCl_2$ solution, a very different trend can be observed. With increasing $CaCl_2$ solution concentration, we see a corresponding increase in aggregate size. This increase becomes even more significant at higher swelling ratios.

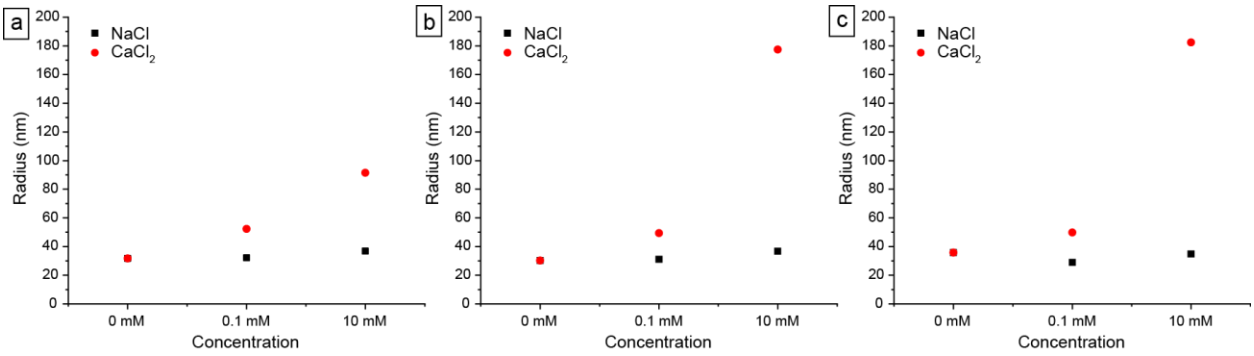

Figure 2.2. Aggregate size, as determined by model-fitting of SAXS curves. Plots indicate feature sizes for NaCl- and $CaCl_2$-swollen hydrogels at Q = 10 (a), Q = 20 (b), and Q = 50 (c).

From these data, we can see that divalent ions are not at all uniformly dispersed throughout the gel like monovalent ions but instead form regions of high electron density within the polymer network. Because of the scattering mechanism of x-rays, we are unable to fully elucidate the composition of these aggregates, which is where the complementary technique of SANS would be extremely valuable. From SAXS alone, we can only theorize as to the true nature of these aggregates. It is our belief to-date that these aggregates are composed of more densely-packed regions of polymer chains forced together by ionic crosslinking. It is feasible that these aggregates also contain salt ions, both positive and negative, due to the collapse of the polymer network by ionic crosslinking, which subsequently forces water out of the hydrogel mesh and entraps ion pairs attracted to both fixed and free charges around the polymer chains. As is evidenced by the lack of crystalline reflection, these ion aggregates are not closely-packed enough to form a crystalline matrix in the current samples. However, the likelihood of ion aggregates raises questions regarding the possibility of gel-driven crystallization that will be discussed further in Chapter 3.

These data have also raised additional questions regarding what information could be gleaned from SAXS experiments. It has been determined in many previous investigations that the reactivity rates of acrylamide and sodium acrylate monomers depend strongly upon the solution conditions under which they are polymerized.[44-48] Specifically relevant to this investigation is the

effect of pH on these reactivity rates.[47] In the currently-employed synthetic procedure, acrylic acid monomer is neutralized to form sodium acrylate by the addition of sodium hydroxide at a stoichiometric ratio of around 1.8 NaOH:AA. As such, the pH of the reaction solution is estimated to be in the range of pH = 8-11, depending upon the ionic fraction of the targeted polymer product. At basic pH, the polymerization rate of acrylamide monomer is significantly higher than that of sodium acrylate, meaning that acrylamide monomers will preferentially be added to polymer chains first. The result of this disparity in reaction rates is that random radically-polymerized copolymers likely possess acrylamide-rich regions and sodium acrylate-rich regions. Researchers have thus far struggled to characterize the distribution of these regions, but the current results suggest SAXS of these copolymers under ionic conditions may offer a path forward. It is hypothesized that the calcium-induced clusters observed in the current experiments represent ionic crosslinks within sodium acrylate-rich regions, which, upon further investigation, could provide information regarding the distribution of sodium acrylate functionalities within this polymer system.

Finally, we briefly discuss the scattering results of hydrogel nanocomposites. As seen in Figure 2.3, these scattering curves exhibited multiple reflections, which indicates the distribution of a highly uniformly-sized component. When the SiO_2 particle size (d = 80.7 nm), as determined by DLS, is considered, the primary reflection of the nanoparticles is expected to appear around q = 0.008 $Å^{-1}$. As such, the peaks observed in Figure 2.3 are expected to be secondary reflections of the scattering off of these nanoparticles, with the primary reflection being blocked by the beamstop at the current sample-to-detector distance. Unfortunately, the dominance of these secondary reflections distorts any scattering produced by the polymer network or ion aggregates, and no

further information can therefore be extracted regarding changes to aggregate sizes on the order of 10s of nanometers.

Model-fitting can still be used to determine the l_p of these systems from the curves at high q-values, and the persistence length of the polymer chains remains consistent with values obtained in neat hydrogel samples. This suggests that, during polymerization, the polymer chains are constructed around the particles with no strong particle-polymer interactions. If there were a stronger attraction of the nanoparticles to acrylamide as previously suggested, we could expect to see a change in persistence length, as the attraction between nanoparticles and polymer functionalities would restrict hydration of and electrostatic repulsion between the polymer chains. However, the swelling capacity has been proven to decrease with the addition of nanoparticles through macroscale experiments, which supports some researchers' proposals that the nanoparticles induce only physical restrictions. It may be hypothesized that the overall extension of the polymer chains is limited due to restricted mobility between distant segments of the network imposed by the presence of nanoparticles (*i.e.*, physical crosslinks), but once again a complementary experimental method such as SANS is necessary to support or refute this hypothesis and fully elucidate the effects of nanoparticles on the hydrogel system.

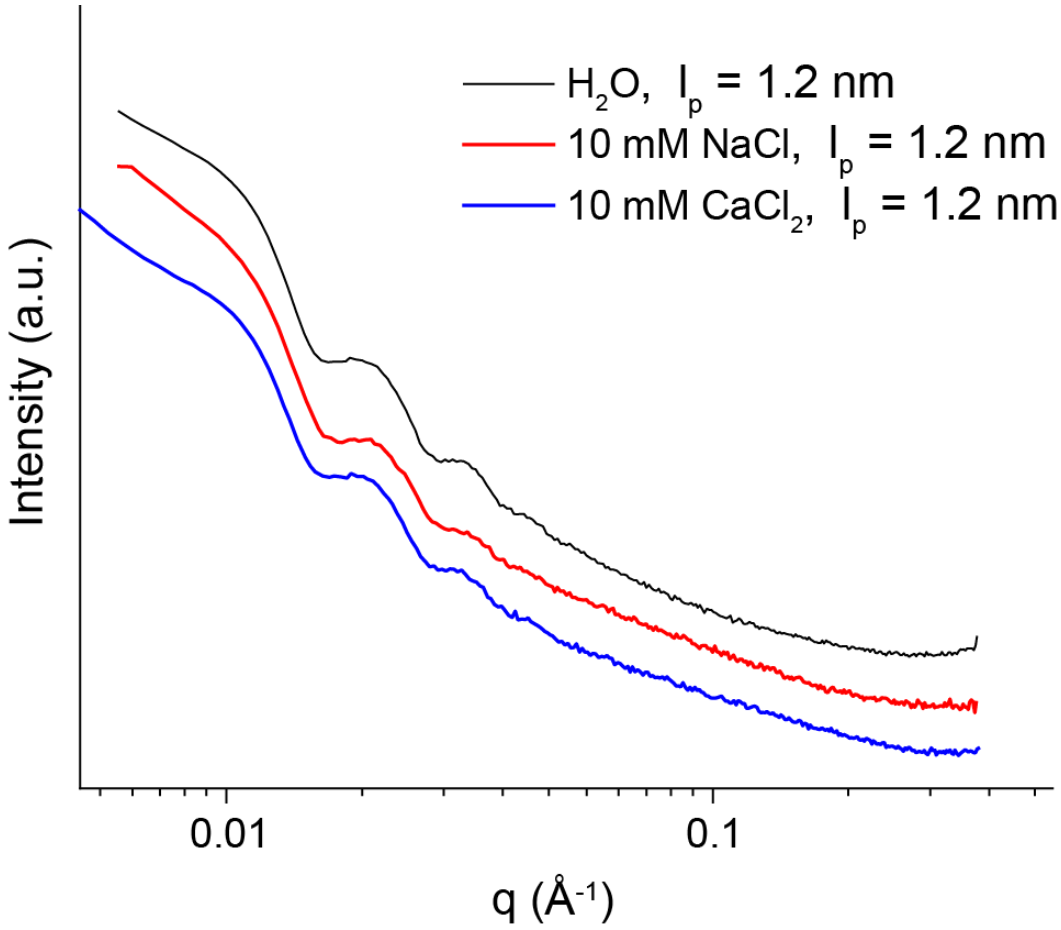

Figure 2.3. Scattering curves of PANa-PAM-SiO_2 nanocomposites in DI water and salt solutions at $Q = 10$.

2.5 Conclusions

This study has striven to lay a thorough groundwork through which researchers will ultimately be able to fully comprehend the nanoscale structural changes in hydrogel nanocomposites and the chemical phenomena that produce such changes. A complete understanding of this system will allow us to tailor hydrogel and composite chemistries to achieve the desired network structures and specific targeted response to a wide range of external stimuli.

This study has determined that ionic crosslinking in PANa-PAM networks by divalent counter-ions disrupts the gradual decrease in swelling ratio observed in monovalent saline solutions. Crosslinks restrict the network at lower solution concentrations and impede additional

swelling decreases induced by electrostatic shielding of fixed charges. We have also discovered that ionic crosslinks do not distribute evenly throughout the hydrogel network but rather aggregate to form highly electron-dense regions within the gel, the dimensions of which increase with increasing divalent salt concentration. This discovery has raised new questions regarding what novel information may be obtained from SAXS experiments on this polymer system. Furthermore, we have determined that, although nanoparticles certainly introduce additional crosslink-like restrictions to the polymer network, these restrictions are unlikely to have a significant chemical component. The consistency of the polymer persistence length across all solute types, solute concentrations, and the presence or absence of nanoparticles, suggests that the polymer chains themselves retain a similar amount of rotational freedom within short chain segments (*i.e.*, 10s of monomer units) regardless of non-aqueous components.

There is still much to be understood about this hydrogel system through further experimentation, but the findings presented here will allow us to take a step toward more facile design of new hydrogel systems and applications and diminish the necessity or scope of trial-and-error experimentation. One disclaimer to the work presented above is as follows: the amount of initiator used in these experiments was later determined to be only half that of the initial syntheses established by Krafcik, *et al.* As such, the hydrogels used in these experiments likely contained a higher dispersity in mesh size and a greater amount of unreacted material than assumed in calculating values such as theoretical mesh size and anticipated chain lengths. In turn, the numerical values given for swelling capacity and feature size will likely differ from experiments conducted using the original synthesis method. However, it is believed that this error does not invalidate the ion-polymer and nanoparticle-polymer interactions elucidated in the report above.

2.6 Acknowledgements

Special thanks to Dr. Gamini Mendes and Dr. Travis Thornell for their initial instruction in material synthesis and Dr. Mendes' continued assistance in troubleshooting synthetic and characterization methodologies through the early stages of this study.

2.7 References

1. Okada, A.; Usuki, A., Twenty Years of Polymer-Clay Nanocomposites. *Macromol. Mater. Eng.* **2006,** *291* (12), 1449-1476.
2. Schexnailder, P.; Schmidt, G., Nanocomposite polymer hydrogels. *Colloid Polym. Sci.* **2009,** *287* (1), 1-11.
3. Karimi, A.; Wan Daud, W. M. A., Harmless hydrogels based on PVA/Na+-MMT nanocomposites for biomedical applications: Fabrication and characterization. *Polym. Compos.* **2015,** *38* (6).
4. Krafcik, M. J.; Macke, N. D.; Erk, K. A., Improved Concrete Materials with Hydrogel-Based Internal Curing Agents. *Gels* **2017,** *3* (46).
5. Krafcik, M.; Bose, B.; Erk, K., Synthesis and Characterization of Polymer-Silica Composite Hydrogel Particles and Influence of Hydrogel Composition on Cement Paste Microstructure. *Adv. Civ. Eng. Mater.* **2018,** *7* (4).
6. Wang, C.; Bai, J.; Gong, Y.; Zhang, F.; Shen, J.; Wang, D.-A., Enhancing Cell Affinity of Nonadhesive Hydrogel Substrate: The Role of Silica Hybridization. *Biotechnol. Prog.* **2008,** *24* (5), 1142-1146.
7. Panic, V. V.; Spasojevic, P. M.; Radoman, T. S.; Dzunuzovic, E. S.; Popovic, I. G.; Velickovic, S. J., Methacrylic Acid Based Polymer Networks with a High Content of Unfunctionalized Nanosilica: Particle Distribution, Swelling, and Rheological Properties. *J. Phys. Chem. C* **2015,** *119*, 610-622.
8. Pourjavadi, A.; Tehrani, Z. M.; Salimi, H.; Banazadeh, A.; Abedini, N., Hydrogel nanocomposite based on chitosan-g-acrylic acid and modified nanosilica with high adsorption capacity for heavy metal ion removal. *Iran. Polym. J.* **2015,** *24* (9), 725-734.

9. Chen, L.; Wang, J.; Yu, L.; Zhang, Q.; Fu, M.; Zhao, Z.; Zuo, J., Experimental Investigation on the Nanosilica-Reinforcing Polyacrylamide/Polyethylenimine Hydrogel for Water Shutoff Treatment. *Energy Fuels* **2018**, 6650-6656.
10. Zhang, C.; Liang, K.; Zhou, D.; Yang, H.; Liu, X.; Yin, X.; Xu, W.; Zhou, Y.; Xiao, P., High-Performance Photopolymerized Poly(vinyl alcohol)/Silica Nanocomposite Hydrogels with Enhanced Cell Adhesion. *ACS Appl. Mater. Interfaces* **2018,** *10* (33), 27692-27700.
11. *Colloidal Silica Fundamentals and Applications*. Taylor & Francis Group: Boca Raton, FL, 2005; p 895.
12. Thornell, T. L. Synthesis and Characterization of Model Acrylic-based Polymer Gels. Purdue University, West Lafayette, IN, 2018.
13. Stober, W.; Fink, A.; Bohn, E., Controlled growth of monodisperse silica spheres in the micron size range. *J. Colloid Interface Sci.* **1968,** *26* (1), 62-69.
14. Afridi, S.; Sikandar, M. A.; Waseem, M.; Nasir, H.; Naseer, A., Chemical durability of superabsorbent polymer (SAP) based geopolymer mortars (GPMs). *Constr. Build. Mater.* **2019,** *217* (30), 530-542.
15. Krafcik, M. J.; Erk, K. A., Characterization of superabsorbent poly(sodium-acrylate acrylamide) hydrogels and influence of chemical structure on internally cured mortar. *Mater. Struct.* **2016**.
16. Erk, K. A.; Bose, B., Using Polymer Science to Improve Concrete: Superabsorbent Polymer Hydrogels in Highly Alkaline Environments. In *Gels and Other Soft Amorphous Solids*, American Chemical Society: 2018; pp 333-356.
17. Davis, C. R.; Kelly, S. L.; Erk, K. A., Comparing laser diffraction and optical microscopy for characterizing superabsorbent polymer particle morphology, size, and swelling capacity. *J. Appl. Polym. Sci.* **2017,** *135* (14).
18. Chamerski, K.; Korzekwa, W.; Filipecki, J.; Shpotyuk, O.; Stopa, M.; Jelen, P.; Sitarz, M., Nanoscale Observation of Dehydration Processin in PHEMA Hydrogel Structure. *Nanoscale Res. Lett.* **2017,** *12*, 303-311.

19. Filipecka, K.; Budaj, M.; Chamerski, K.; Miedzinski, R.; Sitarz, M.; Miskowiak, B.; Makowska-Janusik, M.; Filipecki, J., PALS, MIR and UV-vis-NIR spectroscopy studies of pHEMA hydrogel, silicon- and fluoro-containing contact lens materials. *J. Mol. Struct.* **2017,** *1148*, 521-530.
20. Horkay, F.; Basser, P. J.; Hecht, A.-M.; Geissler, E., Calcium Induced Volume Transition in Polyelectrolyte Gels. *Macromol. Symp.* **2003,** *200* (1), 21-30.
21. Horkay, F.; Hecht, A. M.; Rochas, C.; Basser, P. J.; Geissler, E., Anomalous small angle x-ray scattering determination of ion distribution around a polyelectrolyte biopolymer in salt solution. *J. Chem. Phys.* **2006,** *125* (23).
22. Waters, D. J.; Engberg, K.; Parke-Houben, R.; Hartmann, L.; Ta, C. N.; Toney, M. F.; Frank, C. W., Morphology of Photopolymerized End-Linked Poly(ethylene glycol) Hydrogels by Smal-Angle X-ray Scattering. *Macromolecules* **2010,** *43*, 6861-6870.
23. Whittaker, J. L.; Balu, R.; Knott, R.; de Campo, L.; Mata, J. P.; Rehm, C.; Hill, A. J.; Dutta, N. K.; Choudhury, N. R., Structural evolution of photocrosslinked silk fibroin and silk fibroin-based hybrid hydrogels: A small angle and ultra-small angle scattering investigation. *Int. J. Biol. Macromol.* **2018,** *114*, 998-1007.
24. Clark, N., Small-Angle Neutron and X-ray Scattering and Atomistic Modeling of Intrinsically Flexible Proteins: Reflections of an AMGEN/NIST Post-doc. National Institute of Standards and Technology, 2014.
25. Garcia-Astrain, C.; Guaresti, O.; Gonzalez, K.; Santamaria-Echart, A.; Eceiza, A.; Corcuera, M. A.; Gabilondo, N., Click gelatin hydrogels: Characterization and drug release behaviour. *Mater. Lett.* **2016,** *182*, 134-137.
26. Akalin, G. O.; Pulat, M., Preparation and Characterization of Nanoporous Sodium Carboxylmethyl Cellulose Hydrogel Beads. *J. Nanomater.* **2018,** *2018*.
27. Abuelfilat, A. Y.; Kim, Y.; Miller, P.; Hoo, S. P.; Li, J.; Chan, P.; Fu, J., Bridging structure and mechanics of three-dimensional porous hydrogel with x-ray ulramicroscopy and atomic force microscopy. *RSC Adv.* **2015,** *5*, 63909-63916.
28. Esteki, M. H.; Alemrajabi, A. A.; Hall, C. M.; Sheridan, G. K.; Azadi, M.; Moeendarbary, E., A new framework for characterization of poroelastic materials using indentation. *Acta Biomater.* **2020,** *102*, 138-148.

29. Kiracofe, D.; Kobayashi, K.; Labuda, A.; Raman, A.; Yamada, H., High efficiency laser photothermal excitation of microcantilever vibrations in air and liquids. *Rev. Sci. Instrum.* **2011,** *82* (1).
30. Melcher, J.; Martinez-Martin, D.; Jaafar, M.; Gomez-Herrero, J.; Raman, A., High-resolution dynamic atomic force microscopy in liquids with different feedback architectures. *Beilstein J. Nanotechnol.* **2013,** *4*, 153-163.
31. Cartagena, A.; Hernando-Perez, M.; Carrascosa, J. L.; de Pablo, P. J.; Raman, A., Mapping in vitro local material properties of intact and disrupted virions at high resolution using multi-harmonic atomic force microscopy. *Nanoscale* **2013,** *5*, 4729-4736.
32. Shaik, N. H.; Reifenberger, R. G.; Raman, A., High-resolution dynamic atomic force microscopy in liquids with different feedback architectures. *Appl. Phys. Lett.* **2014,** *104*.
33. Phoon, P. Y.; Narsimhan, G.; San Martin-Gonzalez, M. F., Effect of Thermal Behavior of B-Lactoglobulin on the Oxidative Stability of Menhaden Oil-in-Water Emulsions. *J. Agric. Food Chem.* **2013,** *61*, 1954-1967.
34. Schram, C. J.; Beaudoin, S. P.; Taylor, L. S., Impact of Polymer Conformation on the Crystal Growth Inhibition of a Poorly Water-Soluble Drug in Aqueous Solution. *Langmuir* **2015,** *31*, 171-179.
35. Purohit, H. S.; Taylor, L. S., Phase Behavior of Ritonavir Amorphous Solid Dispersions during Hydration and Dissolution. *Pharm. Res.* **2017,** *34* (12), 2842-2861.
36. Horkay, F.; Tasaki, I.; Basser, P. J., Effect of Monovalent-Divalent Cation Exchange on the Swelling of Polyacrylate Hydrogels in Physiological Salt Solutions. *Biomacromolecules* **2001,** *2*, 195-199.
37. Eichenbaum, G. M.; Kiser, P. F.; Shah, D.; Meuer, W. P.; Needham, D.; Simon, S. A., Alkali Earth Metal Binding Properties of Ionic Microgels. *Macromolecules* **2000,** *33*, 4087-4093.
38. Zhang, F.; Ilavsky, J.; Long, G.; Quintana, J.; Allen, A.; Jemian, P., Glassy Carbon as an Absolute Intensity Calibration Standard for Small-Angle Scattering. *Metall. Mater. Trans. A* **2010,** *41* (5), 1151-1158.
39. Ilavsky, J., Nika: software for two-dimensional data reduction. *J. Appl. Crystallogr.* **2012,** *45* (2), 324-328.

40. Peppas, N. A.; Huange, Y.; Torres-Lugo, M.; Ward, J. H.; Zhang, J., Physicochemical Foundations and Structural Design of Hydrogels in Medicine and Biology. *Annu. Rev. Biomed. Eng.* **2000,** *2*, 9-29.
41. Rubinstein, M.; Colby, R. H., *Polymer physics*. Oxford University Press: Oxford; New York, 2003; p. 440.
42. Muroga, Y.; Noda, I.; Nagasawa, M., Investigation of Local Conformations on Polyelectrolytes in Aqueous Solution by Small-Angle X-ray Scattering. 1. Local Conformations of Poly(sodium acrylates). *Macromolecules* **1985,** *18* (8), 1576-1579.
43. *Characterization and Analysis of Polymers*. John Wiley & Sons, Inc.: Hoboken, NJ, 2008; p 977.
44. Ponratnam, S.; Kapur, S. L. Reactivity ratios of ionizing monomers in aqueous solution. Copolymerizzation of acrylic and methacrylic acids with acrylamide. *Makromol. Chem.* **1977**, *178* (4), 1029-1038.
45. Vinu, R.; Madras, G. Photocatalytic degradation of poly(acrylamide-co-acrylic acid). *J. Phys. Chem. B.* **2008**, *112* (30), 8928-8935.
46. Kurenkov, V.; Gunanova, T.; Kurenkov, A.; Lobanov, F. Copolymerization of acrylamide with sodiuma crylate in aqueous salt solutions. *Russ. J. Appl. Chem.* **2008**, *81* (8), 1414-1418.
47. Riahinezhad, M.; Kazemi, N.; McManus, N.; Penlidis, A. Optimal Estimation of Reactivity Ratios for Acrylamide/Acrylic Acid Copolymerization. *J. Polym. Sci., Part A: Polym. Chem.* **2013**, *51*, 4819-4827.
48. Riahinezhad, M.; Kazemi, N.; McManus, N.; Penlidis, A. Effect of Ionic Strength on the Reactivity Ratios of Acrylamide/Acrylic Acid (sodium acrylate) Copolymerization. *J. Appl. Polym. Sci.* **2014**, *131* (20), 40949.

3. SALT CRYSTALLIZATION AND SWELLING HYSTERESIS IN POLYELECTROLYTE GELS

3.1 Introduction and Motivation

Chapter 2 discussed investigations of polyelectrolyte gels and silica nanoparticle-containing composites at the nanoscale. Here we expand upon a hypothesis formed during one of the experiments in the previous study. Scattering data showed electron-dense aggregates at high salt concentrations and low swelling ratios that were hypothesized to include salt ions trapped in the hydrogel mesh. While the data presented in Chapter 2 indicates that these aggregates remained amorphous, these experiments raised the following questions:

1) Can we induce and control crystallization in neat PANa-PAM hydrogels?
2) How does crystallization in the gel impact subsequent swelling behavior?

Crystallization is an important topic in hydrogel systems, whether it is directed formation of single crystals[1-4] or the hysteretic effects of unintentional crystallization of solutes in the network.[5,6] Many researchers have employed hydrogels and organogels (*i.e.*, superabsorbent networks for organic solvents) for the directed assembly of macromolecular structures.[7-17] Fewer have studied the process of unintended crystallization and how this occurrence affects later hydrogel performance.[5,6,18]

Hydrogels have been employed for the directed assembly of a wide range of constructs, including pure gold nanospheres,[3] metal oxide and tartrate single crystals,[1,2] complex drug particles,[11] polycrystalline salt assemblies for use in synthetic cell scaffolding[7-10,12-17] and as a control handle for gel properties such as porosity.[18] The final item listed here is of most interest to the current study, as controlled salt crystallization could offer an additional handle for tailoring hydrogel properties.

Pre-loading gels could also significantly alter subsequent hydrogel responses in other ionic environments. This possibility makes the effects of unintended crystallization a similar priority. Recent collaborative efforts have begun seeking ways to recycle or "up-cycle" hydrogel-based consumer products, many of which are employed in ionic environments, into secondary applications in fields such as infrastructure. The absorbance performance of such materials is well-known in their initial application. However, little is known about how ions will behave in these gels once the materials are disposed of as waste or recycling, allowed to dry, and washed for use in a secondary application.

In the study described below, we maintain our focus on simple monovalent and multivalent salts sodium chloride (NaCl) and calcium chloride ($CaCl_2$). Unlike the prevalent use of hydrogels for the controlled crystallization of more complex ionic compounds, such simple salts have not been widely investigated in this capacity. Furthermore, these salts are ubiquitous in nature and absorbed in myriad hydrogel applications. This makes a robust understanding of the crystallization behavior of these salts in hydrogels critical for a broad range of primary and recycled applications.

This study can be broken into three sequential investigations through which we proceeded in order to answer the questions outlined above. The first investigation seeks to determine precisely under what conditions crystallization of these salts occurs in the PANa-PAM hydrogel system. The second investigation expands into multiple compositions of PANa-PAM hydrogels to explore whether we can control the size and shape of salt crystals formed in these gels. The third investigation focuses on hydrogel performance following crystallization of these salts inside the network.

3.2 Materials and Methods

3.2.1 Materials

N,N'-methylenebisacrylamide (MBAM), sodium metabisulfite ($Na_2S_2O_5$), sodium persulfate ($Na_2S_2O_8$), acrylamide (AM), sodium hydroxide (NaOH), sodium chloride (NaCl), and calcium chloride ($CaCl_2$) were all obtained from Sigma-Aldrich (St. Louis, MO) and used as received. Acrylic acid (anhydrous, 200 ppm MEHQ inhibitor) (AA) from Sigma-Aldrich was filtered through a pre-packed column (Sigma-Aldrich) to remove MEHQ inhibitor prior to polymerization. Deionized (DI) water (18.1-18.3 MΩ cm^{-1}) was purified in-house using a Barnstead Nanopure system (Dubuque, IA).

Gravimetric swelling tests were conducted using T-Sac Size 3 tea filter bags. All swelling solutions were prepared using DI water. Optical microscopy images were collected using an Olympus BX51 microscope with UIS2 optics, a daylight balancing filter, and a light intensity preset to maintain uniform specimen lighting. X-ray diffraction experiments were conducted using a Bruker D-8 Focus XRD with a Cu-Kα source. Scans were collected across a range of $10° < 2\theta < 90°$.

3.2.2 Synthesis

Hydrogels were synthesized using the same procedure as described in Chapter 2 of this dissertation. Gels of a "low" and "high" ionic fraction and a "low" and "high" crosslinker density were synthesized as outline in Table 3.1. These compositions were chosen as representative materials for deconvoluting the effects of ionic fraction and crosslinking and were based on previous work by Krafcik, *et al.*,[19,20] which established these compositions as highly reproducible

and of interest in concrete applications. As in the previous study, dry hydrogel pieces were ground to a fine powder before being immersed in swelling solutions.

Table 3.1. Hydrogel compositions and reagent amounts used for synthesis of each composition.

Hydrogel Composition	DI Water (mL)	AA (mL)	AM (g)	9.8 M NaOH (mL)	MBAM solution (15 mg/ml)	$Na_2S_2O_5$ solution (30 mg/ml)	$Na_2S_2O_8$ solution (30 mg/mL)
17% ANa/83% AM 2% crosslinker	18.6	1.5	7.5	2.4	12.0	1.5	1.5
17% ANa/83% AM 0.5% crosslinker	9.0	7.5	1.5	12.0	12.0	1.5	1.5
83% ANa/17% AM 2% crosslinker	27.6	1.5	7.5	2.4	3.0	1.5	1.5
83% ANa/17% AM 0.5% crosslinker	18.0	7.5	1.5	12.0	3.0	1.5	1.5

3.2.3 X-ray diffraction

Hydrogel particles were swollen to an equilibrium state in DI water, solutions of 100, 200, and 250 mg/mL NaCl, and solutions of 200, 400, and 600 mg/mL $CaCl_2$. X-ray diffraction (XRD) patterns were collected on at least 3 samples of gels swollen in each solution. Data was also collected for pure NaCl, $CaCl_2$, and dried gels swollen in solutions of no salt, 250 mg/mL NaCl, and 600 mg/mL $CaCl_2$. Samples were prepared by packing gel particles in a flattened layer into a custom acrylic sample tray designed for insertion into the XRD sample holder. XRD patterns were processed and analyzed using Match! powder diffraction software.

3.2.4 Optical microscopy

Optical microscopy images were captured of hydrogels as they were dried at a controlled rate. Drying of the hydrogels at different rates was employed to observe the size and structure of any salt crystals formed as the concentration of salt ions was increased in the gel through water evaporation. Each combination of gel composition, solute, and solution concentration was observed at a variety of temperatures and, in turn, water evaporation rates. Imaging began on gel

particles at equilibrium swelling, and images were collected every 1 to 10 minutes as the sample was heated, dependent upon the rate at which water evaporated from the sample being observed. Hydrogel samples were placed on glass microscope slides and centered on the heating stage of a Linkam TMS 94 programmable temperature controller. Water evaporation and hydrogel drying was observed as samples were heated at temperatures ranging from ambient (~23 °C) to 70 °C in order to monitor the formation of any crystalline structures.

3.2.5 Hysteretic swelling tests

Gravimetric swelling tests were conducted in a manner similar to that described in Chapter 2. However, in the present study swelling was measured at set time points from 0 to 240 minutes as reported in studies by Krafcik, *et al.*[19-21] in order to discern whether the rate of water uptake was affected by salt crystallization in addition to the maximum swelling capacity. Timed swell tests were performed in DI water and 0.1 and 1.0 M NaCl. For samples which are referred to as "fully rinsed" below, hydrogels were swollen in salt solution, air-dried in a fume hood, and rinsed in DI water. After each rinsing cycle, the electrical conductivity (EC) of the rinse water was measured. If the EC was > 5 μS, the polymer was filtered out and placed into fresh rinse water. When the rinse water EC was measured to be ≤ 5 μS, the sample was considered fully rinsed, as this indicates that the ion content in the water, as released by the gel, was below that of traditional RO water. Samples that were fully rinsed were dried completely (*i.e.*, under vacuum) prior to the subsequent swelling test.

3.3 Results and Discussion

3.3.1 Investigation 1: Under what conditions does crystallization occur?

In order to determine under what conditions salt crystallization occurs in the PANa-PAM hydrogels, gels of varied compositions were swollen in DI water and the aforementioned saline solutions and observed, while at equilibrium swelling, using XRD. Initial investigations began with using NaCl solutions at a fraction of the solubility limit of the salt (*i.e.*, 20% or 71.4 mg/mL) to swell gel particles of each composition. Figure 3.1 presents the diffraction patterns from each composition, alongside the diffraction pattern of pure NaCl with Miller indices assigned to the diffraction peaks.

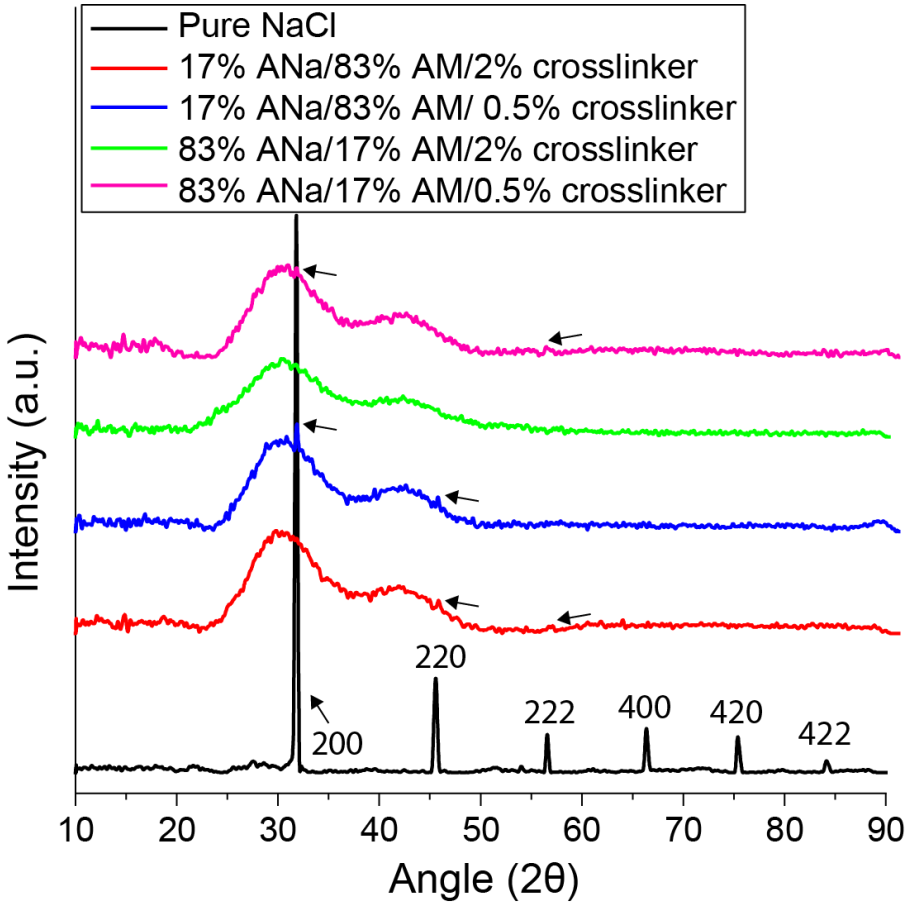

Figure 3.1. XRD patterns for each composition of PANa-PAM hydrogel swollen in 71.4 mg/mL NaCl solution. Pure NaCl diffraction pattern is provided for reference, and visible diffraction peaks are marked with arrows for clarity.

The broad humps produced by the polymer network dominate the diffraction pattern. However, peaks from the [200] plane of the NaCl cubic lattice can be observed in the two samples containing low crosslink density (0.5% crosslinker), peaks from the [220] plane can be seen in the samples containing only 17% ANa, and a slight peak attributable to the [222] plane can be discerned in the low ANa, high crosslinker (17% ANa/83% AM/2% crosslinker) and high ANa, low crosslinker (83% ANa/17% AM/0.5% crosslinker) samples. The location of these peaks and the absence of peak-broadening show that the crystal lattice formed remains unstrained within the polymer network. As these peak signals are weak, however, it was determined that high concentrations of NaCl in the network are necessary to form crystals observable under optical magnification. As the 83% ANa/17% AM/2% crosslinker sample exhibited no crystal diffraction, this sample was omitted from later studies.

The next set of samples investigated contained increasing concentrations of NaCl in a single polymer composition, 17% ANa/83% AM/2% crosslinker, to determine a reasonable salt concentration at which to better evaluate the effects of composition on crystallization. Figure 3.2 presents diffraction patterns for low ANa, high crosslinker hydrogels in DI water, in 100-250 mg/mL NaCl solution and air-dried from the 250 mg/mL NaCl solution. The diffraction pattern for NaCl remains shadowed behind the data for reference.

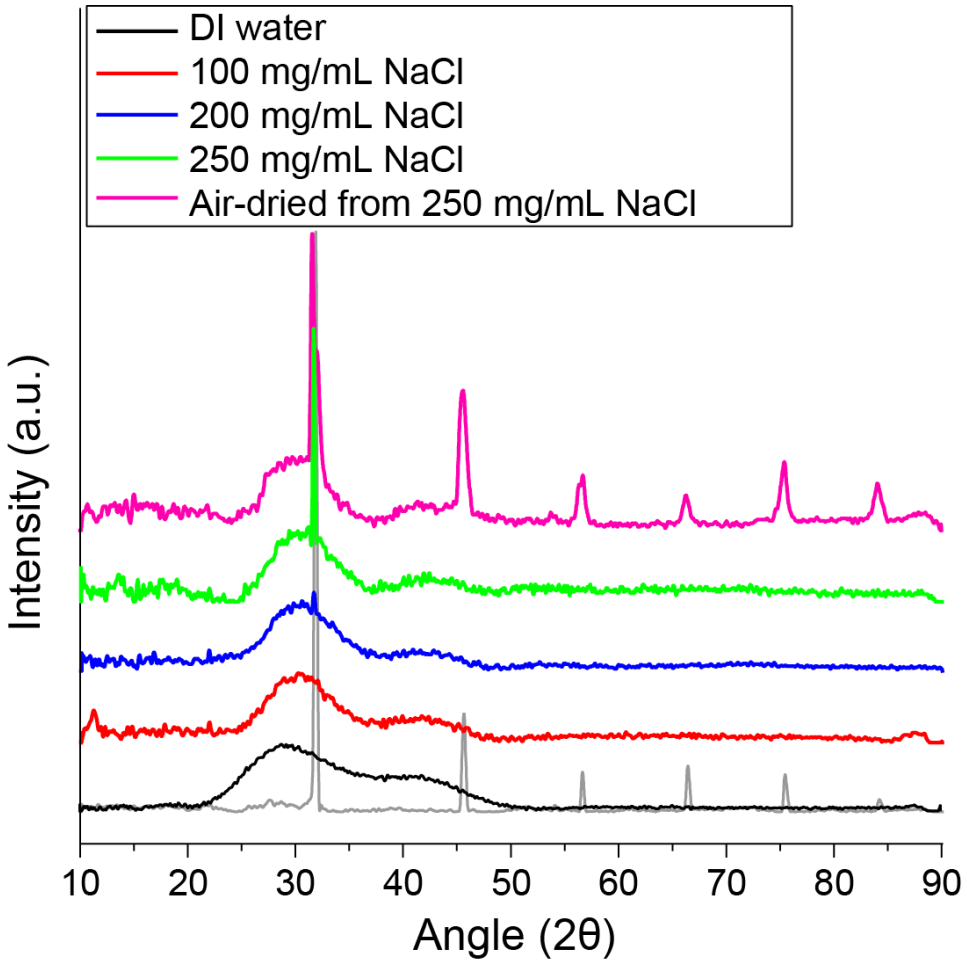

Figure 3.2. XRD patterns for 17% ANa/83% AM/2% crosslinker gels swollen in varying concentrations of NaCl. Pure NaCl diffraction pattern provided in shadow for reference.

The first change to note is that the broad peaks from the polymer network shift to a higher diffraction angle (2θ) with the addition of salt. This is unsurprising, as this diffraction peak is representative of the center-to-center distance of some feature of the network, and a shift to higher 2θ indicates a decrease in that center-to-center distance (*i.e.*, contraction of the network due to electrostatic screening). However, the center-to-center distance observed in these data is on the order of 3 Å, which is only the length of a few atomic bonds. This is a significantly smaller length-scale than that of any ordered structure observed in the polymer network through previous characterization methods. As such, it is unclear at this stage what feature of the network these data

represent. It can also be noted that no further shift in peak value for the polymer occurs with additional increases in salt concentration. This can be understood considering that the lowest concentration used in these studies is above 1 M NaCl, which is drastically greater than the charge concentration within the pure gel when swollen. Therefore, even at the lowest concentration of counter-ions used here, the charges on the polymer chains are screened to the greatest extent achievable.

Regarding salt crystallization, the onset of crystallization was found to be between 100 and 200 mg/mL of NaCl in this system. However, strong diffraction signals were not visible for planes other than the [200] plane until the hydrogel was nearly dried. Initially this was thought to still be a measure of crystallization within the gel. In reality, the strong diffraction peaks representative of all planes in the crystalline unit cell of NaCl is most likely due to the formation of pure NaCl crystals on the surface of the hydrogel, suggesting that even with significant crystallization within the polymer matrix, the only strong signal observable in XRD is the [200] plane. This can be understood in terms of polymer occlusions. The anticipated mesh size of these polymer networks is on the order of 10 nm. As salt crystals grow, they will not typically break polymer chains to do so, but instead will grow around the polymer.[10,14] This occlusion results in defects in the crystal structure in the regions occupied by polymer, causing a significant reduction in the alignment of salt crystals and the subsequent diffraction of x-rays off of those crystalline planes.

In light of this conclusion, XRD studies of salt crystallization in PANa-PAM gels will likely never yield multiple strong diffraction peaks. However, the diffraction of x-rays off of the [200] plane of NaCl crystals is exponentially stronger than the diffraction off of other planes, and the signal from this plane can be used to understand at least a relative relationship between polymer composition and crystallization ability. The next investigation was therefore aimed at comparing

polymer compositions in the same concentration of NaCl. A concentration of 250 mg/mL was chosen in order to increase the likelihood of crystallization without approaching the solubility limit of NaCl and inducing crystallization on the surface of the gel. As mentioned previously, the 83% ANa/17% AM/2% crosslinker hydrogel composition was omitted from later studies.

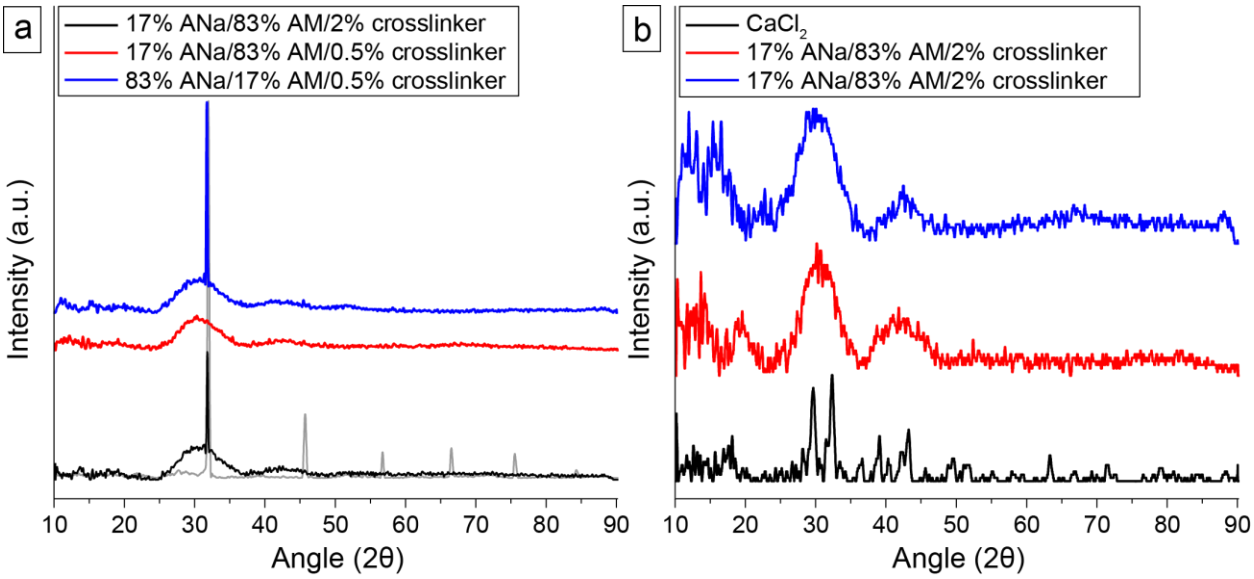

Figure 3.3. XRD patterns for hydrogels in solutions of 250 mg/mL NaCl (a) and 600 mg/mL $CaCl_2$ (b).

Figure 3.3a shows diffraction patterns for the remaining 3 compositions swollen in 250 mg/mL NaCl. These data exhibit minimal crystallization in the 17% ANa/83% AM/0.5% crosslinker gel and much more crystallization in the 17% ANa/83% AM/2% crosslinker and 83% ANa/17% AM/0.5% crosslinker gels. These trends do not directly match observations from Figure 3.1, where more crystallization was seen in the low ANa composition with low crosslink density than high crosslink density at lower salt concentrations. This suggests that the crosslink density affects not only the amount of crystallization achievable but also the concentration threshold above which crystallization occurs. While, in low ionic content gels, low crosslink density produces larger voids for crystal nucleation and allows the onset of crystallization at a lower NaCl concentration than high crosslink density, the achievable amount of crystallization shows the

reverse trend. This may be due to the difference in mesh size and fixed charge density. Table 3.2 presents the molecular weight between crosslinks (M_c), the distance between crosslinks (ξ), and the molecular weight and volume for each given mesh unit cell as calculated based on the method developed by Peppas, *et al*.[22] It can be seen from these values that the decrease in crosslink density resulted in an increase in molecular weight per unit cell of about 500%, while the volume within each unit cell increased by roughly 2000%. The fraction of the M_c that belongs to charged pendant groups remains the same. This means that the density of fixed charges within each mesh unit cell is significantly lower in the 0.5% crosslinker gel. In turn, if the same number of free ions are screening each fixed charge, the Na^+ and Cl^- ions are confined in closer proximity in the gel with the higher crosslink density. As concentration increases, the more densely packed ions in the smaller mesh crystallize more easily, resulting in more overall crystallization in the smaller mesh (*i.e.*, 17% ANa/83% AM/2% crosslinker).

Table 3.2. Theoretical mesh size values for hydrogels in DI water.

Composition	17% ANa/ 83% AM/ 2% crosslinker	17% ANa/ 83% AM/ 0.5% crosslinker	83% ANa/ 17% AM/ 0.5% crosslinker
MW between crosslinks, M_c (g/mol)	1500	8000	10200
MW per mesh unit cell (M_c*12/4) (g/mol)	4400	23900	30600
Charged pendant groups per mesh unit cell	10	60	350
Polymer length between crosslinks, ξ, mesh size (nm)	9	24	45
Mesh volume, ξ^3 (nm^3)	660	13500	93000
Charge density of mesh unit cell (g/mol-nm^3)	.004	.004	.016

Figure 3.3a also shows that more crystallization occurred in the 83% ANa/17% AM/0.5% crosslinker gel than in the 17% ANa/83% AM/2% crosslinker gel. Once again the swelling contributions of crosslink density and ionic fraction do not exhibit a simple scaling relationship. Looking at Table 3.2, the density of polymer pendant groups in the mesh decreases further, which would suggest that crystallization would be even more difficult. However, the values for ξ

calculated in Table 3.2 are for hydrogels swelling in DI water and do not account for the screening of fixed-charges that occurs with the introduction of counter-ions or the subsequent degree of collapse in the network. A much larger portion of the molecular weight between crosslinks is due to ANa monomers for the 83% ANa gel than the 17% ANa gels, which means the density of charged pendant groups in the 83% ANa gel is four times that of the 17% ANa gel. Four times as much of the polymer network will therefore experience polymer chain collapse due to charge-screening. Thus, the true mesh size of the 83% ANa gel in saline solution will be smaller than that of the 17% ANa gel, which results in more densely packed ions at the same solution concentration.

Finally, this investigation sought to determine whether $CaCl_2$ crystals could be formed in these PANa-PAM gels. A concentration of 600 mg/mL $CaCl_2$ was chosen for the swelling solutions via the same reasoning as the chosen NaCl concentration: a highly concentrated solution optimal for crystallization but not nearing the solubility limit of the salt in order to prevent surface crystallization. Diffraction patterns were originally obtained for the 17% ANa containing low and high crosslink densities, as the crosslink density proved to be a significant factor in crystallization of NaCl. Figure 3.3b shows the XRD patterns for these gels in $CaCl_2$. Unfortunately no crystallization could be observed for $CaCl_2$, although it is not clear from these data whether no crystallization occurred. The strongest diffraction peaks of $CaCl_2$ appear at the same ranges of 2θ as the diffraction peaks for the polymer, and, unlike NaCl, there is no peak with significantly stronger diffraction than the polymer. An alternative method is necessary to understand why crystallization peaks are not seen in these cases.

A more thorough quantitative analysis of the XRD presented here may yield the first steps toward a numerical relationship between crosslink density, ionic content, and crystallization, but such work was beyond the scope of the current study. Once it was determined which compositions

yielded significant crystallization and at what salt concentrations, this study moved to investigating the macromolecular structure of the crystals formed in these gels through the use of optical microscopy and controlled evaporation. Furthermore, our understanding of $CaCl_2$ behavior through XRD was limited, leading to the pursuit of alternative methods to visualize $CaCl_2$ crystallization.

3.3.2 Investigation 2: Can we regulate crystal size and shape by hydrogel composition and controlled evaporation?

Hydrogel particles were swollen in solutions of 250 mg/mL NaCl or 600 mg/mL $CaCl_2$ and observed under magnification while heated at different temperatures. Heating causes water from the gel to evaporate at various rates, increasing the concentration of salt in the gel in order to induce crystallization. Particles were also swollen in DI water and heated until dry in order to observe the collapse of gels without salt. Many images were collected in each hydrogel sample, and so only those offering the most valuable information are presented here.

Table 3.3. Drying time of hydrogel composition in 250 mg/mL NaCl or 600 mg/mL $CaCl_2$ solution at elevated temperatures.

Hydrogel Composition	Salt	Q_{equil}	Time to dry, 40 °C (min)	Time to dry, 50 °C (min)	Time to dry, 60 °C (min)	Time to dry, 70 °C (min)
17% ANa/83% AM 2% crosslinker	NaCl	19	76	53	33	--
	$CaCl_2$	16	--	--	--	90
17% ANa/83% AM 0.5% crosslinker	NaCl	35	13	5	4	--
	$CaCl_2$	29	--	30	--	--
83% ANa/17% AM 0.5% crosslinker	NaCl	31	10	9	8	--
	$CaCl_2$	7	--	--	--	--

The heating stage for the optical microscope and glass microscope slide were brought to temperature before placing a swollen hydrogel particle on the slide. Images were taken in set time intervals, the length of which depended on the total time taken for a particle to fully de-swell. It

was quickly discovered that the rate at which de-swelling occurred in saline solution depended strongly on the hydrogel composition. In $CaCl_2$ solution, some hydrogel compositions could not be fully dried even when held at temperatures as high as 70 °C for more than two hours. Table 3.3 presents the time required to fully de-swell each hydrogel composition in a given solution and at a given temperature. Only a few data points of $CaCl_2$ are reported as it was determined that no composition or temperature produced visible crystalline structures. Figure 3.4 presents swollen and dry images of particles swollen in each solution.

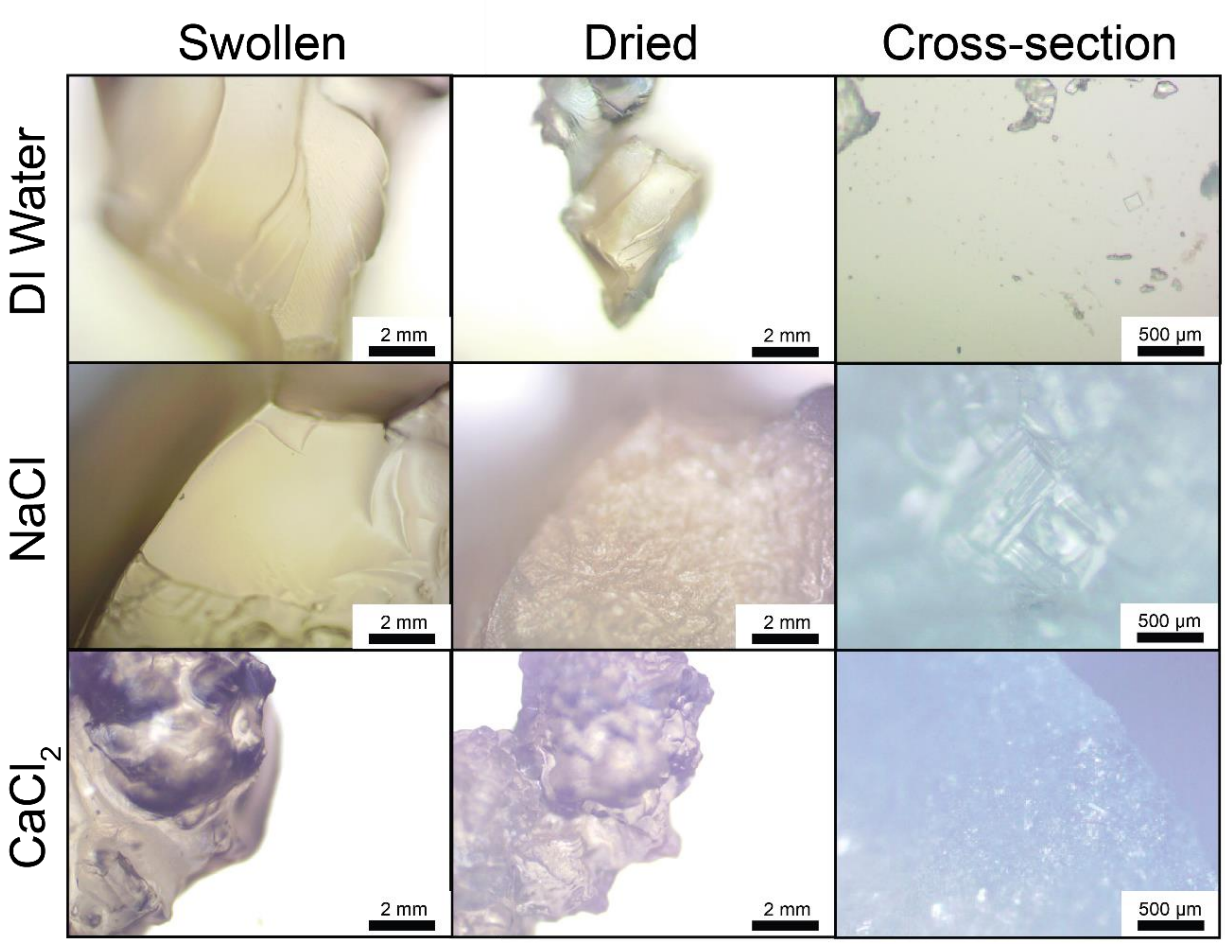

Figure 3.4. Optical microscopy images of hydrogels swollen in DI water, 250 mg/mL NaCl, and 600 mg/mL $CaCl_2$.

One can see from Figure 3.4 that even in the $CaCl_2$-containing samples that could be mostly dried, no defined crystals could be observed. Rather, the images appear to show buckling across the cross-section, while the hydrogel swollen in DI water shrinks uniformly with no buckling on either the surface or interior. This is understandable when ionic crosslinks are considered. The Ca^{2+} ions interact with two different charged polymer functionalities, pulling those segments of polymer closer together and impeding uniform expansion of the hydrated chains.

A sort of surface buckling is observed in the NaCl-containing samples as well. In this case, a dendritic front was observed to move across the hydrogel surface as water evaporated, suggesting that crystallization occurred in stages as each section of the hydrogel reached a threshold salt concentration for which the packing density was great enough to organize into a cubic lattice. However, few clear crystals could be observed at the particle surface, and those observed appeared to be pure salt. The cross-section of NaCl samples, on the other hand, showed discernable crystals throughout. Figure 3.5 shows the cross-sections of two hydrogels containing 17% ANa, one with 2% crosslinker and one with 0.5% crosslinker. These gel particles were dried at the same temperature of 40 °C. It is expected that lower drying temperatures promote larger crystal growth, as the slower evaporation of water allows for more diffusive motion by the salt ions to achieve a crystalline lattice before being locked in place by the absence of water and total collapse of the polymer matrix. Drying at the same temperature allows us to evaluate the effect of polymer composition itself. As can be seen in Figure 3.5, the lower crosslink density, and therefore larger mesh size, gel allows for the growth of somewhat larger crystals. Unfortunately, due likely to the occlusion of polymer in these crystals, a regular crystal shape and size cannot be discerned.

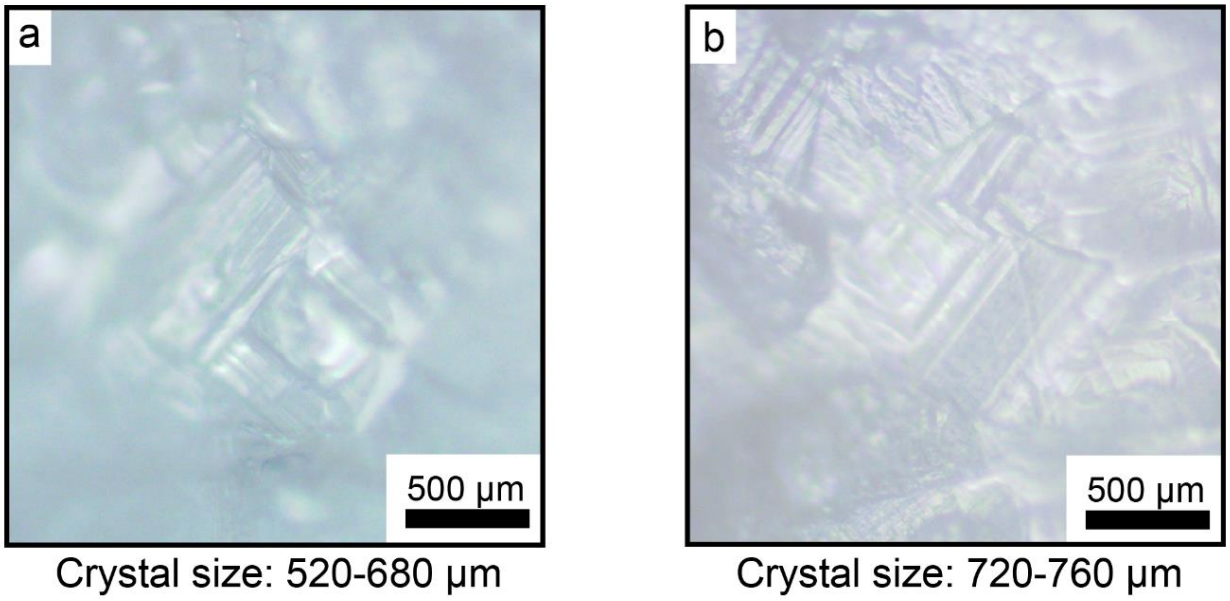

Figure 3.5. Crystal sizes for 17% ANa/83% AM/ 2% crosslinker (a) and 17% ANa/83% AM/0.5% crosslinker (b) dried at 40 °C from equilibrium swelling in 250 mg/mL NaCl solution.

Optical microscopy allowed us to visualize crystallization of NaCl in PANa-PAM hydrogels and confirm that achievable crystal size scales with the mesh size of the polymer. It is possible that we could determine whether crystallization occurs at lower concentrations of salt in the polymer network, but to do so will require a broader combination of characterization techniques to likely include extensive SAXS analysis. Such work was beyond the scope of interest for the present study, and so attention was turned to the effects of crystallization on future hydrogel performance.

3.3.3 Investigation 3: How does crystallization alter subsequent swelling behavior?

As mentioned in our introduction, recent efforts have been undertaken to recycle hydrogels from consumer products and apply them in secondary applications. Therefore, having confirmed that NaCl forms large crystals within the PANa-PAM network upon drying and that said crystals likely confine polymer chains, we chose to investigate the hysteretic effects of crystallization on

hydrogel performance. We evaluated NaCl-swelling under three conditions: dried salt-swollen gels directly into pure water, dried salt-swollen gels into new saline solutions after single swelling in DI water, and dried salt-swollen gels fully rinsed prior to application in new solution.

Figure 3.6 presents gravimetric swelling tests for the first two conditions. The first set of curves, under "Initial Solution," show the swelling performance of pristine 17% ANa/83% AM/2% crosslinker hydrogels in DI water, 0.1 M NaCl solution, and 1 M NaCl solution. After air-drying the same NaCl-exposed gels and placing them in DI water, the curves under "H_2O" are obtained. These swelling tests were performed in a limited volume of DI water, and so it is expected that NaCl migrated out of the gel until the concentration of the external solution matched that of the gel. In light of reaching osmotic equilibrium prior to full removal of salt from the gel, the relative equilibrium swelling ratios are appropriate, with the hydrogel swollen in 1 M NaCl reaching equilibrium swelling near that of the same gel in 0.1 M NaCl and the hydrogel swollen in 0.1 M NaCl reaching equilibrium swelling for a gel swollen in a significantly lower salt concentration.

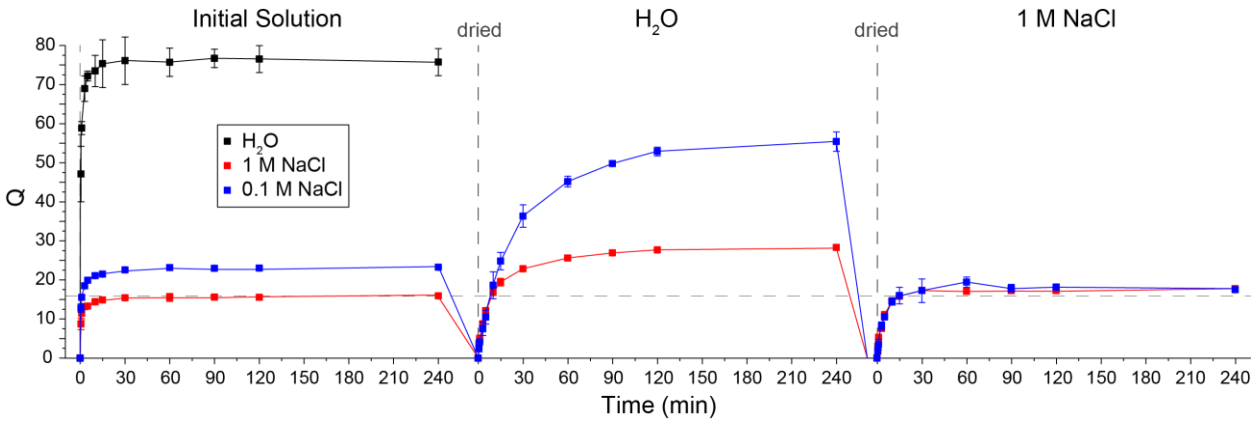

Figure 3.6. Gravimetric swelling ratio as a function of time for 17% ANa/83% AM/2% crosslinker hydrogels in initial solutions (left), in water after drying from salt solutions (center), and in 1 M NaCl after drying from water swelling step (right).

When the gels that received a limited amount of rinsing were placed back in 1 M NaCl solution, both gels approached the equilibrium swelling observed for the pristine gels in the same

concentration solution. A dashed line is provided to mark the level of equilibrium swelling observed for the pristine gel in 1 M NaCl for comparison. Unfortunately this behavior does not give much information on the recyclability of these gels. The volume of DI water in which the salt-exposed gels were swollen was equal for both samples, which means the samples did not reach an equivalent level of salt removal. The next step was therefore to fully rinse the gels prior to re-swelling them in saline solution. These data are reported in Figure 3.7. The curves for H_2O and 0.1 M NaCl initial solutions are provided only for reference.

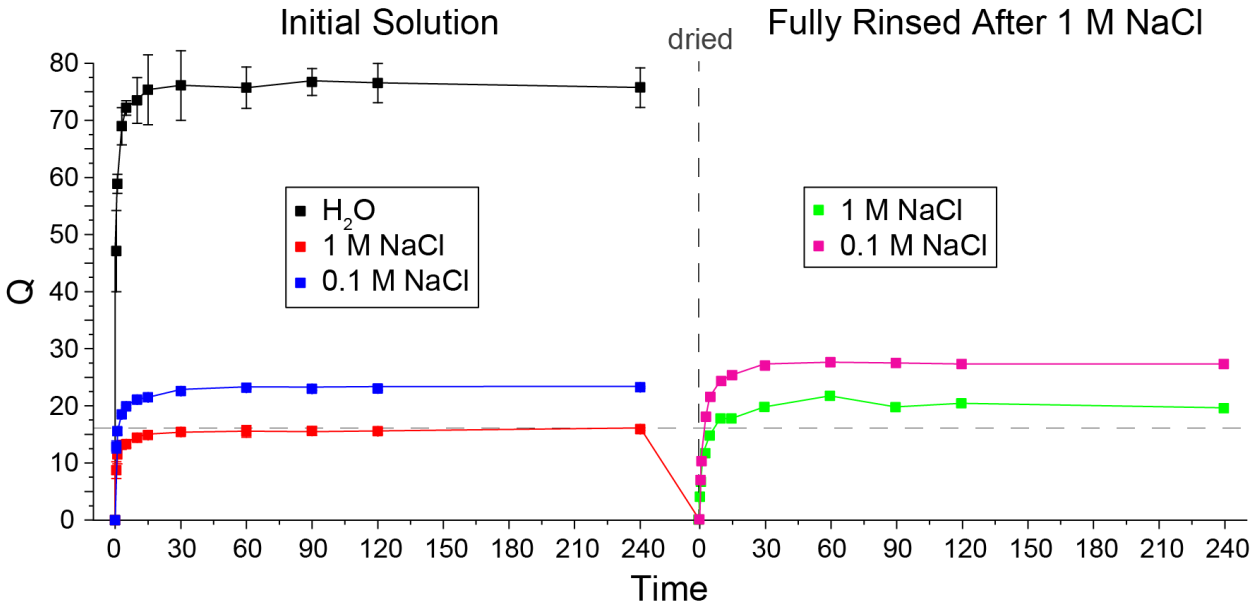

Figure 3.7. Gravimetric swelling ratios of the same initial swelling tests (left) and of the hydrogel in 0.1 and 1 M NaCl after prior exposure to 1 M NaCl and full rinsing (right).

Hydrogels swollen in 1 M NaCl solution were dried, fully rinsed as described in Section 3.2.5, dried once more, and then swollen in either 0.1 M or 1 M NaCl solution. It can be observed in Figure 3.7 that in this case the equillibrium swelling reached in both concentrations of NaCl is higher than the equilibrium swelling reached in the same solutions by gels without previous salt exposure. A guiding line is again provided to delineate equilibrium swelling for pristine hydrogel

in 1 M NaCl solution. This result was unexpected, as it was assumed that further addition of salt would produce equivalent or further reduction in swelling.

After some consideration, we posited a chemical potential-based explanation for this phenomenon as follows. When the hydrogels are fully rinsed, a fraction of free ions remain trapped inside the gel thanks to conformational changes in the polymer mesh produced by crystallization. If free ions remain in the gel upon rinsing and drying, then the charge concentration inside the gel is higher than for the pristine gel. When exposed to the same saline solution, then, the chemical potential gradient between the salt-exposed gel and the exterior solution is smaller than between the pristine gel and the exterior solution. Water molecules and ions are driven into or out of the gel due to this chemical potential gradient in order to balance the concentration of ions in a given unit volume of water. Therefore a lower chemical potential gradient will require more water and fewer ions to enter the gel in order to reach osmotic equilibrium. This idea is illustrated in Figure 3.8.

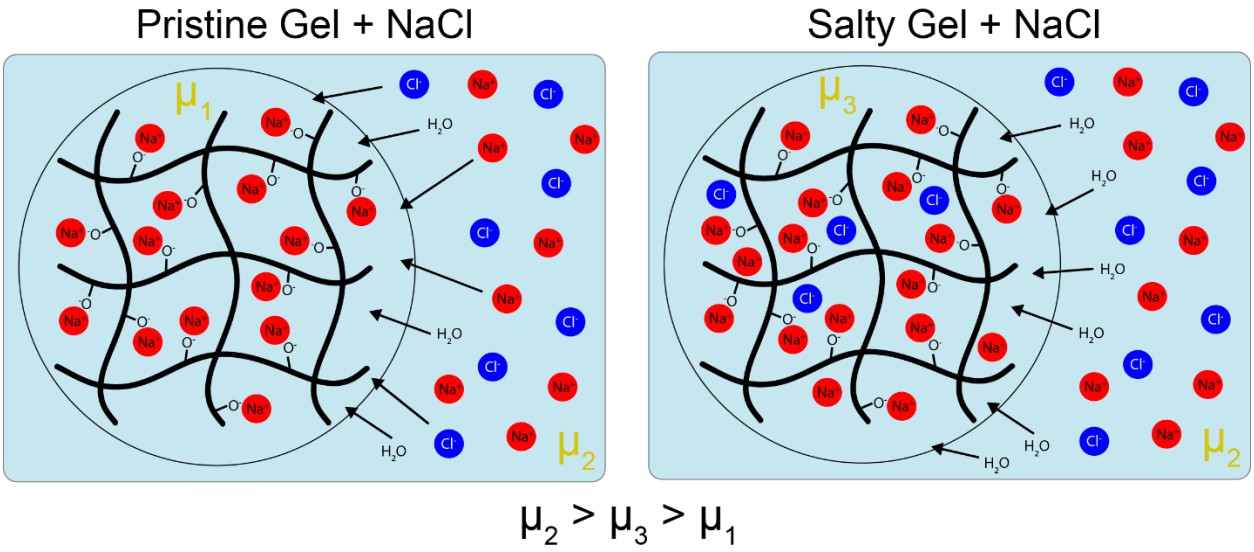

Figure 3.8. Illustration of differences in chemical potential (μ) gradient caused by residual salt ions and its impact on swelling as observed in fully rinsed hydrogels.

However, after a more thorough investigation of the literature, a simpler explanation may also exist. In some hydrogel systems, crystallization is employed to intentionally break covalent bonds in a controlled manner to tailor gel porosity.[25,26] Although this is most often done through the formation of water crystals via freeze-drying, it is possible that the relatively rapid crystallization of NaCl upon drying of a gel may have the same effect. If NaCl crystals indeed break polymer chains as they grow, then after crystallization, the numbers of polymer chains and effective crosslink points are reduced, which allows for increased swelling capacity upon re-swelling.

3.4 Conclusions

The experiments described in this study provided significant insight into the crystallization of simple salts in PANa-PAM hydrogels. We determined that although $CaCl_2$ restricts the polymer network through ionic crosslinks, the salt does not form a crystal lattice at any concentration, even when water is driven out of the gel at elevated temperatures. NaCl, on the other hand, exhibits interesting crystallization behavior and effects in this polymer network. The concentration required for the onset of crystallization, the achievable amount of crystallization, and the size of crystals that can be formed are all dependent upon the composition of the hydrogel. Furthermore, crystals significantly larger than the polymer mesh size were formed, suggesting that the crystals occlude, or incorporate, polymer chains into the crystal structure as they grow.

Previous studies have shown good reproducibility upon swelling and de-swelling PANa and PANa-PAM hydrogels in DI water and NaCl solution, respectively, with no signs of hysteresis.[23,24] However, the final stage of this study suggests that, when crystallized, NaCl exposure can indeed have a hysteretic effect on hydrogel performance. The effect is opposite of what was anticipated in that the hydrogel swells to a greater degree, instead of a lesser degree,

after crystallization of NaCl in the network. We have offered two possible explanations for this phenomenon above, the latter of which (*i.e.*, polymer chain breakage by growing crystal fronts) has proven more likely in subsequent investigations and discussions. Nonetheless, the behavior raises many additional questions, some of which will be addressed in later portions of this dissertation. In particular, after the study described here, we began investigating the hysteretic effects of other salts on the behavior of these hydrogels (Chapter 4) and delving deeper into the binding interactions of these free ions with polymer charge groups (Chapter 5).

3.5 References

1. Arora, S. K.; Patel, V.; Amin, B.; Kothari, A., Dielectric behavior of strontium tartrate single crystals. *Bull. Mater. Sci.* **2004,** *27* (2), 141-147.
2. Arora, S. K.; Kothari, A. J.; Patel, R. G.; Chauhan, K. M.; Chudasama, B. N., Optical absorption in gel grown cadmium tartrate single crystals. *J. Phys.: Conf. Ser*. **2006,** *28*, 48-52.
3. Zhang, J.; Zhao, B.; Meng, L.; Wu, H.; Wang, X.; Li, C., Controlled synthesis of gold nanospheres and single crystals in hydrogel. *J. Nanopart. Res.* **2007,** *9*, 1167-1171.
4. Asenath-Smith, E.; Hovden, R.; Kourkoutis, L. F.; Estroff, L. A., Hierarchically Structured Hematite Architectures Achieved by Growth in a Silica Hydrogel. *J. Am. Chem. Soc.* **2015,** *137*, 5184-5192.
5. Desgrandchamps, F.; Moulinier, F.; Daudon, M.; Teillac, P.; Le Duc, A., An i*n vitro* comparison of urease-induced encrustation of JJ stents in human urine. *Br. J. of Urol.* **1997,** *79*, 24-27.
6. Zhao, X.; Liu, C., Overcoming salt crystallization with ionic hydrogel for accelerating solar evaporation. *Desalination* **2020,** *482*, 114385.
7. Helbig, U., Growth of calcium carbonate in polyacrylamide hydrogel: Investigation of the influence of polymer content. *J. Cryst. Growth* **2008,** *310*, 2863-2870.

8. Yoshida, N.; Higashimura, E.; Saeki, Y., Catalytic Biomineralization of Fluorescent Calcite by the Thermophilic Bacterium G*eobacillus Thermoglucosidasius. Appl. Environ. Microbiol.* **2010,** *76* (21), 7322-7327.
9. Huang, J.; Liu, G.; Song, C.; Saiz, E.; Tomsia, A., Role of Molecular Chemistry of Degradable pHEMA Hydrogels in Three-Dimensional Biomimetic Mineralization. *Chem. Mater.* **2012,** *24*, 1331-1337.
10. Asenath-Smith, E.; Li, H.; Keene, E. C.; Seh, Z. W.; Estroff, L. A., Crystal Growth of Calcium Carbonate in Hydrogels as a Model of Biomineralization. *Adv. Funct. Mater.* **2012,** *22*, 2891-2914.
11. Dawn, A.; Andrew, K. S.; Yufit, D. S.; Hong, Y.; Reddy, J. P.; Jones, C. D.; Aguilar, J. A.; Steed, J. W., Supramolecular Gel Control of Cisplatin Crystallization: Identification of a New Solvate Form Using a Cisplatin-Mimetic Gelator. *Cryst. Growth Des.* **2015,** *15*, 4591-4599.
12. Wang, J.-J.; Zhou, Z.-M.; Zhang, Z.-B.; Du, B.; Zhang, Z.; Wang, Q.; Yuan, P.; Liu, L.-R.; Zhang, Q.-Q., Biomimetic synthesis of platelet-shaped hydroxyapatite mesocrystals in a collagen mimetic peptide-PEG hybrid hydrogel. *Mater. Lett.* **2015,** *159*, 150-153.
13. Gashti, M. P.; Helali, M.; Karimi, S., Biomineralization-Inspired Green Synthesis of Zinc Phosphate-Based Nanosheets in Gelatin Hydrogel. *Int. J. Appl. Ceram. Technol.* **2016**, *13* (6), 1069-1073.
14. Greiner, M.; Yin, X.; Fernandez-Diaz, L.; Griesshaber, E.; Weitzel, F.; Ziegler, A.; Veintemilla-Verdaguer, S.; Schmahl, W. W., Combined Influence of Reagent Concentrations and Agar Hydrogel Strength on the Formation of Biomimetic Hydrogel−Calcite Composites. *Cryst. Growth Des.* **2018,** *18*, 1401-1414.
15. Yin, X.; Griesshaber, E.; Fernandez-Diaz, L.; Ziegler, A.; Garcia-Garcia, F. J.; Schmahl, W. W., Influence of Gelatin-Agarose Composites and Mg on Hydrogel-Carbonate Aggregate Formation and Architecture. *Cryst. Growth Des.* **2019,** *19*, 5696-5715.
16. Yin, X.; Weitzel, F.; Jimenez-Lopez, C.; Griesshaber, E.; Fernandez-Diaz, L.; Rodriguez-Navarro, A.; Ziegler, A.; Schmahl, W. W., Directing Effect of Bacterial Extracellular Polymeric Substances (EPS) on Calcite Organization and EPS-Carbonate Composite Aggregate Formation. *Cryst. Growth Des.* **2020,** *20* (3), 1467-1484

17. Gashti, M. P.; Dehghan, N., Gel diffusion-inspired biomimetic calcium iodate/gelatin composite particles: Structural characterization and antibacterial activity. *J. Solid State Chem.* **2020,** *285*, 121262.
18. Wong, V. W.; Rustad, K. C.; Galvez, M. G.; Neofytou, E.; Glotzbach, J. P.; Januszyk, M.; Major, M. R.; Sorkin, M.; Longaker, M. T.; Rajadas, J.; Gurtner, G. C., Engineered Pullulan–Collagen Composite Dermal Hydrogels Improve Early Cutaneous Wound Healing. *Tissue Eng., Part A* **2011,** *17* (5-6), 631-644.
19. Krafcik, M. J.; Erk, K. A., Characterization of superabsorbent poly(sodium-acrylate acrylamide) hydrogels and influence of chemical structure on internally cured mortar. *Mater. Struct.* **2016**.
20. Krafcik, M. J.; Macke, N. D.; Erk, K. A., Improved Concrete Materials with Hydrogel-Based Internal Curing Agents. *Gels* **2017,** *3* (46).
21. Krafcik, M.; Bose, B.; Erk, K., Synthesis and Characterization of Polymer-Silica Composite Hydrogel Particles and Influence of Hydrogel Composition on Cement Paste Microstructure. *Adv. Civ. Eng. Mater.* **2018,** *7* (4).
22. Peppas, N. A.; Huange, Y.; Torres-Lugo, M.; Ward, J. H.; Zhang, J., Physicochemical Foundations and Structural Design of Hydrogels in Medicine and Biology. *Annu. Rev. Biomed. Eng.* **2000,** *2*, 9-29.
23. Alvarez-Lorenzo, C.; Concheiro, A., Reversible adsorption by a pH- and temperature-sensitiveacrylic hydrogel. *J. Controlled Release* **2002,** *80*, 247-257.
24. Zhang, Y.; Gao, P.; Zhao, L.; Chen, Y., Preparation and swelling properties of a starch-g-poly(acrylic acid)/organo-mordenite hydrogel composite. *Front. Chem. Sci. Eng.* **2016,** *10* (1), 147-161.
25. Annabi, N.; Nichol, J. W.; Zhong, X.; Ji, C.; Koshy, S.; Khademhosseini, A.; Dehghani, F., Controlling the Porosity and Microarchitecture of Hydrogels for Tissue Engineering. *Tissue Eng., Part B.* **2010**, *16* (4), 371-383.
26. Es-haghi, S.S.; Mayfield, M. B.; Weiss, R.A., Effect of Freeze/Thaw Process on Mechanical Behavior of Double-Network Hydrogesl in Finite Tensile Deformation. *Macromolecules* **2018**, *51*, 1052-1057.

4. BEHAVIOR OF POLYELECTROLYTE GELS IN CONCENTRATED SOLUTIONS OF HIGHLY SOLUBLE SALTS

The following was reprinted with permissions from Sargent, J., Chen, X., Brezina, M., Aldwin, S., Howarter, J., & Erk, K. (2020). Behavior of Polyelectrolyte Gels in Concentrated Solutions of Highly Soluble Salts. *MRS Adv.*, *5*(17), 907-915. doi:10.1557/adv.2020.10

4.1 Introduction

Ionic hydrogels are an important class of stimuli-responsive superabsorbent polymers with a rapidly growing breadth of applications.[1-5] These lightly crosslinked networks can contain fractions of or be composed entirely of polyelectrolytes, which imparts the networks with the ability to respond to changes in pH and ionic composition of their environments. These responses include conformational changes in the polymer chains, which leads to changes in permeability, chemical selectivity, and mechanical properties. As such, a thorough understanding of the relationships between hydrogel composition and environmental responses is critical to further advancement of these materials.

The swelling of ionic hydrogels is dominated by osmotic pressure gradients,[6] as illustrated in Figure 4.1. However, there are several complex and interconnected phenomena beyond osmotic pressure that contribute to the performance of these polymer networks, including hydrogen-bonding, electrostatic, and dipole interactions.[7] Several researchers have attempted to decouple and elucidate these interactions, predominately through computational modeling.[8-11] Despite the excellent advances made by such studies, many relationships between hydrogel composition and the physical consequences of these various interactions remain unclear.[12]

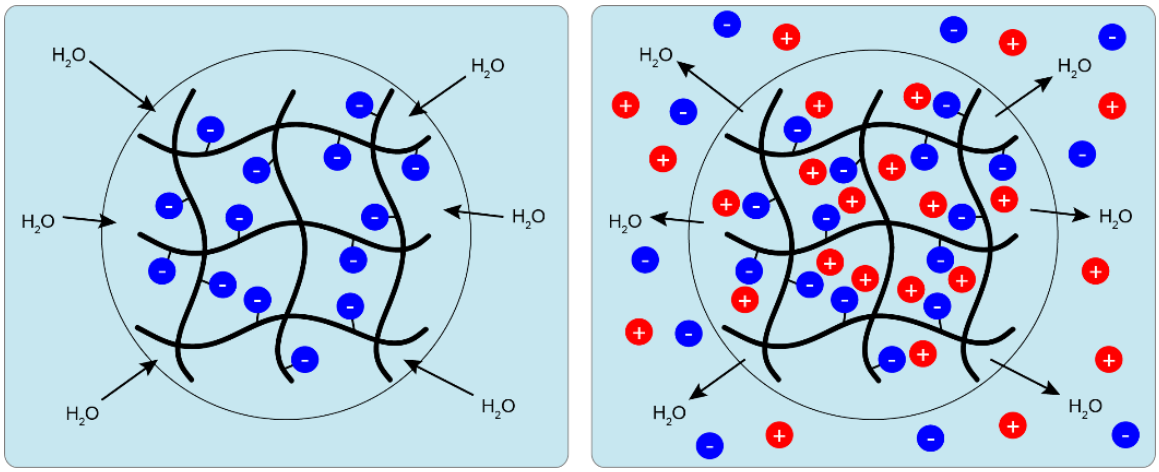

Figure 4.1. Osmotic pressure-driven swelling. In pure water (left), water diffuses into the hydrogel network to balance the chemical potential gradient produced by the polymer's fixed charges. In saline environments (right), counter-ions diffuse into the network to neutralize the polymer's fixed charges, and water diffuses out as necessary to balance chemical potential.

The current study is focused on the response of ionic hydrogels to multivalent ions of different character. In particular, it has been observed that anionic polymer interactions with transition[13] and post-transition[4] metal cations contribute to the mechanical strength of a hydrogel, while interactions with main group metals possessing the same charge valency do not.[13] This difference suggests that transition and post-transition metal ions form "permanent" ionic crosslinks, while main group metal ions form only transient crosslinks.

Herein we report current results of a work in progress. This work investigates the underlying cause for these differing crosslink strengths and seeks to establish quantitative relationships between hydrogel ionic fraction and changes in swelling and mechanical properties induced by these counter-ions. This work employs the copolymer system of poly(sodium acrylate-*co*-acrylamide) (PANa-*co*-PAM), which is a widely utilized hydrogel system[4,14-19] that allows for facile control over the ionic fraction of the gel. By varying the ionic fraction, the underlying cause of these interactions can be better understood and relationships can be elucidated between gel composition and changes in properties induced by multivalent counter-ions.

4.2 Experiment

4.2.1 Materials and methods

All chemicals were used as received from Sigma-Aldrich unless otherwise noted. MEHQ inhibitor was removed from anhydrous acrylic acid prior to polymer synthesis by passage through a prepacked inhibitor remover column. Deionized (DI) water was purified to 18.0-18.2 MΩ resistance using a Barnstead NANOpure Infinity Water Purification System (Thermo Fisher Scientific). Stock solutions of *N,N'*-methylenebisacrylamide (MBAM), sodium persulfate ($Na_2S_2O_8$), and sodium metabisulfite ($Na_2S_2O_5$) were prepared using DI water for hydrogel synthesis. Elastic modulus measurements were performed using a TA-XTplusC Texture Analyser (Stable Micro Systems). Electrical conductivity was measured using a Hanna Combo pH/EC tester.

4.2.2 Hydrogel synthesis

Hydrogel synthesis was adapted from a previous methodology.[4,18] The amounts of reagents used for each hydrogel composition are reported in Table 4.1. Hydrogels were synthesized in 50 mL polypropylene centrifuge tubes (Fisher Scientific) at room temperature and then placed in a 60°C oven overnight. DI water, acrylic acid (AA), and 10 M sodium hydroxide (NaOH) solution were added to the tube first and stirred for 10 minutes to thermally equilibrate. Acrylamide (AM) and crosslinking agent MBAM were added to the tube and stirred for another 10 minutes. Initiators, $Na_2S_2O_8$ and $Na_2S_2O_5$, were added simultaneously. Reaction was allowed to stir for 15 seconds, shaken vigorously for 30 seconds, and allowed to settle for 10 minutes before placing in the oven.

Table 4.1. Amount of reagents used for synthesis of each polymer concentration. Stock solutions of MBAM (15 mg/mL), $Na_2S_2O_8$ (60 mg/mL), and $Na_2S_2O_5$ (60 mg/mL) were used.

Polymer Composition	AA	AM	DI water	10M NaOH	MBAM solution	$Na_2S_2O_8$ solution	$Na_2S_2O_5$ solution
17% PANa, 83% PAM	1.5 mL	7.5 g	18.6 mL	2.4 mL	12 mL	1.5 mL	1.5 mL
83% PANa, 17% PAM	7.5 mL	1.5 g	9 mL	12 mL	12 mL	1.5 mL	1.5 mL

Centrifuge tubes were cut open to remove hydrogels. Hydrogels were broken into pieces and submerged in DI water to remove any unreacted small molecules. Rinse water was changed daily for 5 days. Hydrogels were then sliced into flat pieces of 1-2 cm thickness for mechanical testing, air-dried, and placed under vacuum at room temperature overnight. Hydrogels were synthesized containing 2 wt% crosslinker and either 17 or 83 wt% sodium acrylate.

4.2.3 Hydrogel characterization

Gravimetric swelling

Dry hydrogel pieces were ground to a fine powder as in previous studies.[18] Gravimetric swell tests were conducted using the "tea bag" method[20] to determine equilibrium swelling ratios and provide a qualitative comparison of swelling kinetics in various aqueous environments. The tea bag was submerged in solution until saturated, removed from solution, shaken for 10 seconds, and weighed. Ground polymer was added to the tea bag and the bag was placed back in solution. The bag was removed, shaken, and weighed at set time intervals from 0.5 to 240 minutes. The swelling ratio (Q) was calculated using Equation (4.1), where m_1 is the mass of dry polymer, m_2 is the mass of the wet teabag, and m_3 is the mass of teabag and swollen polymer.

$$Q = (m_3 - m_2 - m_1)/m_1 \tag{4.1}$$

Swelling measurements were performed on both hydrogel compositions described previously in order to compare responses of gels with low and high fractions of ionic

functionalities. Swell tests were conducted using DI water and 10 mM solutions of NaCl, $CaCl_2$, and $CuSO_4$ in DI water. Experiments were conducted using ~150 mg of polymer per tea bag, with each tea bag immersed in 300 mL of the given solution.

Hysteretic swelling experiments were also conducted in order to investigate the reversibility of changes in swelling performance induced by exposure to counter-ions in saline solution. These experiments were conducted using the same mass of polymer and volume of solution as described previously. However, after exposure to saline solutions, hydrogels in these experiments were collected and dried under vacuum at room temperature. These salt-containing hydrogels were next immersed in DI water to remove all free salt ions. Each polymer was filtered and placed in clean rinse water every 4 hours until electrical conductivity (EC) of the rinse water was ≤ 5 μS/cm. This conductivity threshold, which is used for Type IV Reagent Water,[21] was selected as a low EC value which would indicate that all ions which were removable under neutral pH had been eliminated from the hydrogel. Rinsed hydrogels were then dried under vacuum at room temperature. Finally, these hydrogels were re-swollen in DI water.

Mechanical analysis

Dried flat slices of hydrogel were swollen to a set swelling ratio of Q=5 for all experiments. A swelling ratio below the equilibrium Q of $CuSO_4$-swollen samples was chosen in order to compare all compositions and solutions at the same polymer volume fraction ($\varphi=1/Q$). Solution was added slowly to each sample until the desired Q was obtained in order to mitigate risks of sample cracking due to rapid and uneven swelling. Separate samples were prepared containing DI water, 5 mM, 50 mM, and 100 mM solutions of each salt.

The elastic modulus (E) of each sample was measured via compression using a 2 mm diameter flat punch on a hydrogel sample of 5-20 mm thickness. The maximum compression force

was set to 50 mN, and the approach and return rates were set to 0.01 mm/sec in order to ensure that measurements remained in the elastic regime of the materials and there were no velocity-dependent contributions to the elastic modulus.[22] The elastic modulus was determined from the linear section of each stress-strain curve in order to avoid contributions from an uneven sample surface at low strain. Reported *E* values are averages obtained from 3-6 measurements collected on each sample type. 5 mM was chosen as a saline concentration closer to that of biological fluids.[23] High salt concentrations were chosen at 50 and 100 mM, which approach the typical concentration range for many high salinity environments.[24,25]

4.3 Results and Discussion

Hydrogel swelling response depends upon both hydrogel and solvent composition. The overall trends observed in the time-response curves in Figure 4.2 are as expected from previous observations:[4,18,19] 1) increasing ion valency decreases hydrogel swelling capacity, and 2) increasing ionic fraction in the hydrogel increases the impact of counter-ion-induced de-swelling. The effect of further counter-ion interaction with increasing ionic fraction is also exhibited though visual observation as shown in Figure 4.3. It is the difference in swelling behavior between hydrogels in calcium salts and in copper salts that is of primary interest to this investigation.

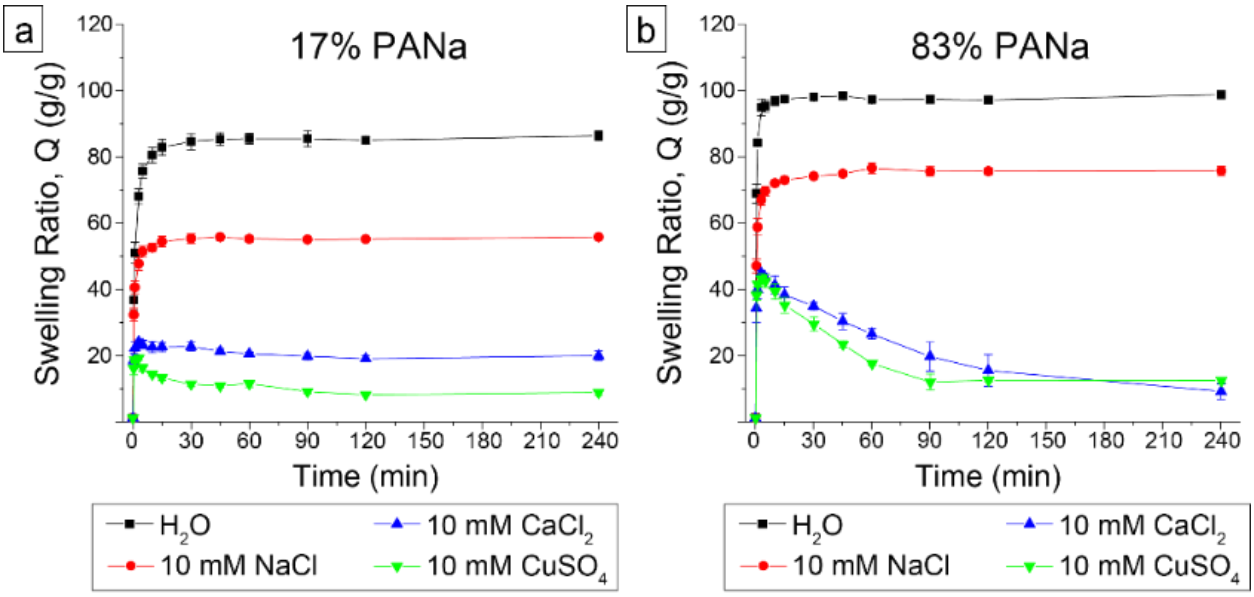

Figure 4.2. Swelling behavior of 17% PANa, 83% PAM hydrogels (a) and 83% PANa, 17% PAM hydrogels (b) in DI water and 10 mM salt solutions.

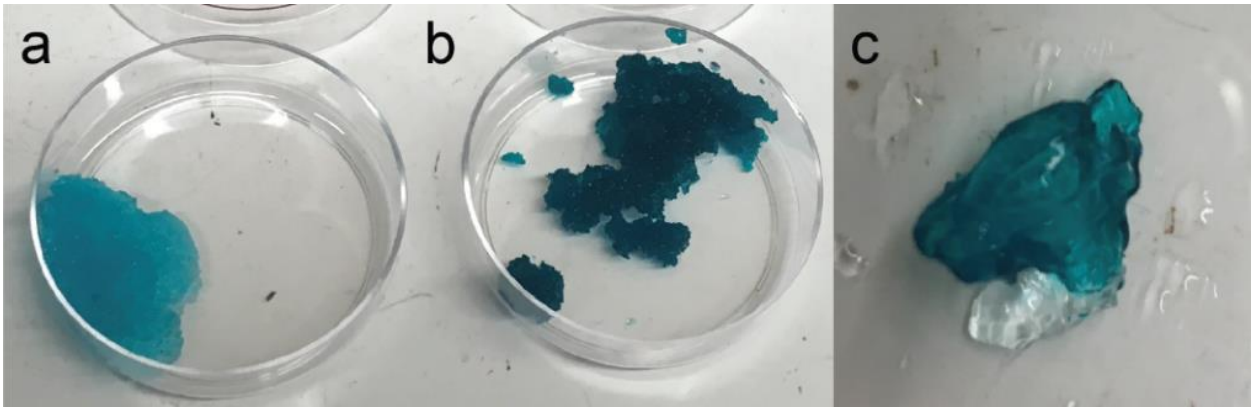

Figure 4.3. PANa hydrogels after swelling in 10 mM $CuSO_4$. The lighter color in the 17% PANa gel (a) and darker color in the 83% PANa gel (b) indicate a higher concentration of copper hydrates present in the 83% PANa gel. Larger pieces of 83% PANa gel (c) formed a measurable copper-crosslinked shell which, when cut into, revealed an un-crosslinked center to the hydrogel.

The time-dependent de-swelling observed in all samples (*i.e.*, high and low PANa hydrogels in solutions of both divalent salts) has been observed and explained in previous works.[13,18] It has also been observed in previous studies that divalent transition metals cause the collapse of ionic networks at lower concentrations than alkaline earth metals.[13] However, the cause of this phenomenon remains poorly understood.

Clues to understanding this phenomenon can be taken from previous studies. In previous PANa-*co*-PAM work, similar observations were made concerning aluminum, which is a post-transition metal of similar character to copper. Krafcik, *et al.*[18] observed that swelling plateaued at a higher Q for Al^{3+} than for Ca^{2+}, while Zhu, *et al.*[4] observed the formation of a solid shell similar to that observed in Figure 4.3c. Horkay, *et al.*[13] observed in pure PANa hydrogels that transition and post-transition metals increase the elastic modulus, while multivalent main group metals do not.

In order to understand how observations in pure PANa and with post-transition metal salts translated to the current system, mechanical analysis of the PANa-*co*-PAM gels was required. Elastic modulus measurements of both hydrogel compositions remained similar in DI water and low concentrations of NaCl and $CaCl_2$. (Figure 4.4) In low concentrations of $CuSO_4$, the elastic modulus of 17% PANa gels increased slightly, while that of 83% PANa gels increased drastically. (Figure 4.5) These results indicate that PAM does not play a role in counter-ion-induced changes in mechanical properties, as the trends observed in PANa-*co*-PAM reflect those observed in pure PANa.[13] These data also show that Cu^{2+} contributes more strongly to the elastic modulus in high PANa gels.

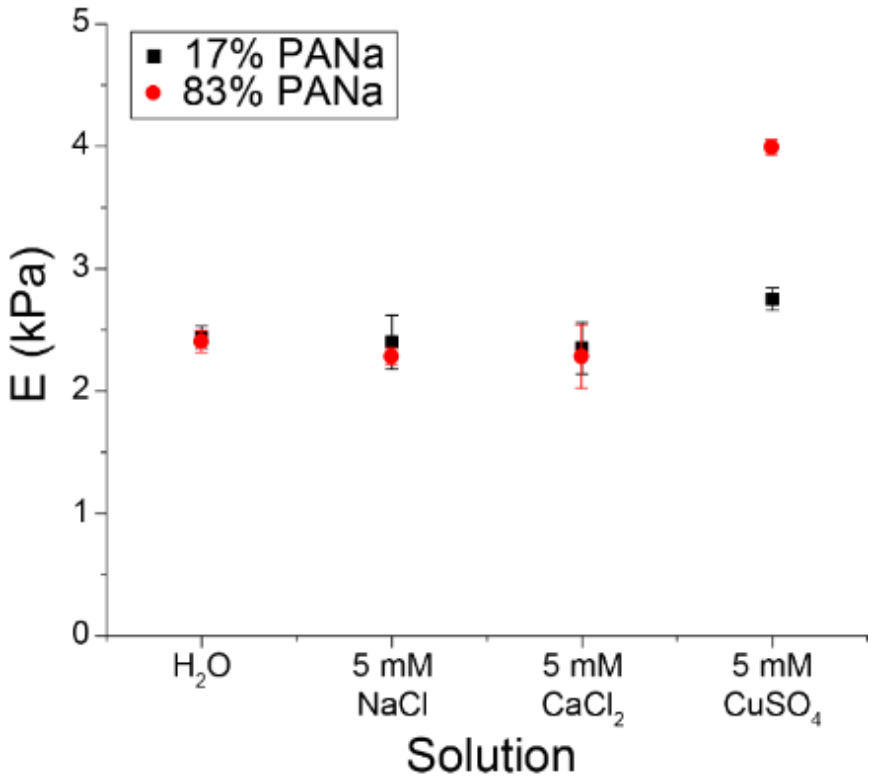

Figure 4.4. Mechanical responses between the two hydrogel compositions were compared as a function of metal cation at low salt concentrations.

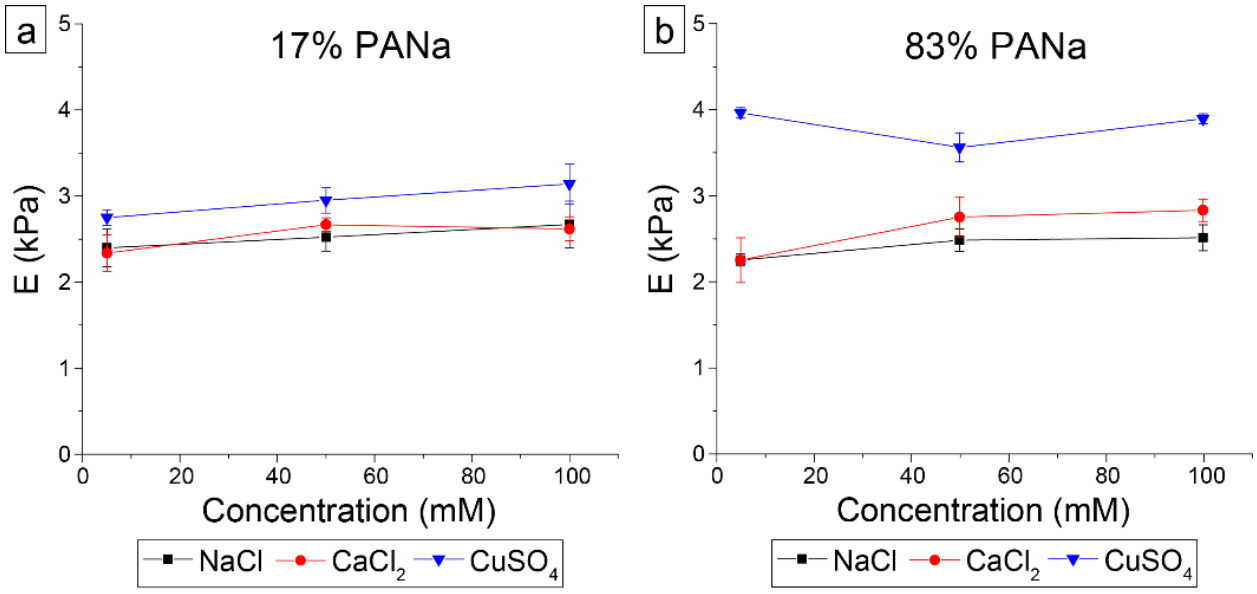

Figure 4.5. Elastic modulus as a function of salt concentration. 17% ANa (a) and 83% ANa (b) hydrogels were examined in 5 mM, 50 mM, and 100 mM solutions of NaCl, $CaCl_2$, and $CuSO_4$.

Such behavior can be understood within the context of metal ion characteristics. Calcium, an alkaline earth (main group) metal, is only weakly electronegative. It is capable of ionic attraction between itself and the anionic polymer functionalities, but it is unable to form covalent bonds. In turn, these ionic crosslinks, or ion bridges, formed by calcium are only transient in nature, as illustrated in Figure 4.6. Transition metals (*e.g.*, copper) and post-transition metals (*e.g.*, aluminum), on the other hand, are strongly electronegative and capable of forming coordinate covalent bonds as observed in ceramic matrices.[26] This ability in turn allows transition and post-transition metals to form permanent, covalent-strength bonds with the anionic polymer functionalities. Only by the formation of permanent bonds can an ion bridge be formed that contributes to the mechanical strength of the polymer network.

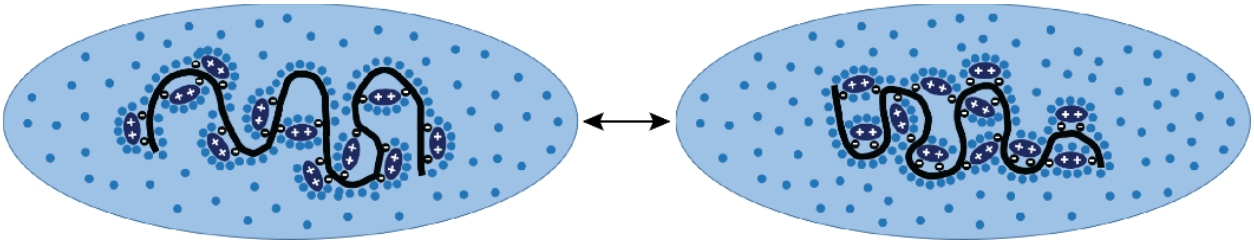

Figure 4.6. Illustration of fluctuation of transient crosslinks as occurs with multivalent main group metal ions.

This study also investigates how these interactions scale with increasing salt concentration. One must recall that electrostatic repulsion contributes to hydrogel swelling, and counter-ion-screening of those repulsions changes the conformation of the polymer chains. At 5 mM, the ionic strength of the saline solutions is lower than the ionic strength of either hydrogel, which is 9.8 mM for 17% PANa and 42 mM for 83% PANa. However, many saline environments, such as seawater or concrete pore solution, can have ionic strengths well into the millimolar range, significantly above the ionic strength of the hydrogels.[24,25]

In Figure 4.5a, it can be observed that for 17% PANa gels, the elastic modulus remains relatively constant through all concentrations of each salt, with the modulus in $CuSO_4$ remaining higher than in NaCl or $CaCl_2$. This is believed to be because even at 5 mM, a majority – or all, in the case of divalent cations - of the anionic sites in the polymer should be occupied, and increasing counter-ion concentration does not significantly increase the amount of charges being screened from electrostatic repulsion. Conversely, in 83% PANa gels (Figure 4.5b) we observe that the modulus in NaCl and $CaCl_2$ increases between 5 mM and 50 mM. In this case, there were still unscreened charges along the polymer chain in 5 mM salt solutions, and so additional screening by higher cation concentrations induced further changes in chain conformation and therefore elastic modulus.

An unexpected result appears in Figure 4.5b for 83% PANa hydrogels in $CuSO_4$ solution. Here, the elastic modulus remains high and relatively constant for all concentrations. This data is contrary to the idea of changes in chain conformation as the ionic strength of the gel is surpassed. However, this behavior can be explained in light of the copper-crosslinked shell formation observed as in Figure 4.3c. Quantification of this shell's thickness and variation with respect to hydrogel composition remains to be investigated. However, it is clear from visual observations that the shell formation is more significant in high PANa gels. Once this shell forms, minimal amounts of water or solute can permeate, and the outer shell of the hydrogel takes on properties different from the center of the hydrogel. In such a case, compression experiments at low forces are measuring the elastic modulus of this shell and not the un-crosslinked gel beneath it. Since this shell forms in 83% PANa gels even at low concentrations, it can be determined that copper ions fully crosslink the outer layer of the hydrogel, after which there is no further conformational

change in the polymer chains, even with higher solution concentrations. This is supported by the consistent elastic modulus measured at all $CuSO_4$ concentrations.

Finally, initial hysteresis experiments also support the permanence of transition metal-induced crosslinks. It will be noted in Figure 4.7 that there is some level of permanent network constriction even with $CaCl_2$. This restriction can be attributed to entrapment of Ca^{2+} ions within the network, which subsequently decreases the osmotic pressure gradient that drives swelling. In the case of $CuSO_4$, however, the cleaned, re-swollen hydrogels never surpass the equilibrium Q obtained during swelling in salt solution. This swelling behavior provides additional support that a crosslinked shell is formed along the exterior of the hydrogel particles, and water is able to permeate only into the free volume within the outer layers of that shell.

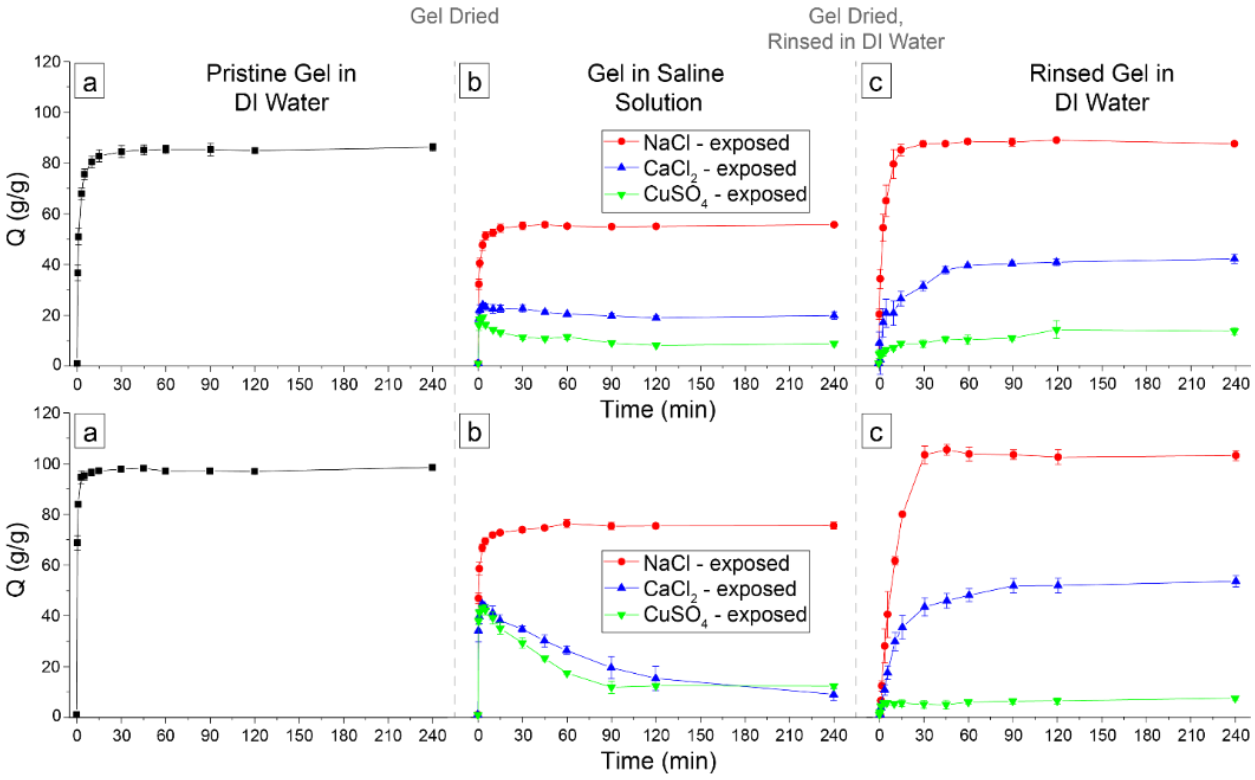

Figure 4.7. Swelling hysteresis experiments. Hydrogels were swollen in DI water (a), dried, swollen in saline solution (b), rinsed, dried, and swollen again in DI water (c). Top row images are of 17% ANa hydrogels and bottom row images are of 83% ANa hydrogels.

4.4 Conclusions

In this work we have investigated PANa-*co*-PAM hydrogels containing a low and a high ionic fraction and their swelling and mechanical performance in saline solutions. We have confirmed the formation of permanent crosslinks between ionic polymer moieties and transition metal counter-ions and the transience of crosslinks formed by main group metal counter-ions. We have further elucidated the reason for this behavioral discrepancy between metal ions and how this discrepancy scales in high salinity environments. This work will be continued in order to investigate a more comprehensive range of hydrogel ionic fractions and establish quantitative scaling relationships between ionic fraction and hydrogel performance properties in solutions of multivalent cations.

4.5 Acknowledgements

We would like to thank Professor Chelsea Davis and Naomi Deneke for advisement and training in conducting mechanical testing. We gratefully acknowledge financial support for this work by the National Science Foundation (CMMI 1454360).

4.6 References

1. Peppas; N. A.; Bures, P.; Leobandung, W.; Ichikawa, H., Hydrogels in pharmaceutical formulations. *Eur. J. Pharm. Biopharm.* **2000**, *50*, 27-46.
2. Nayak, S.; Lyan, L. A., Soft Nanotechnology with Soft Nanoparticles. *Angew. Chem. Int. Ed.* **2005**, *44*, 7686-7708.
3. Rybtchinski, B., Adaptive supramolecular nanomaterials based on strong noncovalent interactions. *ACS Nano* **2011**, *5* (9), 6791-6818.
4. Zhu, Q.; Barney, C. W.; Erk, K. A., Effect of ionic crosslinking on the swelling and mechanical response of model superabsorbent polymer hydrogels for internally cured concrete. *Mater. Struct.* **2015**, *48*, 2261-2276.

5. Cui, H.; Zhao, Q.; Wang, Y.; Du, X., Bioinspired Actuators Based on Stimuli-Responsive Polymers. *Chem. - Asian J.* **2019**, *14*, 2369-2387.
6. Ricka, J.; Tanaka, T., Swelling of Ionic Gels: Quantitative Performance of the Donnan Theory. *Macromolecules* **1984**, *17*, 2916-2921.
7. Muthukumar, M. A, Perspective on Polyelectrolyte Solutions. *Macromolecules* **2017**, *50* (24), 9528-9560.
8. De, S. K.; Aluru, N. R.; Johnson, B.; Crone, W. C.; Beebe, D. J.; Moore, J., Equilibrium swelling and kinetics of pH-responsive hydrogels: models, experiments, and simulations. *J. Microelectromech. Syst.* **2002**, *11* (5), 544-555.
9. Li, H.; Ng, T. Y.; Yew, Y. K.; Lam, K. Y., Modeling and simulation of the swelling behaviour of pH-stimulus-responsive hydrogels. *Biomacromolecules* **2005**, *6*, 109-120.
10. Sing, C. E.; Zwanikken, J. W. de la Cruz, M. O., Effect of ion-ion correlations on polyelectrolyte gel collapse and re-entrant swelling. *Macromolecules* **2013**, *46*, 5053-5065.
11. Chremos, A.; Douglas, J. F., The Influence of Polymer and Ion Solvation on the Conformational Properties of Flexible Polyelectrolytes. *Gels* **2008**, *4*, 20.
12. Horkay, F.; Douglas, J. F., Gels and Other Soft Amorphous Solids in *American Chemical Society Symposium Proceedings*; American Chemical Society: Washington, D.C., 2018; Vol. 1296, pp. 1-13.
13. Horkay, F.; Tasaki, I.; Basser, P. J., Effect of monovalent-divalent cation exchange on the swelling of polyacrylate hydrogels in physiological salt solutions. *Biomacromolecules* **2001,** *2*, 195-199.
14. Gemeinhart, R. A.; Chen, J.; Park, H.; Park, K., pH-sensitivity of fast responsive superporous hydrogels. *J. Biomater. Sci., Polym. Ed.* **2000**, *11* (12), 1371-1380.
15. Bajpai, S. K.; Johnson, S., Superabsorbent hydrogels for removal of divalent toxic ions. Part I: Synthesis and swelling characterization. *React. Funct. Polym.* **2005**, *62*, 271-283.
16. Mudiyanselage, T. K.; Neckers, D. C., Photochromic superabsorbent polymers 1. *Soft Matter* **2008**, *4*, 768-774.
17. Laftah, W. A.; Hashim, S.; Ibrahim, A. N., Polymer Hydrogels: A Review. *Polym.-Plast. Technol. Eng.* **2011**, *50* (14), 1475-1486.

18. Krafcik, M. J.; Erk, K. A., Characterization of superabsorbent poly(sodium-acrylate acrylamide) hydrogels and influence of chemical structure on internally cured mortar. *Mater. Struct.* **2016**, *49*, 4765-4778.
19. Krafcik, M. J.; Macke, N. D.; Erk, K. A. Improved Concrete Materials with Hydrogel-Based Internal Curing Agents. *Gels* **2017**, *3* (46).
20. Davis, C. R.; Kelly, S. L.; Erk, K. A., Comparing laser diffraction and optical microscopy for characterizing superabsorbent polymer particle morphology, size, and swelling capacity. *J. Appl. Polym. Sci.* **2017**, *135* (14).
21. ASTM Standard D1193, 1951 (2018), "Standard Specification for Reagent Water," ASTM International, West Conshohocken, PA, 2018, DOI: 10.1520/D1193-06R18, www.astm.org.
22. Shull, K. R. Contact mechanics and the adhesion of soft solids. *Mater. Sci. Eng., R* **2002**, *36*, 1-45.
23. Horkay, F.; Tasaki, I. Basser, P. J., Osmotic swelling of polyacrylate hydrogels in physiological salt solutions. *Biomacromolecules* **2000**, *1*, 84-90.
24. Millero, F. J.; Feistel, R.; Wright, D. G.; McDougall, T. J., The composition of Standard Seawater and the definition of the Reference-Composition Salinity Scale. *Deep Sea Res., Part I* **2008**, *55*, 50-72.
25. Vollpracht, A.; Lothenbach, B.; Snellings, R. Haufe, J. The pore solution of blended cements: a review. *Mater. Struct.* **2016**, *49*, 3341-3367.
26. Aakeroy, C. B.; Beatty, A. M., *Comprehensive Coordination Chemistry II: From Biology to Nanotechnology*; Elsevier: Amsterdam, 2003.

5. DEVELOPING A CHARACTERIZATION METHODOLOGY FOR ELUCIDATING CHELATION OF METAL IONS BY POLYELECTROLYTE GELS

5.1 Introduction and Motivation: Ion Chelation in Hydrogels

Previous studies regarding PANa-PAM hydrogels reported in the earlier chapters of this dissertation and other publications[1-4] have led to several new questions regarding the behavior of different types of counter-ions in the hydrogel network. In particular, we have found the need for a standard methodology for assessing the counter-ion content and ionic history of hydrogel materials. To our knowledge, there is no current methodology for characterizing the different bonding behavior observed in hydrogels with counter-ions from various classes of molecules (*e.g.*, different groups within the periodic table, macromolecules, amphiphilic compounds). This study therefore aims to build off of previous studies using the PANa-PAM hydrogel system and employ the same alkali metal, alkaline earth metal, and transition metal salts as a model set of variables to develop a characterization protocol. Many commonly-employed superabsorbent polymers contain carboxylate, amide, or other chemical functionalities similar to those found in the PANa-PAM system, and, as such, the protocols developed here may be applied to a broad range of superabsorbent materials, even beyond direct "hydrogel" applications.

As mentioned previously, there is significant interest in employing these materials in changing ionic environments (*e.g.*, sensors for heavy metal contaminants) and recycled applications (*e.g.*, recycling consumer products into infrastructure). Part of this study therefore focuses on being able to characterize the effects of previous exposure history on subsequent ionic interactions and develop tools that use those subsequent interactions to establish what ions were present initially.

5.1.1 Chelation

Metal ion chelation is achievable between more electronegative metals (*e.g.*, transition metals) and several hydrophilic functionalities (*e.g.*, -OH, $-COO^-$, $-NH_2$, C=O), such as those employed in superabsorbent polymers. As seen in Chapter 4 and other works,[1,5-7] chelation of transition and post-transition metals also produces unique ionically-crosslinked shells in some superabsorbent polymers, leading to questions of why this chelation is more "permanent" than weaker ionic crosslinking from alkaline earth metals.

Unlike the weaker electrostatic interactions observed between alkali or alkaline earth metals and these functionalities, transition metal chelation is capable of forming significantly stronger noncovalent bonds. These stronger bonds produce vibration bands that can be observed at low wavenumbers via infrared and Raman spectroscopy. Weaker electrostatic attraction between polymer functionalities and main group metals can sometimes be inferred through shifts they induce in other, stronger vibration bands belonging to the polymer itself, but these weaker bonds often do not have their own signature in an FTIR or Raman spectrum. As such, transition metal-polymer attraction is significantly more conducive to chemical characterization.

This research proposes using transition metals to characterize not only the hydrogel's capacity and strength of transition metal-binding but also as a signaling molecule to discern the previous swelling history and ion content of the gel. It has been observed that hydrogel swelling behavior in transition metal solutions is altered by previous exposure to other salts, and so it is believed that prior exposure changes the character of the gel's interaction with the transition metal ions. Several factors influence the stability of metal-ligand compounds, including the ions' and polymer functionalities' electronegativity, but a direct relationship cannot be assumed between electronegativity and binding affinity as initially presumed. Nonetheless, stability constants have been calculated for many metal-carboxylate compounds, and a clear order of relative stability has

been established (*e.g.*, bond stability of Na^{+}-PAA < Ca^{2+}-PAA < Cu^{2+}-PAA).[8-12] The reported values of these constants vary across literature, but to illustrate the difference in stability, Gustafson and Lirio report stability constants in the range of $8.03 < -\log(K) < 9.39$ for Ca^{2+}-PAA and $4.60 < -\log(K) < 5.49$ for Cu^{2+}-PAA.[11] The attraction between sodium and PAA in water is so weak relative to divalent ion attraction that values for the stability constant are not widely reported in literature.

Furthermore, it has been concluded that, although acrylamide monomer strongly chelates with copper (II),[13] polyacrylamide is likely incapable of strong chelation with copper ions without being first deprotonated.[14,15] This idea is strongly supported by the extensive use of polyacrylamide gels as gel electrophoresis media that diffuse copper-containing compounds or use copper (II) staining procedures (*i.e.*, copper reacts with either a surfactant to form precipitant or is templated by specific proteins).[16-22] Additional literature investigations have found reports that both agree[14,15,23,24] and disagree[25-27] with this theory. Those that disagree present other evidence for polymer-ion coordination, and it is feasible that very weak chelation is occurring for which the attraction does not noticeably impact chemical bond vibrations. It is therefore believed that, particularly relative to copper-acrylate chelation, copper-acrylamide interaction is of minimal consequence to the current study. The amount by which transition metal-polymer binding is altered by ions previously present in the gel can thus be related to the difference between the bond stability of the transition metal-PAA interaction and that of the previously-present species. Therefore, if this change in polymer-transition metal ion interaction can be characterized and understood, a relationship could be developed to determine the amount and type of counter-ions already present in the gel.

5.1.2 Copper as a model transition metal

Copper (II) is useful as a model transition metal for several reasons. First, it possesses the same ion valency as a main group metal under investigation but forms significantly stronger bonds with the polymer. It is not strongly chao- or cosmotropic[28] so that its influence on the structure of the hydrogen-bonding network in the gel is not significantly different from that of calcium and sodium. Furthermore, it is photochromic, which allows for characterization of copper (II) content and confirmation of the metal's ionization state through absorbance measurements and optical observation.

Copper (II) chelation with poly(acrylic acid),[9-12,29,30] acrylamide monomers,[13] and other organic molecules[31-33] has also been studied by many researchers. Copper chelation in similar PANa-PAM systems has been investigated for its effects on swelling,[34] but no studies have been found in which a mixed-polymer system was studied with respect to molecular-scale bonding. Therefore a complete set of spectroscopic reference values for the functionalities in this combined system cannot be compiled from previous studies. Nonetheless, portions of the studies referenced above do offer insight into the spectroscopic signals generated by copper-related interactions and how to interpret alterations observed in spectra for these organic compounds.

5.1.3 Spectrometry and spectroscopy

Due to the photochromic and chelating properties of copper (II), counter-ion uptake by the gel, as well as the strength with which it interacts with different functionalities within the gel, can all be characterized through spectroscopic techniques. UV-Vis spectrometry offers a facile method by which we can measure the concentration of copper (II) in a given solution, and by measuring the concentration of a solution after a hydrogel has been swollen in it, we are able to calculate the

amount of copper absorbed by the gel. Data interpretation in FTIR and Raman spectroscopy is significantly more complex, but the spectra obtained can provide a wealth of information.

UV-Vis spectrometry functions by measuring the absorbance of light by a given volume of solution at a set wavelength. Spectra can be collected across a wide range of wavelengths in the visible to ultraviolet range, and one or more peak absorbance wavelengths can be discerned for any photochromic compound. The molar absorptivity coefficient is well-established for many transition metals, which provides a direct relationship between absorbance and solution concentration.

Fourier-transform infrared spectroscopy (FTIR) and Raman spectroscopy have been used extensively to measure metal-ligand chelation bonds,[31,32,35-37] including a few studies regarding superabsorbent materials.[38,39] In general, FTIR data collection is simpler than that of Raman spectroscopy, but it has proven not to be an ideal characterization method for superabsorbent materials in their swollen state, including the current system. This is because the O-H bond in water molecules is highly absorbent of infrared wavelengths. In a highly swollen system such as a hydrogel, this results in signal from other bond vibrations being buried within the broad, intense signal produced by the water. As described in previous chapters, this work has been heavily focused on understanding ionic interaction in hydrogels in their end-use state (*i.e.*, swollen), and so it is important to be able to conduct spectroscopy experiments on fully swollen gels. Raman spectroscopy provides an alternative method to overcome the strong absorption signal produced by water in FTIR.

Raman spectroscopy functions by measuring the Raman scattering of a monochromatic laser off of vibrating atomic bonds. Raman scattering is weak relative to scattering by other means (*e.g.*, fluorescence) or absorbance measurements (*e.g.*, UV-Vis, FTIR), which makes data

collection more complex. Scattering is therefore most efficient at high microscope magnifications (*i.e.*, 50-100X) using a laser spot size on the order of microns.[40] Nonetheless, this method is capable of superior resolution at low wavenumbers (*e.g.*, less than 800 cm^{-1}) where metal-organic bonds often appear and is minimally affected by H_2O bond vibrations, making it the preferred characterization method for the current study.

An additional benefit of Raman spectroscopy is that scattering is only measured from a sample thickness of around 1 micron. This makes it possible to produce a depth profile in which spectra are collected from different layers in a stepwise manner by changing the focal plane of the microscope. This depth profile would be highly beneficial for measuring the concentration gradient of copper that has been observed optically in some hydrogel samples and which is likely responsible for the "shell" formation often observed in hydrogels swollen in solutions containing transition metals. This process was not completed in the current study due to constraints on laboratory access during the COVID-19 pandemic. However, it is proposed here as a valuable follow-up experiment to be conducted in future studies.

As mentioned previously, Raman spectroscopy allows us to overcome strong signals from water molecules. This is because Raman scattering is produced by different vibrational modes than those that absorb infrared light in FTIR. However, most data collection programs present spectra according to their Raman shift, which aligns vibration bands at the same wavenumber as those produced in FTIR, making the translation of information between the two methods straightforward.

Due to the multiple vibration modes that produce Raman scattering, information can be drawn from these spectra regarding both bond strength and character, and changes in stretching symmetry can even indicate changes to vibrations of neighboring bonds. The latter capability further increases the usefulness of Raman spectroscopy in the current study, as weaker interactions

between the polymer and main group metal ions can be observed by changes in the vibration of adjacent bonds. More detail as to the relationships between bond vibrations will be discussed in the results section of this study.

5.1.4 Experimental considerations

In contrast to previous studies discussed in this dissertation, the method by which swelling experiments are conducted has been altered for the present investigation. This study focuses on an 83% ANa/17% AM/2% crosslinker hydrogel. Scaling laws may be developed at a later date to relate ANa content and the extent of copper chelation, but the current study focuses on gels with the highest ANa content in order to most clearly illustrate the interactions of counter-ions with the ionic polymer functionalities.

Hydrogel samples were also fabricated in a new fashion for this study. The high sensitivity and small collection volume of Raman spectroscopy requires flat sample surfaces that can be probed at high magnifications of an optical microscope. Flat hydrogel samples were therefore synthesized as described below. Furthermore, all swelling experiments were conducted on pre-swollen hydrogels. This method was chosen due to the high level of internal stresses produced in gel samples that were swollen from the dry state. Rapid water uptake in previous studies led to extensive curling and fracture of hydrogel samples, which made analysis by Raman spectroscopy impossible.

5.2 Experimental Methods

5.2.1 Materials

N,N'-methylenebisacrylamide (MBAM), sodium metabisulfite ($Na_2S_2O_5$), sodium persulfate ($Na_2S_2O_8$), acrylamide (AM), sodium hydroxide (NaOH), sodium chloride (NaCl),

calcium chloride ($CaCl_2$), and copper (II) sulfate ($CuSO_4$) were all obtained from Sigma-Aldrich (St. Louis, MO) and used as received. Acrylic acid (anhydrous, 200 ppm MEHQ inhibitor) (AA) from Sigma-Aldrich was filtered through a pre-packed column (Sigma-Aldrich) to remove MEHQ inhibitor prior to polymerization. Deionized (DI) water (18.0-18.3 MΩ cm^{-1}) was purified in-house using a Barnstead Nanopure system (Dubuque, IA).

Gravimetric swelling tests were conducted using T-Sac Size 3 tea filter bags. All swelling solutions were prepared using DI water. UV-Vis spectra were collected using a SpectraMax M Series spectrophotometer from Molecular Devices (San Jose, CA). Raman spectra were collected using a Renishaw inVia confocal Raman microscope (Auburn Hills, MI).

5.2.2 Hydrogel fabrication

Flat sample fabrication

Flat pieces of hydrogel were synthesized by creating a multilayer assembly that could be inserted into a 50 mL centrifuge tube prior to synthesis. Three glass microscope slides (Fisher Scientific, Waltham, MA) were placed on top of each other, and aluminum foil spacers were placed at each end to separate each of the three slides. A strip of aluminum foil was folded 12 times and cut to size so that each spacer was composed of 24 layers of foil and was of equal width with the glass microscope slides. The assembly of slide-spacer-slide-spacer-slide was clamped on each end using a mini binder clip and inserted into a centrifuge tube.

Hydrogel synthesis

Poly(sodium acrylate-*co*-acrylamide) hydrogels containing 83% PANa, 17% PAM, and 2% crosslinker were synthesized according to the procedure described in Chapter 4, using the reagent amounts provided in Table 4.1. However, instead of mixing all reagents in the centrifuge tube, the

solution was prepared in a separate beaker. Initiator was added to the solution, the solution was allowed to stir for 30 seconds, and then the solution was poured directly over the slide assembly in the centrifuge tube, making sure the solution fully infiltrated the space between each pair of glass slides. The centrifuge tube was then capped and placed in the oven at 60 °C overnight to drive the reaction to completion.

Sample recovery

The centrifuge tube was removed from the oven and allowed to cool to room temperature, then the cap was removed. A utility knife was used to cut the conical tip of the tube off and make a slit down the side of the tube. The tube could then be pulled apart and the gel could be removed as a single piece. Excess gel was peeled off of the slide assembly, and the binder clips and aluminum foil spacers were removed. The glass slides were not forcibly separated but were placed as one unit in a wide dish filled with DI water.

As the hydrogel layers swelled, they delaminated from the glass slides naturally. Rinse water was decanted out of the dish and replaced with fresh DI water daily for 5 days. After rinsing, hydrogel samples were cut into small pieces of approximately 2-6 cm wide and long. Samples were stored in large petri dishes (Fisher Scientific) in DI water to keep them at equilibrium swelling.

5.2.3 Sample preparation

Hydrogels at equilibrium swelling were placed into various saline solutions for subsequent experiments. For each sample, a small petri dish was zeroed out on a balance, a hydrogel piece was patted dry using a KimWipe and placed in the dish, and the initial mass of the hydrogel was recorded. Ten milliliters of the chosen solution was then added to the dish, and the closed dish was

wrapped with Parafilm to prevent water evaporation. Hydrogels were allowed to swell for at least 12 hours in NaCl and $CaCl_2$ solutions and at least 48 hours in $CuSO_4$ solutions to reach equilibrium.

5.2.4 Charge density calculations

The average charge density of the hydrogel samples was calculated for use in later salt-uptake calculations. Five samples were measured, at equilibrium swelling in DI water, via optical microscope. Images were taken of the full length, width, and cross-section of each gel and dimensions were measured using ImageJ software. Each piece was then dried fully (*i.e.*, under vacuum), and gravimetric swelling tests were conducted as described in previous chapters.

The theoretical charge density of each sample was calculated using the equilibrium swelling ratio (Q_{equil}) and the formulae developed by Peppas, *et al*.[41] The swollen volume of each sample was calculated from the optical microscopy measurements. From these values, an average number of charges per unit volume (mL or mm^3) was determined. The total charge content of each sample used in a subsequent experiment was then calculated using Q_{equil}, the polymer volume fraction at Q_{equil}, the polymer specific volume, and the density of water at 23 °C. Equations for each value mentioned above, including the complete formulae for the theoretical charge density, can be found in Appendix A.

5.2.5 UV-visible spectrometry

UV-vis spectra were collected on the remaining solution from each $CuSO_4$ swelling experiment. Solution from each small petri dish was pipetted into a polystyrene cuvette and analyzed over the wavelength range of 350 nm $\leq \lambda \leq$ 1000 nm. The absorbance (A) was recorded at λ_{max} = 810 nm, and the concentration *[C]* of each sample was calculated using Beer's law, as

shown in Equation 5.1. The molar absorptivity coefficient of copper (II) at 810 nm is ε = 12.3 L/mol-cm, and the path length through the cuvette cell is l = 1 cm.

$$A = \varepsilon[C]l \tag{5.1}$$

From the concentration of the remaining solution and the initial volume of solution (*i.e.*, 10 mL), the number of charges taken up by the gel could be determined. The divalent cation capacity of the gel, assuming ideal chelation where every copper (II) ion is bound to two charged polymer functionalities, was then calculated and the amount of copper absorbed by the gel was expressed as a percent of the theoretical capacity. These calculations are laid out in more detail in Appendix A.

5.2.6 Raman spectroscopy

Raman spectra were collected on hydrogel samples swollen in DI water, 100 mM NaCl, 50 mM $CaCl_2$, solutions of 1-50 mM $CuSO_4$, and in 50 mM $CuSO_4$ *after* swelling in NaCl or $CaCl_2$. Spectra were collected over the range of 100 nm^{-1} to 3200 nm^{-1} using a 532 nm laser at 1-10% laser power, 50-100x magnification, and a scan rate of 10 s^{-1}. At least 3 spectra were collected for each set of swelling conditions. Data were plotted, smoothed, and analyzed using KnowItAll (Bio-Rad) software for spectroscopic analysis, and normalized integrals, amplitudes, and peak values were collected for every spectrum. For peaks that overlap, deconvolution was performed using the "Peak Analyzer" function in OriginPro (OriginLab, Northampton, MA). Peaks were fitted using a Gaussian-Lorentzian Cross Product type curve.

5.3 Results and Discussion

In this section we report results of UV-Vis spectrometry and Raman spectroscopy experiments on PANa-PAM hydrogels swollen in NaCl, $CaCl_2$, and $CuSO_4$ solutions from various

previous swelling conditions (*e.g.*, DI water, NaCl, $CaCl_2$). All data is presented early, followed by a more thorough discussion.

5.3.1 UV-Vis measurements

Copper uptake was first measured by UV-Vis spectrometry. Since UV-Vis absorption deviates from Beer's Law (Equation 5.1) at high absorbance, UV-Vis spectrometry cannot be performed directly on hydrogels containing copper. Instead, a known amount of copper solution (10 mL) was added to a petri dish containing a known mass of hydrogel swollen to Q_{equil} in DI water and allowed to equilibrate for two days. The initial solutions were analyzed using UV-Vis, the spectra of which can be seen in Figure 5.1, to obtain an accurate initial concentration. The remaining solution from each hydrogel sample was analyzed in a similar fashion after the gel reached its new equilibrium swelling capacity in the copper solution. From these data, the initial and final concentrations of each solution could be determined using Beer's Law. The theoretical charge density for the hydrogel was determined using the previously-mentioned formulae developed by Peppas, *et al.*, and the maximum ion capacity for each sample was calculated from these values, Q_{equil}, and the initial volume of each sample as measured by optical microscopy. The steps of these calculations are laid out in detail in Appendix A.

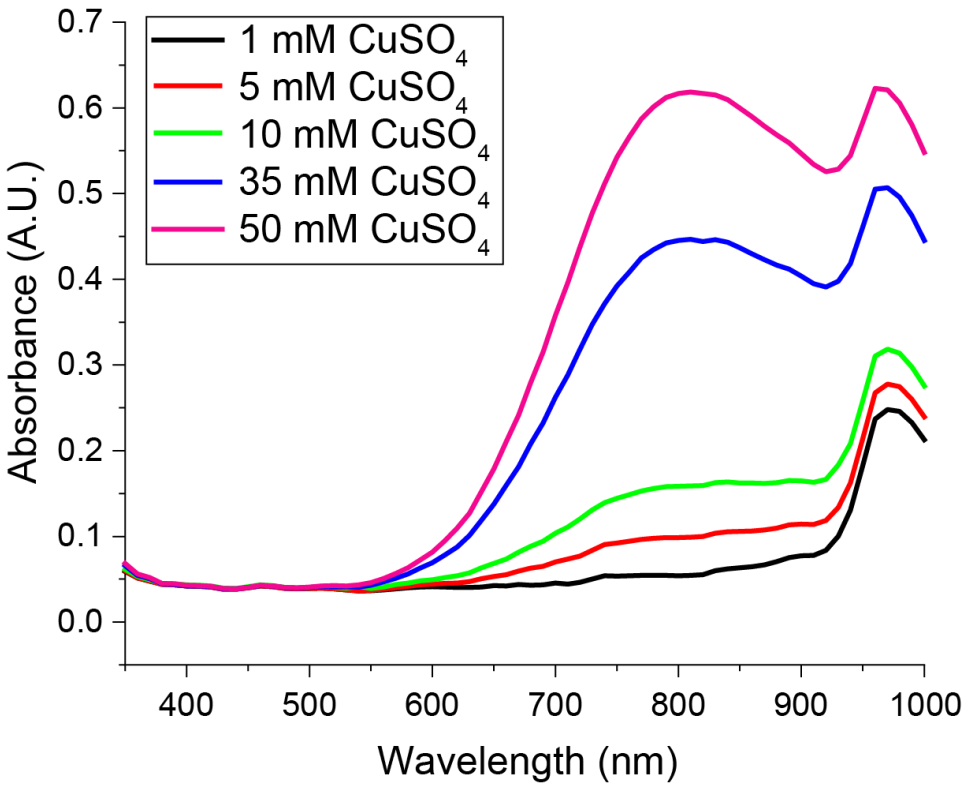

Figure 5.1. UV-Vis spectra for increasing concentrations of $CuSO_4$. Precise concentration was calculated using the absorbance at 810 nm and Beer's Law.

The average amount of copper absorbed from solutions of each concentration, as well as for samples that were swollen in either 100 mM NaCl or 50 mM $CaCl_2$ and then in 50 mM $CuSO_4$, is reported in Figure 5.2. Values are reported as a percentage of the theoretical charge capacity of the gel. One will quickly notice that the copper uptake value for pure gel soaked in 50 mM $CuSO_4$ exceeds 100% of the theoretical charge capacity. This can be explained in light of osmotic pressure, in that even once all PANa charged sites were occupied, the ionic strength of the solution was still greater than that within the gel and excess copper ions were pushed into the gel by the osmotic pressure gradient. Of primary interest to this work is the difference in copper uptake in a pure hydrogel relative to a gel previously swollen in a solution containing a different salt, and so the values to the far right of the plot (*i.e.*, 50 mM $CuSO_4$ solution) are outlined in Figure 5.2 as those of greatest interest.

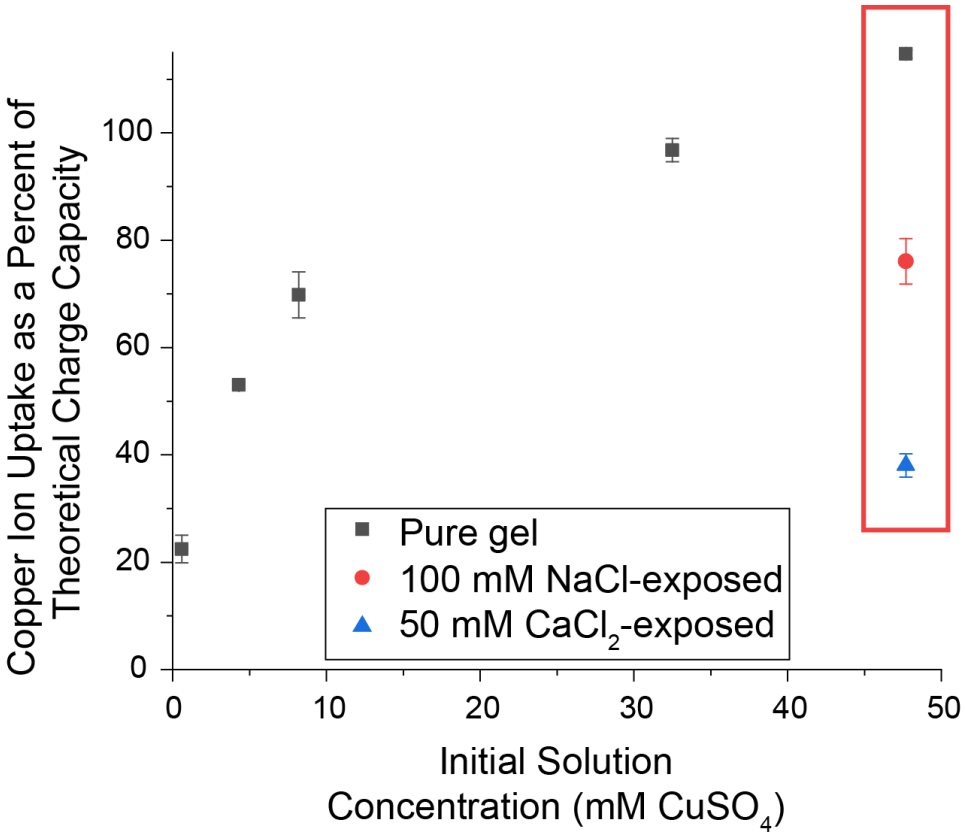

Figure 5.2. Copper ion uptake as determined by UV-Vis. Uptake is presented as a percentage of theoretical charge capacity at different concentrations of $CuSO_4$ (x-axis) with different initial conditions (see Legend).

5.3.2 Raman spectra

Although excess copper may be present in the pure hydrogels swollen in 50 mM $CuSO_4$, only the ions strongly coordinated with polymer functionalities will appear in vibrational spectroscopy analyses such as FTIR or Raman spectroscopy. As mentioned above, Raman spectroscopy was chosen for this study due to the minimal contribution from H_2O bond stretching and higher resolution at low wavenumbers. Raman spectroscopy was therefore conducted on all of the previously described hydrogel samples. Bond assignments and their respective wavenumber ranges are tabulated in Table 5.1, and representative spectra of hydrogels swollen under each set of conditions are plotted in Figure 5.3. Peak assignments have been confirmed with previous literature[31,32,35-38,42,43] and spectroscopy databases.[44,45]

Table 5.1. Peak assignments of interest and their respective spectral ranges for Raman scattering from hydrogel samples.

Peak Assignment	Wavenumber (cm^{-1})		
O-Metal (*v*)	400-515		
CO-O^- (*str*)	860-870	895-910 (primary)	981
CO-O^- (*v*)	1090-1105		
C-NH_2 (*str*)	1405-1430		
C-COO^- (*str*)	1440-1460 (*s*)	1540-1615 (*a*)	
C=O (*str*)	1635-1675 (AM)	1705-1745 (ANa)	

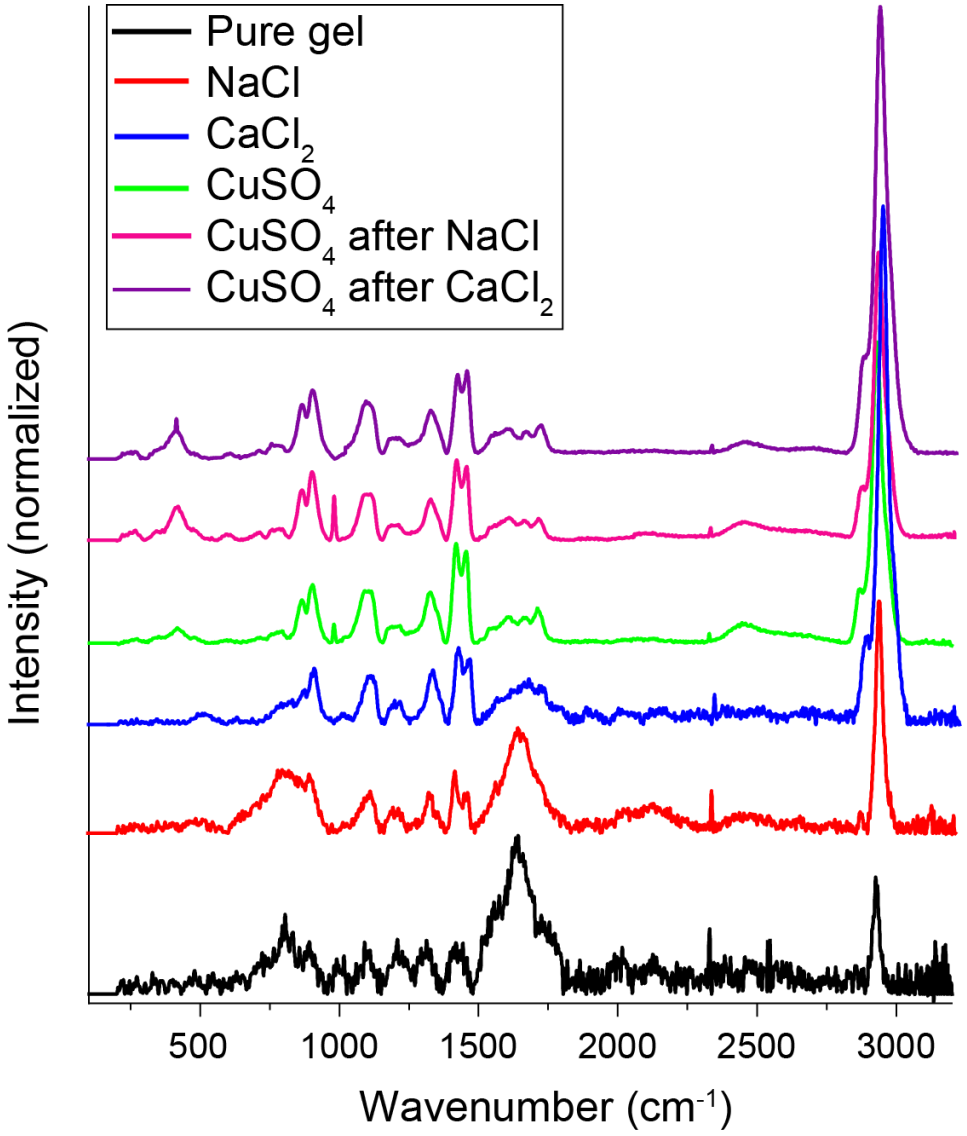

Figure 5.3. Representative Raman spectra for each swelling condition, normalized to peaks from backbone C-C stretching.

Peak-splitting features

There are several features to note in the spectra in Figure 5.3. Beginning at wavenumbers in the range of 860 to 981 cm^{-1}, we observe a splitting of the $CO\text{-}O^-$ stretching peak with the inclusion of divalent salts. This splitting is caused by the introduction of a new asymmetrical stretching mode induced by ionic-crosslinking from the divalent ions. The ratio of the amplitude of the primary peak to that of the split peak in this region can therefore be used as a measure of the relative amount of singly- and doubly-bound divalent ions. An additional stretching or vibrational mode at higher wavenumbers appears for $CuSO_4$ swelling, the location of which remains stable for all conditions under which it appears (*i.e.*, 981 cm^{-1}), suggesting that this peak is unique to the CO-OCu stretch. We hypothesize that this peak is specifically representative of O-Cu-O crosslinks where the copper is chelated with two carboxylate groups. The logic behind this hypothesis is as follows: in an excess of $CuSO_4$ solution (50 mM) only a portion of the copper ions are chelated on both sides by carboxylate groups. When an excess of NaCl is previously present in the gel ($CuSO_4$ after NaCl), a smaller number of copper ions migrate into the gel to reach osmotic equilibrium. However, the copper-carboxylate (Cu-O) bond is exceedingly more stable than the sodium-carboxylate bond (Na-O), and so the copper ions that do enter the gel essentially all interact with two carboxylate groups, producing more O-Cu-O crosslinks and a stronger peak at 981 cm^{-1}. In the case of an excess of $CaCl_2$ previously present ($CuSO_4$ after $CaCl_2$), although the Cu-O bond is more stable than the Ca-O bond, the difference in stability is significantly less. As such, the prior presence of Ca^{2+} crosslinks further limits the influx of Cu^{2+} ions into the gel and also appears to prevent the Cu^{2+} ions entering the gel from chelating with two carboxylate groups, thereby eliminating the peak at 981 cm^{-1} caused by the O-Cu-O double chelation.

The peaks attributed to stretching of the C-C bond of the carboxylate group (C-COO^-) (*i.e.*, 1440 to 1615 cm^{-1}) and the C=O stretches of both the carbonyl and the carboxylate groups (*i.e.*, 1635-1745 cm^{-1}) also offer broad insight from both their peak wavenumber and their relative intensities. The C-C bond adjacent to the C=O bond is bound on one side by a more neutral C-C bond and on the other side by significantly more electronegative oxygen atoms, inducing a dipole in the C-C bond of the carboxylate. As the pull from a metal cation on the carboxylate anion increases, it decreases the polarity of the C-C bond by pulling electrons away from the carbon atom and toward the negatively charged oxygen atom. This in turn decreases the asymmetrical stretch of the C-C bond and decreases the ratio of asymmetrical-to-symmetrical C-COO^- (*str*) peaks. The same increasing pull from a metal cation increases the intensity of the C=O stretching for the PANa carboxylate found at 1705-1745 cm^{-1}, as it increases the polarity of the C=O bond by pulling electrons toward the negatively charged oxygen and away from the carbon atom. This pull does not change the strength of the C-C bond itself, so no shift in wavenumber occurs. However, it does weaken the C=O bond as it draws electrons away from the C=O bond toward the C-O^- bond and delocalizes the double bond, causing the PANa C=O bond signal to "red-shift" to lower wavenumbers.

In order to explain more precise peak changes and their implications, we first offer Table 5.2, where we report the wavenumber for each peak of interest under each set of swelling conditions.

Table 5.2. Peak assignments of interest and their values for each set of swelling conditions.

	Peak Center (cm^{-1})					
Peak Assignment	DI Water	NaCl	$CaCl_2$	$CuSO_4$	$CuSO_4$ after NaCl	$CuSO_4$ after $CaCl_2$
O-Metal (*v*)	-	-	513	403	419	415
$CO\text{-}O^-$ (*str, asym*)	-	-	864	860	862	862
$CO\text{-}O^-$ (*str, sym*)	895	899	905	903	903	905
$CO\text{-}O^-$ (*str, O-Cu-O*)	-	-	-	981	981	-
CO-O- (*v*)	1104	1091	1103	1091	1101	1094
$C\text{-}NH_2$ (*str*)	1414	1409	1420	1426	1419	1420
$C\text{-}COO^-$ (*str, sym*)	1441	1451	1458	1454	1454	1454
$C\text{-}COO^-$ (*str, asym*)	1543	1553	1608	1605	1604	1602
C=O (*str, AM*)	1642	1649	1666	1672	1663	1663
C=O (*str, ANa*)	1732	1742	1706	1719	1716	1716

Direct signal from metal-polymer coordination

The peak that is attributed by researchers[31,35,37,46,47] to direct metal-polymer coordination (*i.e.*, around 400-900 cm^{-1}) becomes stronger in intensity but shifts to lower wavenumbers with the introduction of Cu^{2+}. It has been thoroughly established in literature that copper (II) binds more strongly with the carboxylate group of PANa than sodium or calcium,[8-12] which would suggest that it should cause a blue-shift (*i.e.*, shift to higher wavenumbers) to correspond with an increase in bond strength. However, the red-shift (*i.e.*, shift to lower wavenumbers) observed in this region can be understood regarding the difference in mass between the cations. If atomic bonds are envisioned as the popular ball-and-spring model,[48] having a ball or atom with a larger mass (Cu^{2+}) will cause a lower frequency vibration (*i.e.*, lower wavenumber, in this case ~400 cm^{-1}) relative to one with a smaller mass (Ca^{2+}).

The amplitude of this peak can be directly related to the number of bonds in the sample volume vibrating at this frequency and therefore can be used as a relative measure of the amount

of copper-chelation occurring in the gel. It is believed that a scaling relationship between the density of copper-polymer bonds and either the amplitude or integral of this peak could be derived, although such a relationship was not the primary focus of the work described herein. With previous salt exposure, this peak shifts to higher wavenumbers, suggesting contribution from other metal-polymer interactions, but continues to increase in intensity. Unfortunately, since a slight signal arises from Ca-polymer interactions in $CaCl_2$-soaked gels at ~510 cm^{-1}, the gels exposed to Ca^{2+} followed by Cu^{2+} salts may require additional deconvolution of peaks in this region as well.

Polyacrylamide signal contributions

It is next simplest to summarize the peaks related solely to the PAM functionality, which include the C-NH_2 stretch and the C=O (AM) stretch. In both of these peaks, one sees shifts in wavenumber with the addition of divalent salts. However, in each case, the shift is to *higher* wavenumbers, not lower, which indicates an *increase* in bond strength. We hypothesize that this increase is due to the preferential interaction of the ions with the PANa functionalities. As the PANa bonds are weakened by the pull of metal ions, each acrylamide group is separated from that pull by 2 or 3 C-C bonds so that it does not "feel" the pull. In the meantime, acrylic acid groups and associated ions are being pulled away from the acrylamide groups, allowing the acrylamide groups more bond stretching and vibrational freedom. Furthermore, it has been documented that high concentrations of salt disrupt hydrogen-bonding networks, and so this blue-shift could be partially due to a breaking of hydrogen bonds around the polymer.

Polyacrylic acid signal contributions

Interpretation of the many spectroscopic signals that are produced by bonds in the carboxylate group becomes more complex. Returning to low wavenumbers, we can examine more

closely the relative intensities and shifts in peak values for the symmetric and asymmetric $CO\text{-}O^-$ peaks. As mentioned previously, shifts to lower wavenumbers (red-shifts) indicate a decrease in bond energy, which occurs whenever one bond is "pulled on" from a new interaction occurring at an adjacent bond. Therefore, red-shifts in signals related to the carboxylate group indicate a stronger draw on an adjacent bond (*e.g.*, the anion coordinating with a metal cation). The asymmetric stretch of the $CO\text{-}O^-$ bond itself splits to a lower wavenumber than the symmetrical stretch observed in gels without divalent ions present. This indicates that the metal-polymer coordination is exerting further strain on the $CO\text{-}O^-$ bond. An additional slight red-shift is observed in the asymmetric stretch of the $CO\text{-}O^-$ bond between the calcium-swollen gel and the copper-swollen gel, indicating that the strain exerted by copper coordination is stronger than by calcium coordination. Gels swollen in copper after a different salt show a slight shift back toward higher wavenumbers, which shows that the impact of the copper coordination has less overall impact on the asymmetrical stretching when the gel already contains a more weakly-coordinating cation.

The relative amplitudes of the asymmetric and symmetric stretches, illustrated in Figure 5.4, also offer information. The asymmetric-to-symmetric ratio of the $CO\text{-}O^-$ bond increases with the addition of copper, indicating that copper ions coordinate strongly with a larger fraction of the carboxylate groups than calcium ions do. In both conditions for which the hydrogel was swollen in a more weakly-coordinating salt prior to copper, this ratio is less than in gels exposed only to copper and remains the same for both NaCl and $CaCl_2$ initial exposure. This suggests that a comparable, lower fraction of carboxylate ions are interacting with divalent cations, although the contributions of calcium and copper ions to that interaction cannot be deconvoluted in this measurement.

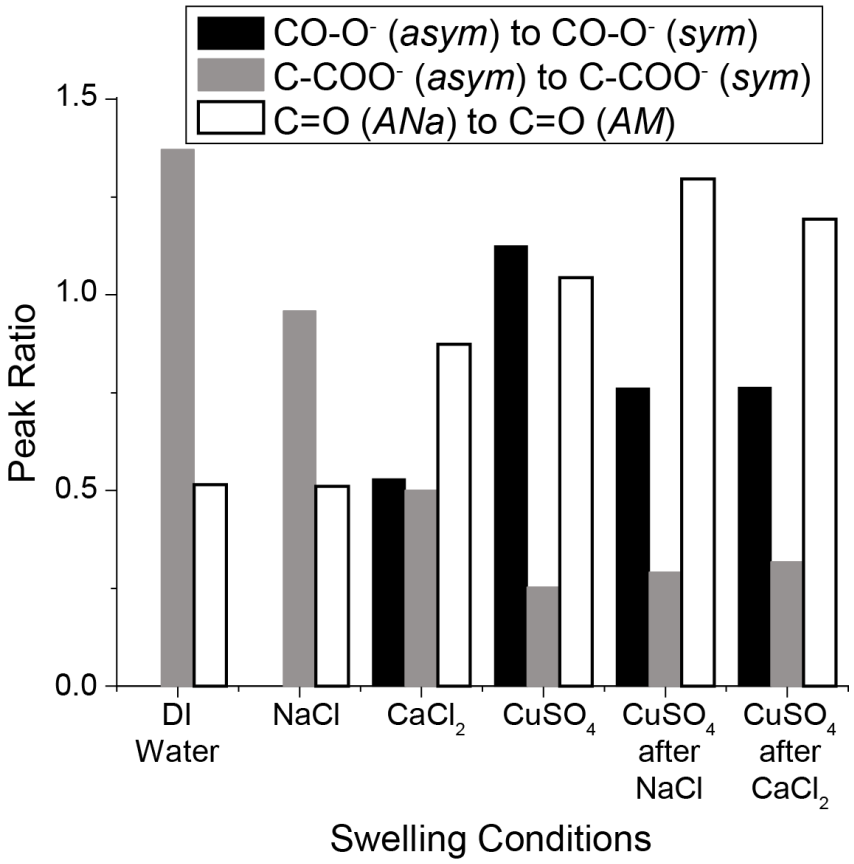

Figure 5.4. Ratios of peak amplitudes for spectra collected under various swelling conditions.

Moving incrementally to higher wavenumbers, we encounter a broad peak attributed to $CO\text{-}O^-$ vibration. The maximum intensity of this peak has been measured at wavenumbers varying between 1091 and 1104 cm^{-1}. It is not anticipated that the vibrational mode of $CO\text{-}O^-$ is strongly impacted by cation coordination, and so this variation is attributed to the broad nature of the peak and shortcomings of model-fitting at this time.

The next contribution from polyacrylic acid groups occurs with the symmetric and asymmetric $C\text{-}COO^-$ stretch at 1441-1458 and 1543-1608 cm^{-1}, respectively. In this instance, there are both symmetric and asymmetric stretching modes regardless of the composition of the swelling solution, as described in section 5.3.2.1. All cations cause a blue-shift in both peaks relative to gels in DI water, with divalent cations inducing a significantly larger shift relative to Na^+ ions.

Surprisingly, calcium cations induce a larger blue-shift than copper cations in these stretching modes. The cause of this is not fully understood, but we hypothesize that it is due to a greater amount of delocalization of the negative charge on the carboxylate group in the presence of Cu^{2+}. Referring back to Figure 5.4, one can observe the ratio of asymmetric-to-symmetric stretching for the $C\text{-}COO^-$ bond as well. The significant decrease in the asymmetric stretching mode, as described in section 5.3.2.1, can be attributed to a shift in charge density on the carboxylate group, in which strong coordination at the carboxylate anion decreases the polarity of the C-C bond.

Finally, the C=O stretch of the carboxylate group can be examined. As mentioned previously, coordination with divalent cations causes an increase in the amplitude of the C=O stretch and a redshift in its peak center. Once again, the amount by which the peak center is shifted is larger in $CaCl_2$ than in $CuSO_4$ solution. This seems counter-intuitive due to the copper cation having a stronger coordination bond with the negatively charged oxygen, but once again we must consider that this stretching mode belongs to an adjacent bond and not the bond being stretched by metal-polymer coordination. At this stage we attribute this difference again to greater delocalization of the negative charge between the two oxygen atoms in the carboxylate group, but further investigation would be beneficial.

5.3.3 Changes in Copper Chelation Induced by Previous Salt Content

Here we outline the significant changes induced by concentrated $CuSO_4$ (*e.g.*, 50 mM solution), relative to hydrogel samples swollen in DI water, before specifying the impact of previous salt content. Copper-polymer coordination produces a new spectral band centered at 403 cm^{-1}. The symmetric $CO\text{-}O^-$ stretch at 895 cm^{-1} splits into an asymmetric peak at 860 cm^{-1}, a symmetric peak at 903 cm^{-1}, and a double-chelation peak (*i.e.*, O-Cu-O bonding) at 981 cm^{-1}. The symmetric and asymmetric $C\text{-}COO^-$ stretching bands shift from 1543 to 1605 cm^{-1} and from 1642

to 1672 cm^{-1}, respectively. The C=O stretch of the carboxylate shifts from 1732 to 1719 cm^{-1}. The C-NH_2 stretching band from the carbonyl group shifts from 1414 to 1426 cm^{-1}, and the carbonyl C=O stretching band shifts from 1642 to 1672 cm^{-1}. The ratio of the amplitudes of asymmetric to symmetric C-COO^- stretching changes from 1.4 to 0.3. The ratio of the amplitudes of carboxylate to carbonyl C=O stretching increases from 0.5 to 1.0.

In the presence of NaCl, copper-polymer coordination generates a vibrational band at a higher wavenumber of 419 cm^{-1}. Since sodium-polymer coordination is not strong enough to produce a vibrational band in this range, it is expected that the blue-shift observed is a function of the high salt concentration in the gel. As mentioned previously, the hydrogen-bonding between unbound water molecules inside a polymer network, as well as between water molecules and hydrophilic polymer groups, is disrupted by increasing salt concentrations. The disruption of the hydrogen-bond network increases the vibrational strength of other bonds, which in this case causes the vibration of the Cu-O bond to shift to a higher wavenumber.

From the increased intensity of the O-Cu-O peak at 981 cm^{-1}, it is believed that a larger fraction of the copper ions present in the gel is chelated with two carboxylate groups each, as described previously. The presence of NaCl does not impact the symmetric stretching of either the CO-O^- bond (903 cm^{-1}) or the C-COO^- (1454 cm^{-1}), but it marginally decreases the magnitude of the red-shift observed in the asymmetric CO-O^- stretching (*i.e.*, from 860 to 862 cm^{-1}) and the blue-shift observed in the asymmetric C-COO^- stretch (*i.e.*, from 1605 to 1604 cm^{-1}). Due to the higher concentration of ions already in the gel, fewer copper ions enter the gel, which means they produce, as an average across the sampled section, less pull on the negatively charged carboxylate oxygen and cause a less significant shift in asymmetric stretches. The ratio of asymmetric-to-symmetric CO-O^- amplitude decreases from 1.1 to 0.8, again indicating that the averaged effect of

copper-polymer coordination is diminished by previous presence of NaCl. The C-NH_2 stretch and the carbonyl C=O stretch shift back to a lower wavenumber of 1419 cm^{-1} and 1716 cm^{-1}, respectively, which is believed to be attributable to less pull on the carboxylate groups and less freedom for the carbonyl groups. Finally, the ratio of C=O peaks for carboxylate to carbonyl groups increases from 1.1 in $CuSO_4$-only samples to 1.3 under the current conditions. This too can be explained by a smaller fraction of carboxylate groups being chelated with copper ions. Chelation increases the intensity of the C=O stretch as it further polarizes the bond, and predominantly double-chelation (O-Cu-O) further increases the polarity of the bond. All of the changes described above agree well with the concept that the presence of NaCl diminishes the amount of $CuSO_4$ taken up by the gel, as indicated by UV-Vis measurements (Figure 5.2), but that the fraction of copper ions in the gel that are chelated with *two* carboxylate groups increases.

In the presence of $CaCl_2$, some of the shifts observed follow the same trend as NaCl-swollen gels, but some shifts suggest that Ca^{2+} alters copper-binding by a different mechanism than Na^+. This dissimilarity may prove useful in differentiating between gels initially containing each cation. First, we can delineate which shifts in spectral bands follow a similar trend to NaCl-swollen gels: signals for asymmetric stretching of the CO-O^- bond, stretching of the C-NH_2 bond, symmetric stretching of the C-COO^- bond, and stretching of both the carbonyl and carboxylate C=O bonds remain the same as in "$CuSO_4$ after NaCl" gels.

As for signals that differ, several conclusions can be drawn from the O-Metal peak in "$CuSO_4$ after $CaCl_2$" spectra. The ion content in the gel after this set of swelling conditions should be a mixture of Cu^{2+} and Ca^{2+} cations but with far fewer Cu^{2+} ions than under other conditions, as confirmed by UV-Vis. It would therefore be logical that the O-Metal peak shifts to somewhere between the peaks for pristine gels swollen in $CaCl_2$ and $CuSO_4$. However, the previous exposure

to $CaCl_2$ causes less of a blue-shift than NaCl. One will also note that the peak entirely disappears at 981 cm^{-1}. These features lend credence to the idea that the peak at 981 cm^{-1} is produced specifically by fully-chelated copper (O-Cu-O) assemblies, and that the presence of Ca^{2+} ions in the gel limits the Cu^{2+} ions to binding with only one carboxylate group each. In this case, we can also conclude that the O-Metal peak is produced predominantly by single copper-polymer binding interactions.

In the previous set of gels, the presence of NaCl caused a slight blue-shift in asymmetric stretching of the $CO\text{-}O^-$ bond, relative to a $CuSO_4$-swollen gel, but did not shift the peak for the symmetric stretch. Here, the presence of $CaCl_2$ blue-shifts both the symmetric and asymmetric stretching of this bond by 2 cm^{-1}, corresponding to an overall weaker pull on the carboxylate anion. We must remember that these shifts in wavenumber represent only the peak center of the vibrational band, not the intensity. Therefore an overall decrease in pull simply means the average pull is lessened, which correlates with the idea that O-Cu-O assemblies are prohibited by the presence of Ca^{2+}. The ratio of the amplitudes of these two signals (*i.e.*, asymmetric to symmetric $CO\text{-}O^-$) implies that there is still a mixed contribution from Cu^{2+} and Ca^{2+}, as the ratio for this case, 0.8, falls between the ratios observed in $CuSO_4$-only (1.1) and $CaCl_2$-only (0.5) swelling conditions.

The asymmetric stretch of the $C\text{-}COO^-$ bond exhibits a small red-shift with the previous presence of $CaCl_2$, which indicates a slight decrease in the strength of this bond's asymmetric stretching relative to $CuSO_4$-only swelling conditions. As previously described, it is believed that Cu^{2+} causes greater delocalization of the negative charge on the carboxylate group. This small shift again supports the idea that Ca^{2+} prevents Cu^{2+} ions from chelating with two carboxylate groups

each, which decreases the delocalization effect on the carboxylate charge, increases the polarity of the C-C bond, and slightly weakens the C-COO^- stretch.

Finally, The ratio of C=O groups appears larger in "$CuSO_4$ after $CaCl_2$" gels than in $CuSO_4$-only gels but lower than in "$CuSO_4$ after NaCl" gels. This is unsurprising, as Ca^{2+} ions pull more on the carboxylate group than Na^+ ions, but the pull from Cu^{2+} ions is diminished both by their limited presence and if they are unable to chelate two carboxylate groups. All of the changes described above agree with the idea that the presence of $CaCl_2$ is more restrictive on copper-uptake, as confirmed by UV-Vis, and Ca^{2+} ions at least largely prevent Cu^{2+} ions from chelating with two carboxylate groups per ion.

5.4 Conclusions and Outlook

The studies described in this chapter have established a more thorough understanding of the differences in ion-polymer interactions between metal cations of different classes and outlined specific effects of previous salt content on the chelation of hydrogel functionalities by transition metal ions. We have confirmed the lack of chelation between copper and polyacrylamide functionalities and hypothesized several specific changes in the charge distribution and bond vibration modes that occur under various swelling conditions. The ideas expressed in this chapter have laid a foundation, but there is still work to be done to establish a standard methodology for identifying hydrogel ion content and swelling history.

Our conclusions to-date include the following:

1) Peak-splitting in the range of 860-990 cm^{-1} can indicate the relative amount of singly- and double-bound divalent counter-ions.
2) The full (double) chelation of Cu^{2+} produces a unique scattering peak at 981 cm^{-1}.

3) Copper-chelation produces a unique vibrational band at 403 cm^{-1} from the direct Cu-O bond vibration.
4) High concentrations of salt cause the Cu-O vibration to shift to higher wavenumbers, likely due to disruption of the hydrogen-bond network in the gel.
5) Strong metal coordination weakens the bond between the negatively charged oxygen atom and the rest of the carboxylate group.
6) Strong metal coordination alters the polarity of the C-C and C=O bonds of a carboxylate group by drawing electrons toward the negatively charged oxygen atom with which the cation is coordinating.
7) Previous presence of Na^+ ions in the gel decreases the number of Cu^{2+} ions that enter the gel due to osmotic pressure gradients but promotes a large fraction of chelation due to the large difference in metal-polymer bond stability.
8) Previous presence of Ca^{2+} ions in the gel more drastically limits the number of Cu^{2+} ions that can enter the gel and also prevents true chelation by the Cu^{2+} between multiple carboxylate groups.

The above conclusions may be expanded to other alkali, alkaline earth, and transition metals thanks to trends in electronegativity and metal-ligand bond stability values. Additionally, the shifts that occur between pristine gels swollen in $CuSO_4$ and previously-exposed "salty" gels swollen in $CuSO_4$ all shift toward the peak observed in the initial salt solution (*i.e.*, NaCl or $CaCl_2$-swollen gel samples). This indicates that if a transition metal is introduced into a "salty" gel, then a reference set of spectra for the gel composition of interest swollen in different salts from the pristine state may be used to identify the prior content of the "salty" gel. For example, if reference spectra are compiled for gel composition X swollen in salts 1, 2, and 3, where one of those salts is

the transition metal salt used to test the previously-exposed "salty" sample, then the differences between those spectra may be used to interpret the changes observed in a spectrum of the "salty" sample. With more data available, this process may even be extendable into samples containing a mixture of two or more counter-ions.

Future work necessary to develop a robust characterization protocol for hydrogel content and history will require additional UV-Vis and Raman spectroscopy analysis on gels containing different fractions of PANa and possibly swollen in different salt concentration combinations in order to fully elucidate the relationship between polymer ionic fraction and metal cation binding. Furthermore, a depth profile study of copper binding in these gels would offer insight into the "shell" formation induced by transition metals and the permeation distance of transition metal ions into a gel sample.

An additional valuable step will be the inclusion of mechanical analysis of the hydrogels under these various swelling conditions. The formation of a "shell" by transition metals, as described in earlier results, produces an increase in the elastic modulus of the sample. The anticipated changes in modulus values under each condition may be calculated using stability constants and other thermodynamic data reported in literature,[8-12] and these values can be compared to experimental mechanical data to gain more insight into shell formation. Comparing calculated values to experimental data may help us understand not only the magnitude of these contributions and the relative strength of weaker ionic crosslinks that do not form a "shell," but also how the "shell" crosslink density varies with depth and hydrogel composition. Samples have been prepared for mechanical testing using a three-point-bending apparatus on a Texture Analyzer, but such experiments were delayed due to COVID-19 related lab access restrictions. Additionally, rheological studies have been considered as an alternative method by which to measure

coordination bond strength. Shear rheology at low strain rates may be employed to break metal coordination bond crosslinks without breaking chemical or physical crosslinks.[43,49]

This study has laid foundational work for a robust, widely-applicable characterization methodology for assessing ionic hydrogel content and history. Such a methodology, when fully developed through the follow-up experiments described above, we believe could be invaluable in understanding how superabsorbent materials will perform in changing ionic environments and recycled applications. With this understanding, more polymeric materials could be up-cycled, improving both future applications and sustainability efforts.

5.5 References

1. Zhu, Q.; Barney, C. W.; Erk, K. A., Effect of ionic crosslinking on the swelling and mechanical response of model superabsorbent polymer hydrogels for internally cured concrete. *Mater. Struct.* **2015,** *48*, 2261-2276.
2. Krafcik, M. J.; Erk, K. A., Characterization of superabsorbent poly(sodium-acrylate acrylamide) hydrogels and influence of chemical structure on internally cured mortar. *Mater. Struct.* **2016**.
3. Krafcik, M. J.; Macke, N. D.; Erk, K. A., Improved Concrete Materials with Hydrogel-Based Internal Curing Agents. *Gels* **2017,** *3* (46).
4. Krafcik, M.; Bose, B.; Erk, K., Synthesis and Characterization of Polymer-Silica Composite Hydrogel Particles and Influence of Hydrogel Composition on Cement Paste Microstructure. *Adv. Civ. Eng. Mater.* **2018,** *7* (4).
5. Budtova, T.; Navard, P., Swelling-Induced Birefringence of a Polyelectrolyte Gel Strongly Interacting with Metal Ions. *Macromolecules* **1997,** *30*, 6556-6558.
6. Budtova, T.; Navard, P., Swelling Kinetics of a Polyelectrolyte Gel in Water and Salt Solutions. Coexistence of Swollen and Collapsed Phases. *Macromolecules* **1998,** *31*, 8845-8850.
7. Budtova, T., Absorption/ release of polyvalent metal ions by a polyelectrolyte gel. *J. Controlled Release* **1998,** *54*, 305-312.

8. David, C.; Companys, E.; Galceran, J.; Garces, J. L.; Mas, F.; Rey-Castro, C.; Salvador, J.; Puy, J., Competitive Ion Complexation to Polyelectrolytes: Determination of the Stepwise Stability Constants. The Ca2+/H+/Polyacrylate System. *J. Phys. Chem. B* **2007**, *111*, 10421-10430.
9. Tomida, T.; Hamaguchi, K.; Tunashima, S.; Katoh, M.; Masuda, S., Binding Properties of a Water-Soluble Chelating Polymer with Divalent Metal Ions Measured by Ultrafiltration. Poly(acrylic acid). *Ind. Eng. Chem. Res.* **2001,** *40*, 3557-3562.
10. Miyajima, T.; Mori, M.; Ishiguro, S.-I., Analysis of Complexation Equilibria of Polyacrylic Acid by a Donnan-Based Concept. *J. Colloid Interface Sci.* **1997,** *187*, 259-266.
11. Gustafson, R. L.; Lirio, J. A., Binding of divalent metal ions by crosslinked polyacrylic acid. *J. Phys. Chem.* **1968,** *72* (5), 1502-1505.
12. Roma-Luciow, R.; Sarraf, L.; Morcellet, M., Complexes of poly(acrylic acid) with some divalent, trivalent and tetravalent metal ions. *Eur. Polym. J.* **2001,** *37*, 1741-1745.
13. Girma, K. B.; Lorenz, V.; Blaurock, S.; Edelmann, F. T., Coordination chemistry of acrylamide. *Coord. Chem. Rev.* **2005,** *249* (11-12), 1283-1293.
14. Sigel, H.; Martin, B., Coordinating Properties of the Amide Bond. Stability and Structure of Metal Ion Complexes of Peptides and Related Ligands. *Chem. Rev.* **1982,** *82*, 385-426.
15. Kasgoz, H.; Ozgumus, S.; Orbay, M., Preparation of modified polyacrylamide hydrogels and application in removal of Cu(II) ion. *Polymer* **2001,** *42*, 7497-7502.
16. Lee, C.; Levin, A.; Branton, D., Copper Staining: A Five-Minute Protein Stain for Sodium Dodecyl Sulfate-Polyacrylamide Gels. *Anal. Biochem.* **1987,** *166*, 308-312.
17. Vanfleteren, J. R.; Peeters, K., Chromatographic recovery of polypeptides from copper-stained sodium dodecyl sulfate polyacrylamide gels. *J. Biochem. Biophys. Methods* **1990,** *20*, 227-235.
18. Jewett, S. L.; Rocklin, A. M., Two Applications Using N,N*-Diethyldithiocarbamate as a Stain for Copper in Native Polyacrylamide Gels of Superoxide Dismutase. *Anal. Biochem.* **1996,** *237*, 65-69.
19. Wang, Z.; Liu, X.; Baeyens, W. R. G.; Delanghe, J. R.; Ouyang, J., Copper(II)-Alizarin Red S Complex as an Efficient Chemiluminescent Probe for the Detection of Human Serum Proteins after Polyacrylamide Gel Electrophoresis. *J. Proteome Res.* **2008,** *7*, 5075-5081.

20. Saito, S.; Kawashima, K.; Ohshima, H.; Enomoto, K.; Sato, M.; Yoshimura, H.; Yoshimoto, K.; Maeda, M.; Shibukawa, M., Separation of metalloproteins using a novel metal ion contaminant sweeping technique and detection of protein-bound copper by a metal ion probe in polyacrylamide gel electrophoresis: distribution of copper in human serum. *Analyst* **2013,** *138*, 6097-6105.
21. Zhu, X.; Shi, H.; Shen, Y.; Zhang, B.; Zhao, J.; Li, G., A green method of staining DNA in polyacrylamide gel electrophoresis based on fluorescent copper nanoclusters synthesized *in situ*. *Nano Res.* **2015,** *8* (8), 2714-2720.
22. Ozcesmec, M.; Bas, S. S.; Akkurt, B.; Bolkent, S.; Hamuryudan, E., Synthesis, characterization and staining performance of peripherally and non-peripherally substituted metallo-phthalocyanines bearing 1,3-bis-(trimethylamino)-2-propoxy groups. *New. J. Chem.* **2020,** *44*, 7786-7794.
23. Wu, R.; Zhang, S.; Lyu, J.; Lu, F.; Yue, X.; Lv, J., A visual volumetric hydrogel sensor enables quantitative and sensitive detection of copper ions. *Chem. Commun.* **2015,** *51*, 8078- 8081.
24. Szewczuk-Karpisz, K.; Nowicki, P.; Sokolowska, Z.; Pietrzak, R., Hay-based activated biochars obtained using two different heating methods as effective low-cost sorbents: Solid surface characteristics, adsorptive properties and aggregation in the mixed Cu(II)/PAM system. *Chemosphere* **2020,** *250*, 126312.
25. Moulay, S.; Bensacia, N.; Garin, F.; Fechete, I.; Boos, A., Polyacrylamide-Based Sorbents for the Removal of Hazardous Metals. *Adsorpt. Sci. Technol.* **2013,** *31* (8), 691-709.
26. Pourjavadi, A.; Motamedi, A.; Hosseini, S. H.; Nazari, M., Magnetic starch nanocomposite as a green heterogeneous support for immobilization of large armounts of copper ions: heterogeneous catalyst for click synthesis of 1,2,3-triazoles. *RSC Adv.* **2016,** *6*, 19128.
27. Sun, Y.; Gao, J.; Liu, Y.; Kang, H.; Xie, M.; Wu, F.; Qiu, H., Copper sulfide-macroporous polyacrylamide hydrogel for solar steam generation. *Chem. Eng. Sci.* **2019,** *207*, 516-526.
28. Marcus, Y., Effect of Ions on the Structure of Water: Structure Making and Breaking. *Chem. Rev.* **2009,** *109*, 1346-1370.
29. Gregor, H. P.; Luttinger, L. B.; Loebl, E. M., Metal-Polyelectrolyte Complexes. I. The Polyacrylic Acid-Copper Complex. *J. Phys. Chem.* **1955,** *59* (1), 34-39.

30. Fan, H.; Sun, T.; Li, W.; Sui, D.; Jin, S.; Lian, X., Sodium polyacrylate as a binding agent in diffusive gradients in thin-films technique for the measurement of Cu^{2+} and Cd^{2+} in waters. *Talanta* **2009,** *79*, 1228-1232.
31. Undabeytia, T.; Morillo, E.; Maqueda, C., FTIR Study of Glyphosate-Copper Complexes. *J. Agric. Food Chem.* **2002,** *50*, 1918-1921.
32. Okuno, D.; Iwase, T.; Shinzawa-Itoh, K.; Yoshikawa, S.; Kitagawa, T., FTIR Detection of Protonation/Deprotonation of Key Carboxyl Side Chains Caused by Redox Change of the CuA-Heme a Moiety and Ligand Dissociation from the Heme a3-CuB Center of Bovine Heart Cytochrome c Oxidase. *J. Am. Chem. Soc.* **2003,** *125*, 7209-7218.
33. Marinsky, J. A.; Anspach, W. M., Complexation of Copper (II) by a Polymethacrylic Acid Gel. *J. Phys. Chem.* **1975,** *79* (5), 439-444.
34. Ricka, J.; Tanaka, T., Swelling of Ionic Gels: Quantitative Performance of the Donnan Theory. *Macromolecules* **1984,** *17*, 2916-2921.
35. Adongo, J. A.; Neubert, T. J.; Sun, G.; Janietz, S.; Lauermann, I.; Rademann, K.; Rappich, J., Fabrication and Characterization of Surfaces Modified with Carboxymethylthio Ligands for Chelate-Assisted Trapping of Copper. *ACS Appl. Mater. Interfaces* **2017,** *9*, 24273-24281.
36. Wang, C.; Wang, C.; Li, B.; Li, H., Zn(II) chelating with peptides found in sesame protein hydrolysates: Identification of the binding sites of complexes. *Food Chem.* **2014,** *165*, 594-602.
37. Torreggiani, A.; Jurasekova, Z.; Sanchez-Cortes, S.; Tamba, M., Spectroscopic and pulse radiolysis studies of the antioxidant properties of (+)catechin: metal chelation and oxidizing radical scavenging. *J. Raman Spectrosc.* **2008,** *39*, 265-275.
38. Magalhaes, A. S. G.; Neto, M. P. A.; Bezerra, M. N.; Ricardo, N. M. P. S.; Feitosa, J. P. A., Application of FTIR in the Determination of Acrylate Content in Poly(sodium acrylate-*co* -acrylamide) superabsorbent hydrogels. *Quim. Nova* **2012,** *7*, 1464-1467.
39. Zhang, X.; Wang, L.; Weng, L.; Deng, B., Strontium ion substituted alginate-based hydrogel fibers and its coordination binding model. *J. Appl. Polym. Sci.* **2019,** *137* (16), 48571.
40. *Handbook of Raman Spectroscopy: From the Research Laboratory to the Process Line*. Marcel Dekker: New York, NY, 2001; p 1054.

41. Peppas, N. A.; Huange, Y.; Torres-Lugo, M.; Ward, J. H.; Zhang, J., Physicochemical Foundations and Structural Design of Hydrogels in Medicine and Biology. *Annu. Rev. Biomed. Eng.* **2000,** *2*, 9-29.
42. Baigorri, R.; Garcia-Mina, J. M.; Gonzalez-Gaitano, G., Supramolecular association induced by Fe(III) in low molecular weight sodium polyacrylate. *Colloids Surf., A* **2007,** *292*, 212-216.
43. Zheng, P.; Cao, Y.; Lissel, F.; Linder, C.; You, X.-Z.; Bao, Z., A highly stretchable autonomous self-healing elastomer. *Nat. Chem.* **2016,** *8*, 618-624.
44. Millipore Sigma, IR Spectrum Table & Chart. Millipore Sigma: St. Louis, MO, 2020.
45. Yvon, J., Raman Spectroscopy for Analysis and Monitoring. Horiba: Edison, NJ.
46. Ferraro, J. R.; Walker, W. R., Infrared Spectra of Hydroxy-Bridged Copper(II) Compounds. *Inorg. Chem.* **1965,** *4* (10), 1382-1386.
47. Pereira, D. C.; de Faria, D. L. A.; Constantino, V. R. L., Cu^{II} Hydroxy Salts: Characterization of Layered Compounds by Vibrational Spectroscopy. *J. Braz. Chem. Soc.* **2006,** *17* (8), 1651-1657.
48. Ashenhurst, J. Bond Vibrations, Infrared Spectroscopy, and the "Ball and Spring" Model. https://www.masterorganicchemistry.com/2016/11/11/bond-vibrations-ir-spectroscopy/.
49. Li, X.; Wang, H.; Li, D.; Long, S.; Zhang, G.; Wu, Z., Dual Ionically Cross-linked Double-Network Hydrogels with High Strength, Toughness, Swelling Resistance, and Improved 3D Printing Processability. *ACS Appl. Mater. Interfaces* **2018,** *10* (37), 31198-31207.

6. CONCLUSIONS AND FUTURE RECOMMENDATIONS

6.1 Summary of Research

This dissertation set out to develop a more thorough understanding of structure-property relationships in hydrogels driven by ionic interactions. To achieve this, a model hydrogel system composed of poly(acrylic acid-*co*-acrylamide) crosslinked with MBAM was utilized to investigate noncovalent interactions within a pH- and ion-sensitive superabsorbent network. Interactions were probed relative to polymer composition, solution composition, and solute character across multiple lengthscales using a broad range of non-destructive characterization techniques.

The initial investigation in this dissertation sought to provide a more robust understanding of the changes in polymer conformation and distribution of network components induced by monovalent and multivalent counter-ions. It employed a previously-established synthetic protocol to produce polymer gels and their nanocomposite counterparts that are of interest for a wide range of applications so that this work might offer the broadest impact. Characterization relied heavily on macroscale swelling experiments and spatially-averaged nanoscale measurements via small-angle x-ray scattering. This work determined that while monovalent counter-ions produce a gradual reduction in swelling through increasing electrostatic screening, multivalent ions induce a significant degree of network collapse at low concentrations due to the formation of ionic crosslinks between polymer functional groups. These ionic crosslinks do not distribute evenly throughout the polymer network but instead aggregate to form clusters of electron-dense regions. The incorporation of nanoparticles further decreases the swelling capacity of these hydrogels by adding physical crosslinks to the system. However, we found no evidence that these crosslinks contain a chemical component, as the persistence length of the polymer chains was unaffected by nanoparticle presence. As for ion-induced reductions in swelling in the presence of nanoparticles,

evidence suggests that there is a preferential association of free counter-ions around the negatively charged nanoparticles. This results in minimal ion-induced decreases in hydrogel swelling until the solution concentration exceeds the saturation concentration for the nanoparticles.

Motivated by the appearance of polymer-salt aggregates in scattering spectra, the next portion of this research sought to understand crystallization of simple salts in PANa-PAM hydrogels. This study discovered unexpected relationships between hydrogel composition and the onset concentration and capacity of the gel for crystallization of NaCl. A deeper investigation into the anticipated mesh size of each polymer composition offered insight into these relationships. This study also discovered that despite the aggregates observed via SAXS in hydrogels containing $CaCl_2$, crystallization of $CaCl_2$ in these gels could be achieved. The size of crystals formed by NaCl could be somewhat controlled by hydrogel composition and the rate at which salt concentration in the gel increases, although the probable occlusion of polymer by the salt crystals limited the uniformity and measurement capacity of these crystals. This investigation further probed the effects of NaCl crystallization on subsequent hydrogel performance, finding that salt crystallization, even after fully rinsing the hydrogels in DI water, still has a hysteretic impact on gel swelling.

Investigation of the hysteretic impact of salts in these hydrogels was expanded to other solute types, resulting in the investigation using metal cations of different character (*i.e.*, ions with the same valency but from different groups within the periodic table) presented in Chapter 4. Here, the permanence of ionic crosslinks was investigated as a function of polymer composition. It was confirmed that transition metals such as copper (II) form “permanent” ionic crosslinks, which contribute to the mechanical properties of the polymer gel and can be broken only under extremely acidic conditions. The magnitude of ionic contributions to the elastic modulus of the polymers was

determined with respect to solute concentration, and theories were developed for the chemical cause of the discrepancies between hydrogel properties when swollen with alkaline earth metal ions versus transition metal ions.

The final portion of this dissertation sought to obtain a deeper understanding of the physical chemistry behind these hydrogel-ion interactions and develop a robust characterization protocol by which the contents of such polyelectrolyte gels could be measured. This study employed a combination of spectroscopic techniques to more fully elucidate the effects of alkali, alkaline earth, and transition metal cations on the noncovalent bonding interactions within a PANa-PAM network. Spectroscopic shifts were identified and quantified for polymer interactions with NaCl, $CaCl_2$, $CuSO_4$, and $CuSO_4$ after prior exposure to NaCl and $CaCl_2$. From these measurements, we have been able to hypothesize the effects of main group metal cations on the subsequent binding of transition metal ions. Specifically, we conclude that the presence of sodium (or monovalent) ions in the gel decreases the number of copper (or transition metal) ions that enter the gel through osmotic pressure gradients but increases the fraction of copper ions that chelate with *two* carboxylate groups. We anticipate that this is due to the significantly higher stability of Cu-O bonds over Na-O bonds. Similarly, the presence of calcium (or divalent main group) ions further limits the influx of copper when placed in the same concentration solution. However, in the case of calcium-copper competition, the difference in Cu-O and Ca-O stability is less significant, and calcium ions appear to wholly preclude copper ions from interacting with more than one carboxylate group, rather than being replaced entirely by copper ions as is the case with sodium ions.

6.2 Future Work and Outlook

The investigations described herein have elucidated a range of ionically-driven structure-property relationships in polyelectrolyte gels and have the built a foundation for several different paths forward. As such, a few recommendations for future studies are laid out below.

6.2.1 Non-destructive characterization

This research will continue to benefit from non-destructive characterization techniques that allow investigation of nanoscale features of hydrogels in the swollen state. Additional scattering and spectroscopic analysis, including the methods described in this dissertation as well as new analysis techniques proposed below, will allow future investigators to obtain a complete understanding of the nanoscale phenomena investigated in this dissertation as a function of polymer composition.

Scattering

This dissertation has designed x-ray scattering experiments for the analysis of PANa-PAM hydrogels and PANa-PAM-SiO_2 nanocomposites. The experiments described here may be reproduced using properly-synthesized (*i.e.*, higher initiator content) hydrogels and should be expanded to include gels swollen with transition metal salts. Further expansion in SAXS experimentation may include data collection at larger sample-to-detector distances in order to fully characterize the PANa-PAM-SiO_2 nanocomposites. At sufficiently low q-values (*i.e.*, large scattering distances), changes in the size of nanoparticle-based features, such as increases in the measured radius of the particles that appear due to the coordination of cations on their surfaces. The inclusion of neutron scattering experiments on the same materials would provide a more complete understanding of polymer conformation and ionic interactions in these gels, if feasible.

Spectroscopy

Perhaps even more valuable than SANS, however, would be the addition of PALS characterization. Positron annihilation can provide information about changes in free volume of the polymer network, complementing correlation length measurements obtained through scattering. It can also measure alterations in hydrogen-bonding induced by counter-ions in the gel by determining the relative amount of bound and unbound water in the system. Furthermore, a PALS instrument is readily accessible within the department, and experiments can be conducted on it without incurring additional costs or facing time limits on access to the instrument.

Building off of the Raman spectroscopy experiments described in this dissertation, future work should also prioritize conducting depth profiling experiments on transition metal-crosslinked gels of varying polymer composition. This step will be particularly important, as the formation of crosslinked "shells" has been observed to strongly depend on polymer composition, and such shell formation will drastically impact any subsequent mechanical characterization attempts. As mentioned previously, these experiments can be conducted using the same Raman microscope used for prior experiments.

This same Raman microscope assembly can further be combined with an AFM chamber that is currently available for the instrument but not in use. This AFM chamber can be used to conduct force measurements on swollen hydrogel samples under ambient conditions, which will provide an *in situ* method to gain insight regarding the distribution and strength of ionic crosslinks. This form of non-destructive mechanical analysis could prove particularly valuable in measuring more "permanent" ionic crosslinks from transition metals, as well as nanoparticle distribution in PANa-PAM-SiO_2 nanocomposites.

6.2.2 Mechanical Characterization

Finally, some characterization in which the hydrogel sample is destroyed may prove valuable for elucidating the strength of ionic bonds and the crosslink gradient formed by the "shell" observed in transition metal-swollen gels. Mechanical analysis will allow researchers to more thoroughly connect the nanoscale interactions with macroscale hydrogel performance. As mentioned in Chapter 5, three-point-bending experiments have been planned for quantifying mechanical contributions made by stronger "permanent" ionic crosslinks. Once the shell thickness and transition metal concentration gradient have been determined, mechanical characterization of hydrogels swollen in main group metal salt solutions, transition metal salt solutions, and transition metal solutions *following* main group metal solutions should be conducted in order to fully quantify bonding interactions. In the case of transition metal-containing gels, this will require exfoliation of the shell layers such that the mechanical properties of test materials are more uniform throughout the thickness of the test sample.

6.2.3 Outlook

Quantification of the strength and distribution of ion-polymer interactions, changes to polymer bonding and conformation, and competitive ion effects, all as a function of polymer composition, would provide a complete and robust understanding of ionically-driven structure-property relationships in this polymer system. Many facets of these phenomena have been elucidated in this dissertation, but more investigation remains in order to complete our understanding. With this information, scaling relationships can be derived in order to tailor hydrogel composition for targeted ionic environments. Furthermore, this understanding of the ionically-driven changes in polymer properties can be applied to polymer systems well beyond the PANa-PAM copolymer.

Finally, a unified characterization protocol for recyclable materials, as represented by "$CuSO_4$ *after* NaCl" or $CaCl_2$ conditions in Chapter 5, would open the door for understanding the full performance capacity of recycled hydrogel materials and allow researchers to decide where and how such used materials could be applied in a secondary field without extensive Edisonian experimentation.

APPENDIX A. RELEVANT EQUATIONS

EQUATIONS RELATING SAX PARAMETERS

Scattering vector: $q = \frac{4\pi \sin\theta}{\lambda}$

Feature diameter, or center-to-center distance: $d = \frac{2\pi}{q}$

CALCULATIONS RELATED TO THEORETICAL POLYMER MESH SIZE

Input Parameters:

N_{AA} – moles of AA in reaction

N_{AM} – moles of AM in reaction

$N_{init,1}$ – moles of $Na_2S_2O_5$ in reaction

$N_{init,2}$ – moles of $Na_2S_2O_8$ in reaction

N_{MBAM} – moles of MBAM in reaction

N_{NaOH} – moles of NaOH in reaction

V_{tot} – total volume of reaction

M_{init} – mass of reagents in reaction

M_{rec} – recovered mass of polymer

Q – equilibrium swelling ratio

Constants:

M_{AA} – mass of AA monomer – 72.06 g/mol

M_{AM} – mass of AM monomer – 71.08 g/mol

N_A – Avogadro's number

ρ_w – density of water – 1

ρ_{AA} – density of AA – 1.41

ρ_{AM} – density of AM – 1.3

V_1 – molar volume of water – 18 mL/mol

χ_1 – AA-AM interaction parameter – 0.4707*

φ – functionality of crosslinking agent – 4

K_a – acid dissociation constant AA – 4.5

l – length of C-C bond – 0.154 nm

Calculated Parameters:

X – molar ratio AM:AA

$$X = \frac{N_{AM}}{N_{AA}}$$

Conv. – conversion

$$Conv. = \frac{M_{init}}{M_{rec}}$$

Mon. – monomer units in reaction

$$Mon. = (N_{AA} + N_{AM}) * N_A$$

Rad. – radicals produced in reaction

$$Rad. = 2 * N_{init,2} * N_A$$

R – repeat units per chain at 100% conversion

$$R = \frac{Mon.}{Rad.}$$

N_{avg} – average repeat units per chain

$$N_{avg} = R * Conv.$$

$\bar{M}_n$ = average molecular weight of polymer chain

$$\bar{M}_n = \left(N_{avg} * \frac{1}{1+X} + M_{AA}\right) + \left(N_{avg} * \frac{X}{1+X} * M_{AM}\right)$$

ρ_p – density of polymer

$$\rho_p = \left(\rho_{AA} * \frac{N_{AA}}{N_{AA}+N_{AM}}\right) + \left(\rho_{AM} * \frac{N_{AM}}{N_{AA}+N_{AM}}\right)$$

$v_{2,r}$ – volume of polymer in relaxed state (*i.e.*, immediately after polymerization)

$$v_{2,r} = \frac{M_{rec}}{\rho_p} * \frac{1}{V_{tot}}$$

$v_{2,s}$ – swollen volume fraction

$$v_{2,s} = \frac{\rho_w}{\rho_p} * \frac{1}{Q}$$

$\bar{v}$ – specific volume of polymer (mL/g)

$$\bar{v} = \frac{1}{\rho_p}$$

I – ionic strength of gel (see table)

$$I = \sum \frac{1}{2}(C_i Z_i^2)$$

Reagent	$Z_{Ion\ 1}$	$Z_{Ion\ 2}$	$C_{Ion\ 1}$	$C_{Ion\ 2}$
NaOH	+1	-1	N_{NaOH}	N_{NaOH}
AA	+1	-1	N_{AA}	N_{AA}
AM	0	0	N_{AM}	N_{AM}
MBAM	0	0	N_{MBAM}	N_{MBAM}
$Na_2S_2O_5$	+1	-2	$N_{init,1}$	$N_{init,1}$
$Na_2S_2O_8$	+1	-2	$N_{init,2}$	$N_{init,2}$

M_r – average monomer mass

$$M_r = M_{AA}\left(\frac{1}{1+X}\right) + M_{AM}\left(\frac{X}{1+X}\right)$$

pH – pH of gel

$$pH = 14 + \log N_{NaOH}$$

C_n – Flory characteristic ratio of the polymer**

$$C_n = \left(\frac{N_{AA}}{N_{AA}+N_{AM}} * 6.7\right) + \left(\frac{N_{AM}}{N_{AA}+N_{AM}} * 2.72\right)$$

Governing equation for ionic gels:

$$\frac{V_1}{4IM_r}\left(\frac{v_{2,s}}{\bar{v}}\right)\left(\frac{K_a}{10^{-pH}+K_a}\right)^2$$

$$= \left[\ln(1-v_{2,s}) + v_{2,s} + \chi_1 v_{2,s}^2\right] + \left(\frac{V_1}{\bar{v}\bar{M}_c}\right) v_{2,r}\left(1 - \frac{2\bar{M}_c}{\bar{M}_n}\right)\left(\left(\frac{v_{2,s}}{v_{2,r}}\right)^{1/3} - \frac{v_{2,s}}{2v_{2,r}}\right)$$

Solve for M_c – molecular weight between crosslinks

ξ – mesh size (nm)

$$\xi = (v_{2,s})^{-1/3}\left(\frac{2C_n\bar{M}_c}{M_r}\right)^{1/2} l$$

*interpolated value based on Turan, E.; Caykara, T.; "Swelling and network parameters of pH-sensitive poly(acrylamide-*co*-acrylic acid) hydrogels" *J. Appl. Polym. Sci.* **2007**, *106* (3), 2000-2007.

interpolated value based on Thakur, A.; Wanchoo, R. K.; Singh, P. "Structural Parameters and Swelling Behavior of pH Sensitive Poly(acrylamide-*co*-acrylic acid) Hydrogels" *Chem. Biochem. Eng. Q*. **2011, *25* (2), 181-194.

CALCULATIONS RELATED TO HYDROGEL FIXED CHARGE CONCENTRATION, THEORETICAL CHARGE DENSITY, AND COPPER-UPTAKE

Useful conversions:

1 nm = $1.0*10^{-6}$ mm

1 nm^3 = $1.0*10^{-18}$ mm^3

1 mL = 1 cm^3 = 1000 mm^3

Equations:

ρ_{charge} – gel charge density (chains/mm^3)*

$$\rho_{charge} = \frac{\left(\frac{M_c}{M_r} * \frac{M_{AA}}{M_{AA}+M_{AM}}\right) * \frac{12}{4}}{\xi^3} * \frac{1 * 10^{-18} nm^3}{1 mm^3}$$

ρ_{gel} – average gel density

m_{equil} – mass of sample at Q_{equil}

V_{equil} = (length * width * thickness) as measured by optical microscopy at Q_{equil}

$$\rho_{gel} = \frac{m_{equil}}{V_{equil}}$$

C_i – concentration of copper solution in UV-Vis, *i* designates before/after gel uptake

$C_i = \frac{A_{810}}{12.3}$ (Beer's Law)

Cap_{gel} – charges in gel at Q_{equil}

$$Cap_{gel} = \rho_{gel} * m_{equil}$$

Cap_{div} – capacity for divalent charge interactions

$$Cap_{div} = \frac{Cap_{gel}}{2}$$

Abs – cations absorbed from solution**

$$Abs = \left(C_{after} - C_{before}\right) * 0.01\ L * N_A$$

$\%_{abs}$ – percent of theoretical capacity occupied by absorbed ions

$$\%_{abs} = \frac{Abs}{Cap_{div}} * 100$$

* 12/4 factor assumes cubic structure, where 12 chain lengths make up a cube, and each chain length between crosslinks is shared between 4 cubes

** 10 mL solution per sample

APPENDIX B: STANDARD OPERATING PROCEDURE FOR SAXSANALYSIS SOFTWARE

1. Locate the .h5z data files (individual and averaged) collected from your experiments and transfer them to a personal computer using an external storage device.
2. Open the SAXSanalysis package on your personal computer.
3. Start an empty session.
4. Right click on Source Data, select Add File(s). Choose the files you wish to process.
5. Expand the Source Data banner, select a frame.
6. Click Figures across the top, select 2D graphs, and click "select data" on right panel
7. Load the frame of interest. *You should see a 2D scattering pattern.*

   Notes on Settings:
   a. The gear icon on the left side of the image panel can be used to scale colors and bring out subtle scattering rings.
   b. The symbol composed of four diamonds next to the Figure title to dock/undock a panel.
8. Right click on Source Data and select Add Process. *If you have individual frames, proceed to step 9. If you have averaged frames, skip to step 13.*
9. Select Process type: Combiner and click Create process.
10. Right click on Process and click the "Select" button to choose which files to include in the process.
11. Right click on Process again and choose Insert Tool. Select the "Frame Averager" tool.
12. Click Calculate to run the process and average your frames.
13. Right click on the Process (or on Source Data if you have not added a Combiner process). Select Insert Process and choose Process type: Sequential.
14. Right click on the most Process to select your data. Click "Select" to choose the files you wish to include. *If you used a combiner process, choose the frame under the "Frame Averager" menu.*
15. Right click on the Process again and select Insert Tool.
16. Select "Zero Point by Moments 2D" and create tool. *You can filter tools by data type at the top of this menu.*

17. Click on the Zero Point by Moments 2D tool and click “Select Dataset” and choose the most recent frames.
18. To set your zero point, go to the graph settings (gear icon) and select color mapping. Turn off scale, and zoom to the center of your scattering pattern by clicking and dragging a box around the area.
19. Select the “Box” (dashed line box with a plus in the corner). Box in only the signal that is passing through the center of the beamstop but clicking at one corner, releasing the mouse button, moving to the opposite corner, and clicking again. *If you click and drag, you will zoom. Double click to zoom back out to your full frame.* Click Apply in the bottom right and Calculate.
20. If masking is needed, right click on the Zero Point by Moments 2D tool and insert tool. Select 2D Masking. *If you do not want to mask portions of your pattern, skip to step 23.*
21. Select your dataset, making sure you select the frame under your last tool. Use the box, slice, or arc tools on the left side of the frame to draw masking boxes to cover the beamstop or select portions of your pattern. *Masking parts of your pattern is primarily useful if you have a flare on one side of the pattern caused by scattering off the edge of a capillary tube sample holder.*
22. Click Mask and Calculate.
23. Right click on your last tool, Add tool, and select Q Transformation. Click on the tool.
    a. For transmission SAXS, select Transformation type: Transmission.
    b. For GISAXS, select Transformation type: Gisaxs and select Type of GISAXS projection: (qy,q_z).
24. Calculate.
25. Right click on Q Transformation and Insert tool. Select Data Reduction 2D.
26. Click on the tool and Select Dataset. Make sure to select the frame under Q transformation.
27. Use the box, slice, and arc tools to highlight the area of scattering that you wish to reduce.
    a. For isotropic samples, you will typically use the slice tool. Click at the center of your beamstop, release the mouse button and drag up the highlighting section to the top edge of your frame. Click again.
    b. For anisotropic samples, box and arc tools are helpful for highlighting the desired sections of data.

c. To make sure your slice is centered at the zero point, click “Set 0” on the menu that appears once you’ve highlighted an area. You can then change your x and y out, which moves the far end of the slice, and choose the angle over which you want to integrate.

28. Click Apply and Calculate.
29. Go to the Figures tab across the top and select a 1D graph. Select data. *You should now see the 1D reduction of you scattering pattern.*
30. For 1D masking, right click on Data Reduction 2D, Insert tool, and select Masking 1D.
31. Click on the tool and select your most recent data set. Use the “x Range” tool on the left side of the frame to mask sections like signal from the center of the beamstop or trim noise at large *q* ranges. *You will likely skip this step if you conducted 2D masking.*
32. Click Mask and Calculate.
33. If you would like to subtract a background file, right click your last tool, Insert tool, and select Standard Operations 1D. Select a Reference background under the Subtract intensity heading. Click apply and Calculate. *You may choose to skip this step.*
34. Right click your most recent tool, Insert tool, Export ASCII. *This will generate a general comma-separated file. Depending on additional software you are using, you may choose to export in a different format.*
35. Create tool, choose your Output File Name and Path. Click apply and Calculate. *This will generate a file that can be opened in Excel or any program that can read ASCII or .csv.*

Note on removing the gap between detectors on your 2D data: Collect an additional set of data at an SDD approximately 10 cm closer to the detector. When processing, perform a standard sequential process until you reach the Q transformation step. Calculate the Q transformation, and then create a new Combiner process. Check the box for “Separate output per input file,” and select inputs. Right click on the process to insert a tool, and Insert tool: Binning 2D combiner.

VITA

Jessica Sargent was born and raised in Lawrenceville, GA. She graduated *summa cum laude* from Auburn University with her Bachelor of Science degree in Polymer & Fiber Engineering and a minor in Music Performance. While attending Auburn, she was an undergraduate researcher under Professor Maria Auad and assisted in the development of antimicrobial polyurethanes and naturally-derived epoxy resins. She completed her M.S., Thesis degree at Purdue University in Chemical Engineering, where she studied self-assembly of triblock copolymers for application in water purification membranes. In 2017, she joined the Materials Engineering program at Purdue University to complete her PhD studies. She is interested in synthesis and characterization of soft and composite materials with a focus on polymer chemistry. She is the primary author of four publications, one of which is related to Engineering Education through the Purdue University Women in Engineering Program. She has co-authored five other research papers, of which three have been published to date.